



Master Thesis

Anapole Moment of Majorana Fermions and Implications for Direct Detection of Neutralino Dark Matter

**Anapolmoment von Majorana-Fermionen und Implikationen für den
direkten Nachweis von Neutralino Dunkler Materie**

Merlin Emanuel Reichard

18. February 2021

last compiled: 20. Dezember 2022

First Reviewer (Supervisor): Prof. A. Ibarra
Second Reviewer: Dr. J. Harz

Abstract

After an introduction to dark matter and supersymmetry, the calculation of the anapole moment as loop induced electromagnetic interaction of a generic Majorana fermion is carried out. For this, the contributions of both a scalar and a vector in the corresponding loop diagram is considered, of which the latter is a novel calculation. After motivating this inherent electromagnetic moment in the context of dark matter direct detection experiments, where observation based on this interaction may occur, a numerical analysis of the anapole moment is carried out. After a brief model-independent study, the focus is drawn on the dark matter candidate of the minimal supersymmetric standard model, the lightest neutralino. In particular the parameter space of the gravity- and anomaly mediated supersymmetry breaking scenarios are investigated. For this, the experimental constraints on the Higgs boson and the dark matter relic density are employed.

Zusammenfassung

Nach einer Einführung in die Dunkle Materie und die Supersymmetrie wird die Berechnung des Anapolumoments als schleifeninduzierte elektromagnetische Wechselwirkung eines generischen Majorana-Fermions durchgeführt. Dazu werden die Beiträge sowohl eines Skalars als auch eines Vektors im entsprechenden Schleifendiagramm betrachtet, wobei letzteres eine neuartige Berechnung ist. Nach einer Motivation dieses inhärenten elektromagnetischen Moments im Kontext von Experimenten zum direkten Nachweis dunkler Materie, bei denen eine Beobachtung aufgrund dieser Wechselwirkung erfolgen kann, wird eine numerische Analyse des Anapolumoments durchgeführt. Nach einer kurzen modellunabhängigen Untersuchung wird der Fokus auf den Dunkle-Materie-Kandidaten des minimalen supersymmetrischen Standardmodells, das leichteste Neutralino, gelenkt. Insbesondere wird der Parameterraum der Gravitations- und Anomalie-vermittelten supersymmetriebrechenden Szenarien untersucht. Dazu werden die experimentellen Ergebnisse für das Higgs-Boson und die Reliktdichte der Dunklen Materie herangezogen.

Acknowledgements

I would like to thank Ryo Nagai for helpful discussions.

Contents

1	Introduction	1
2	Basics of Dark Matter	3
2.1	Standard Cosmology	3
2.2	Observational Evidence	5
2.3	Production Mechanisms and WIMPs	9
3	Supersymmetry in a Nutshell	13
3.1	Symmetries in Particle Physics	13
3.2	Why Supersymmetry?	15
3.3	Supersymmetric Lagrangians	16
3.4	The Minimal Supersymmetric Standard Model	25
3.5	SUSY-Breaking Scenarios	34
4	The Anapole Moment	37
4.1	Electromagnetic Interactions of Fermions	37
4.2	The SM Neutrino Charge Radius and Anapole Moment	40
4.3	The Pinch-Technique and the Background Field Method	43
4.4	General Anapole Moment for Majorana Fermions	44
4.5	The SM Neutrino Charge Radius: Revisited	48
5	Connection to Direct Detection Experiments	51
5.1	Experiments and Constraints	51
5.2	Basics of Direct Detection Experiments	52
5.3	Standard SI and SD Contributions	54
5.4	Magnetic Dipole Interaction	56
5.5	Anapole Interaction	57
6	Numerical Analysis	59
6.1	Model-Independent Analysis	59
6.2	MSSM: General Framework	64
6.3	SUGRA	65
6.4	AMSB	68

7 Summary and Outlook	71
A Classical Multipole Expansion and Toroid Moment	75
B Treatment of γ_5	81
C Feynman Rules	85
C.1 Majorana Fermion Interactions	85
C.2 Background Field Vertices	86
C.3 Supersymmetric Vertices	87
C.4 Vertices in the MSSM	88
Bibliography	95

Chapter 1

Introduction

Observational evidence suggests that around 80% of matter in our universe is not visible, but composed of an unknown, dark type of matter instead [1]. These pieces of evidence can be seen in many astrophysical and cosmological systems, ranging from rotation curves of galaxies, cluster movements, to large scale structure and the omnipresent cosmic microwave background [2]. This dominating type of matter is substantially driving the gravitational dynamics of the structures in our Universe. If this dark matter (DM) is a particle, it is expected to be truly dark, e.g. it does not interact with the photon in the same way as the electrons and the nuclei of the intergalactic medium. Furthermore, it has to be stable; otherwise their content would have decayed [3]. One typical type of DM candidate is a *weakly interacting massive particle* (WIMP), whose present relic abundance is described by the *freeze-out* mechanism: The candidate is in thermal equilibrium with the bath of Standard Model particles at high temperature (early times), but once the annihilations cannot keep the WIMP in equilibrium with the thermal bath, it stops interacting with the visible sector [3] and its (comoving) number density becomes constant. Furthermore, the same couplings leading to the correct dark matter abundance may allow the detection of WIMPs.

Different strategies both experimentally and theoretically have been developed trying to detect the DM particle. On the experimental side the approaches can be separated roughly into three categories: direct detection experiments, where DM interacts with material in the detector directly, indirect detection experiments, where signals like hard gamma-rays originating from extraterrestrial DM interactions are looked out for, and collider searches, where DM may be produced via high-energetic particle collisions. On the theoretical side, many models have been proposed with varying particle content and interactions allowing both predicting the present observational evidence for DM and offering a prospect for its detection.

Current evidence does not completely exclude the possibility that the DM particle can interact with ordinary matter via electromagnetic interactions. In fact the assumption of Lorentz- and electromagnetic gauge invariance do not forbid that DM can have a charge or other higher electromagnetic moments. In many models, these higher electromagnetic moments can be generated via quantum corrections. Con-

cretely, Dirac fermions can carry electric charge, an electric- and magnetic dipole moment, and an anapole moment. Majorana fermions, due to the fact that they are self-conjugate fields, can only carry an anapole moment. In this thesis we will consider the anapole moment of a spin 1/2 Majorana fermion and its application to the scenario in which it dominates the interaction between the DM particle and nuclei in direct detection experiments.

One candidate for WIMPs is found in the framework of *supersymmetry* (SUSY). This additional symmetry of nature proposes that all particles have a corresponding supersymmetric partner called sparticle. These new fields differ from their counterparts by their spin quantum number. Applying this framework to our currently best model - the Standard Model (SM) of particle physics - leads to the *minimal supersymmetric standard model* (MSSM). Consequently, all matter particles, like quarks and leptons, have corresponding force-carrier particles called squarks and sleptons respectively. Similarly the gauge bosons of the strong-, weak- and electromagnetic interaction have matter fields called gauginos as partners. Apart from addressing many still-standing issues of the SM, this framework can be studied on its own and has interesting theoretical features and consequences for quantum field theories in general.

The thesis is structured as follows, chapter 2 introduces dark matter and some of the evidence hinting at it followed by a discussion of the *freeze-out* production mechanism of a *weakly interacting massive particle* (WIMP).

Supersymmetry as a framework of physics beyond the Standard Model of particle physics is introduced in chapter 3. Basics of the construction of supersymmetric theories and the simplest supersymmetric extension of the Standard Model in the form of the minimal supersymmetric standard model (MSSM) is given subsequently.

Then, the definition and calculation of the anapole moment of a generic Majorana fermion is covered in chapter 4. For this, the possible contributions from both scalar and vector interactions are covered, of which the latter is a novel consideration. Furthermore, the historic issues surrounding the calculation of the SM neutrino charge radius is presented and the solution in the form of Pinch-Technique and Background Field Method are discussed.

In chapter 5 the basics of direct detection experiments are discussed and the possibility of the detection of a Majorana WIMP via the anapole moment is illuminated.

Chapter 6 contains the numerical analysis of the anapole moment in both, a model-independent manner and in the context of the MSSM. For the latter, the lightest neutralino as WIMP DM candidate is considered. Under the assumption that it is the only WIMP responsible for the present dark matter energy density, some of the underlying parameter spaces of the supergravity- and anomaly mediated MSSM is considered and the anapole moment is evaluated in this regions.

Finally, the key results are summarized in chapter 7 and an outlook is given.

Chapter 2

Basics of Dark Matter

In this chapter the concept of dark matter (DM) is introduced and some of the observational evidence and basic production mechanisms are presented. We will also summarize the basics of today's understanding of cosmology in the form of the Λ CDM model.

2.1 Standard Cosmology

Based on the observation by Hubble, that the velocity of which galaxies drift apart from each other is proportional to their distance, the Big Bang scenario was developed. The basic idea is, that if the distance between galaxies grows with time, they were closer together in the past. Thus, a common origin in both space and time was proposed. The present value of this rate is given by the Hubble constant

$$H_0 = 100 \cdot h \text{ km s}^{-1} \text{Mpc}^{-1}, \quad (2.1)$$

where $h \approx 0.67$ is introduced as a dimensionless quantity [1, 3] and allows the study of H_0 irrespective of the issues surrounding its measurement. For this reason many quantities in this framework depend on h .

More general, the time dependent expansion of the Universe is described by the Hubble rate

$$H(t) \equiv \frac{da/dt}{a}, \quad (2.2)$$

where a is the scale factor (with the value today set to $a_0 \equiv 1$) describing the change of length due to the Universe's expansion and accompanies the spacial components of the line element

$$ds^2 = dt^2 - a^2 \left(\frac{dr^2}{1 - kr^2} + r^2 d\Omega^2 \right), \quad (2.3)$$

for which homogeneity and isotropy is assumed. Further, this line element defines the Friedmann-Robertson-Walker (FRW) metric $g_{\mu\nu}$. The factor $k \in \{-1, 0, +1\}$ describes the curvature of an open, flat and closed Universe respectively.

A common choice to describe the content of the Universe is to model it as a perfect fluid with energy momentum tensor

$$T^\mu{}_\nu = \begin{pmatrix} \rho & \\ & -p \mathbb{1}_{3 \times 3} \end{pmatrix}, \quad (2.4)$$

where ρ is the energy density and p is the pressure. Its dynamics are described by the Einstein equation

$$R_{\mu\nu} - \frac{1}{2}Rg_{\mu\nu} - \Lambda g_{\mu\nu} = 8\pi GT_{\mu\nu}, \quad (2.5)$$

where $R_{\mu\nu}$ and R are the Ricci-tensor and Ricci-scalar respectively, while Λ is the cosmological constant. For a pressureless fluid, one can solve the time- and space-like components and obtain the Friedmann equations

$$H^2 = \frac{8\pi G}{3}\rho + \frac{\Lambda}{3} - \frac{k}{a^2} \quad (2.6a)$$

$$\frac{\ddot{a}}{a} + \frac{1}{2}\frac{\dot{a}^2}{a^2} = -4\pi Gp + \frac{\Lambda}{2} - \frac{1}{2}\frac{k}{a^2} \quad (2.6b)$$

It is useful to rewrite eq. (2.6a) as

$$\mathcal{H}^2 \left[\Omega_m + \Omega_r + \Omega_\Lambda - 1 \right] = k, \quad (2.7)$$

where $\mathcal{H} \equiv \text{dln}(a)/\text{dt} = Ha$ is the conformal expansion rate, $\Omega_m \equiv \rho_m/\rho_c$, $\Omega_r \equiv \rho_r/\rho_c$ and $\Omega_\Lambda \equiv \frac{\Lambda}{8\pi G}/\rho_c$ are the dimensionless energy density of non-relativistic matter, radiation and vacuum energy respectively, and $\rho_c \equiv \frac{3H^2}{8\pi G}$ is the critical density. Observations tell us, that the curvature is flat, e.g. $k \approx 0$ [1], such that eq. (2.7) reduces to

$$\Omega_m + \Omega_r + \Omega_\Lambda = 1. \quad (2.8)$$

In general, the thermodynamic equation of state (no summation implied),

$$p_j = w_j \rho_j, \quad \text{with } w_j = \begin{cases} 0 & \text{non-rel. matter} \\ 1/3 & \text{rel. matter} \\ -1 & \text{vacuum energy} \end{cases} \quad (2.9)$$

describes the relationship between pressure and density of any type of matter (and vacuum energy here). One consequence is, that the energy density of the respective type of energy has a different time-dependency. Explicitly [4],

$$\rho_j(a) \sim \begin{cases} a^{-3} & \text{non-rel. matter} \\ a^{-4} & \text{rel. matter} \\ \text{const.} & \text{vacuum energy} \end{cases} \quad (2.10)$$

implying that in the very early stages of the Universe, the dominating type of energy was relativistic matter (radiation). With ongoing expansion, this contribution decreased and the non-relativistic matter started dominating eventually. The intermediate epoch, at which the radiation and matter energy densities were equal, is called *matter-radiation equality* and plays an important role for the large scale structures and the cosmic microwave background. Today, the dominating source of energy density is the vacuum energy, contributing around 70% to the total energy content of the Universe.

The Λ CDM model is then realized by the spatially flat $k = 0$ FRW metric of eq. (2.3). The matter contribution Ω_m is further separated into baryonic (visible) matter Ω_b and cold dark matter (CDM) Ω_χ . The latter - the *DM relic density* - serves as key quantity for testing new models describing DM candidates and depends heavily on the exact framework of the physics beyond the SM. Some ideas are summarized in section 2.3.

2.2 Observational Evidence

Some examples of evidence hinting at DM ranging from scales of galaxies and galaxy clusters to cosmological scales are summarized here [2].

2.2.1 Galaxies and Galaxy Cluster

The apparent deviation of the rotation curves of galaxies from the Newtonian prediction is hinting strongly towards a new form of matter. The discrepancy is due to the fact, that the observed velocity of the outer parts of galaxies is approximately constant, while from Newtonian physics one would expect a relation

$$v(r) = \sqrt{\frac{GM(r)}{r}}, \quad (2.11)$$

with $M(r) = 4\pi \int dr r^2 \rho(r)$ leading to a dependency beyond the optical disk of

$$v \sim 1/\sqrt{r}, \quad (2.12)$$

where v is the circular velocity of the galaxy with radius r . The measurement, that the velocity of objects in the outer regions is nearly constant with respect to r , can only be explained if there is additional - non-visible - matter with a density distribution $\rho_{\text{new}} \sim 1/r^2$. This new presence of non-visible, or *dark matter* (DM), is then dominantly responsible for the comparably high- and constant velocities in the outer region of galaxies. This characteristic is best studied by the observation of Low Surface Brightness (LSB) galaxies, whose mass distribution is dominated by the presence of DM. How this distribution, also known as DM halo, is shaped in the

inner regions, is still subject of research: it could present a cored or cuspy profile. For the outer regions on the other hand, the rotation curves of disk galaxies strongly suggest a spherical halo shape.

Another form of observational evidence of DM can be found via the effect of weak gravitational lensing around elliptical galaxies. The strong gravitational potential generated by the mass aggregated in the galaxy bends the spacetime around the center. Since light from behind the galaxy (from our point of view) follows the geodesic "around" the galaxy, a unique shape is generated. Then, the mass generating this effect can be deduced and compared to the mass from visible matter.

On the scale of galaxy clusters the first hints of DM were observed in 1933 by F. Zwicky [5, 6] who found using velocity dispersion measurements that the mass-to-light ratio in the Coma cluster is two orders of magnitudes higher than that in the solar neighborhood. There are several ways of determining the mass of a cluster. Common methods include gravitational lensing, the profile of X-ray emissions and relating the observed kinetic energy with the potential using the Virial theorem. Then, one can compare this data with estimates of the mass of visible matter only.

2.2.2 Cosmic Microwave Background

The evidence based on galaxies and galaxy clusters allows us to study the DM distribution on comparably small scales. In order to quantify its contribution to the total energy density of the Universe, larger scales have to be probed. In fact, valuable information can be extracted from the omnipresent *Cosmic Microwave Background* (CMB).

At early times when the temperature was high enough, neutrinos, photons and electrons were in thermal equilibrium via the processes

$$\bar{\nu}_e e^- \rightarrow W^* \rightarrow \bar{\nu}_e e^- \quad \text{and} \quad e^- \gamma \rightarrow e^* \rightarrow e^- \gamma. \quad (2.13)$$

The interaction rate is given by

$$\Gamma := \sigma v n, \quad (2.14)$$

where σ is the cross section, v the relative velocity and n the number density. Since the Universe expands, the number density persistently dropped until the processes of eq. (2.13) could no longer occur. The equilibrium stopped once the Hubble rate, eq. (2.2), became larger than the interaction rate. The epoch, where they were equal,

$$\Gamma(T_{\text{dec.}}) = H(T_{\text{dec.}}), \quad (2.15)$$

defines the decoupling temperature $T_{\text{dec.}} \approx 0.26 \text{ eV} \approx 3000\text{K}$ at which the photons decoupled from matter [4]. In fact, these photons are still present but with reduced

temperature $T_0 \approx 2.7\text{K} \approx 60\text{GHz}$ due to the expansion of the Universe. As apparent, this temperature lays in the microwave band, thus giving rise to the name *Cosmic Microwave Background* (CMB). First signs of this signature were observed in 1941 by McKellar [7], but it took until 1964 where Penzias and Wilson accidentally discovered a background noise in the microwave band [8], now identified with the CMB. This discovery was a major milestone for the Big Bang hypothesis and delivered observational evidence contradicting the competing steady state theory.

Instruments to study the CMB include the Wilkinson Microwave Anisotropy Probe (WMAP) mission [9] on the observational side, which surveyed the background over the full sky. After accounting for relative corrections due to earth's movement, it was found that the CMB is remarkably smooth, with deviations being of order $\delta T/T \lesssim 10^{-5}$. However, the whole sky - as a surface - should not be causally connected, so there needs to be an explanation of why the temperature is so uniformly similar. One theory is that the Universe underwent an epoch of very rapid expansion such that these regions were causally connected. As it turns out, this inflationary period would be driven by a cosmological constant and not by any type of matter.

In conclusion, the CMB permits the study of all cosmological model parameters, since it has all physical information present at the decoupling epoch encoded. These will be imprinted into temperature fluctuations around T_0 and inhabit statistical information about physical quantities. Leading physical effects on the CMB are

- At the time of photon decoupling there are *acoustic oscillations* in the photon-baryon composite due to the presence of gravitational wells caused by DM. While the composite is pulled down the potential, and if its temperature cannot adjust fast enough, a pressure is generated acting against the potential. This induces a temperature fluctuation.
- The *Sachs-Wolfe effect* describes the effect of general relativity on the CMB photons, namely the effect caused by a strong gravitational potential changing over the time a photon is traveling through it. Before and during the decoupling epoch, this effect is hardly separable from the acoustic oscillations. After decoupling however, when the photons are streaming through the Universe, this effect can have sizeable effects and has to be integrated over the line of sight.

From the analysis of the CMB one can infer the values of

$$\Omega_{\text{total}}(t_0), \quad \Omega_{\Lambda}, \quad \Omega_{\text{m}}(t_0)h^2, \quad \Omega_{\text{b}}(t_0)h^2, \quad (2.16)$$

where each has a separate effect on the shape of the CMB power spectrum (see [4, Chapter 1.4]).

2.2.3 Large Scale Structures

Hints at dark matter can also be found in the visible matter distribution in the Universe. In particular how the large scale structures like (super-) galaxy clusters and voids are distributed. Their history is governed by the time evolution of primordial seeds in the energy distribution in the very early epoch of the Universe. Since DM is the dominating matter form, the gravitational dynamics are mainly governed by it, driving the aggregation and formation [10].

The basic idea here is, that one studies the deviations of the matter density field with respect to its mean. That is, one separates the local density $\rho(\mathbf{x}, t)$ into

$$\rho(\mathbf{x}, t) = \bar{\rho}(\tau)(1 + \delta(\mathbf{x}, \tau)), \quad (2.17)$$

where $\bar{\rho}$ is the spatial average and $\delta(\mathbf{x}, \tau)$ is the *density contrast*. The *peculiar velocity* is given by the velocity deviating from the Hubble flow, e.g.

$$u_i(\mathbf{x}, \tau) \equiv v_i(\mathbf{x}, \tau) - \mathcal{H}x_i. \quad (2.18)$$

where v_i is the ordinary velocity. In both eq. (2.17) and eq. (2.18), $x_i \equiv ar_i$ and $\tau \equiv \int_{t_0=0}^t \frac{dt'}{a(t')}$ are the *comoving distance* and *comoving time* respectively. The conservation of the number density in phase space $f(\mathbf{x}, \mathbf{p}, \tau)$ implies that its total derivative vanishes:

$$\frac{df}{d\tau} = \frac{\partial f}{\partial \tau} + \frac{\partial \mathbf{x}}{\partial \tau} \cdot \nabla f + \frac{\partial \mathbf{p}}{\partial \tau} \cdot \nabla_{\mathbf{p}} f \quad (2.19a)$$

$$= \frac{\partial f}{\partial \tau} + \frac{\mathbf{p}}{am} \cdot \nabla f - am \nabla \Phi \cdot \nabla_{\mathbf{p}} f = 0. \quad (2.19b)$$

This equation is called *Vlasov-equation* where Φ is the cosmological potential describing the gravitational source due to the fluctuations only. Taking momentum moments of the Vlasov-equation, one obtains in lowest order the equations

$$\frac{\partial \delta(\mathbf{x}, \tau)}{\partial \tau} = -\nabla \cdot [(1 + \delta(\mathbf{x}, \tau))\mathbf{u}(\mathbf{x}, \tau)] \quad (2.20a)$$

$$\frac{\partial u_j}{\partial \tau} + \mathcal{H}u_j + u_i \nabla_i u_j = -(\nabla \Phi)_j - \frac{1}{\rho} \nabla_i (\rho \sigma_{ij}) \quad (2.20b)$$

corresponding to the continuity- and Euler equation respectively. The term σ_{ij} is the stress-tensor and can be taken to be diagonal and proportional to the pressure of the fluid. Since in this context, the structure formation is mainly governed by cold DM modeled as a pressureless fluid, the tensor σ_{ij} vanishes at first order. However this approximation is not valid on all scales [10].

With these equations one can study the formation of large scale structures and test the resulting statistical predictions in the form of the matter power spectrum $P(k)$ defined by

$$\langle \delta(\mathbf{k})\delta(\mathbf{k}') \rangle = (2\pi)^3 \delta^{(3)}(\mathbf{k} + \mathbf{k}') P(k). \quad (2.21)$$

Here, $\delta(\mathbf{k})$ is the density contrast in momentum space and $\langle \cdot \rangle$ is the correlation function. This powerspectrum can be compared with both observations and N -body simulations. The key point is, that the smoothness of the CMB, and thus the homogeneous distribution of the photon-baryon composite in the early epoch, cannot serve as a source for the observed structures alone. Instead, one needs additional matter in order for the observed structures to have formed in the given time of the Universe. This additional matter is identified with the DM, whose effect on the structure formation dominates over the contribution from visible matter.

2.3 Production Mechanisms and WIMPs

Several mechanism have been developed to explain the present energy density of DM, its *relic abundance*. The most popular ideas are [11]:

1. **Freeze-out mechanism:** Similar to the decoupling of photons, starting in thermal equilibrium, when the interaction rate between the DM and SM drops below the Hubble rate, its comoving number density becomes constant and freezes out due to lack of interaction processes occurring.
2. **Freeze-in mechanism:** Here, the DM was never in equilibrium with the SM (for example achieved with a small coupling $y \sim \mathcal{O}(10^{-7})$). Once the visible sector producing the DM becomes Boltzmann suppressed, the comoving number density of the DM freezes-in.
3. **Dark Freeze-out mechanism:** Similar to the freeze-in mechanism, DM was never in equilibrium with the visible sector. However, it was in equilibrium with its own dark sector populated by a freeze-in type yield from the visible sector. The DM particle annihilates into particles of the dark sector only until the Hubble rate dominates over this interaction rate.
4. **Reannihilation mechanism:** Here, the dark sector is thermalized and dark freeze-out happened prior to the ending of the yield from the visible sector. Thus, the relic abundance is increased by these processes until the yield stops, after which the abundance freezes out.

In this work we will focus on *weakly interacting massive particles* (WIMPs), whose relic abundance is produced via the freeze-out mechanism. An advantage of the model is, that a WIMP naturally obtains the correct relic abundance in the early epoch of the Universe via the same interactions, with which it is detectable [12]. The WIMP relic density is coined by the physics in the era preceding Big Bang Nucleosynthesis (BBN). Currently, BBN is the earliest time we can probe, where the elements D, ^3He , ^4He and ^7Li were synthesized within approximately the first

three minutes. Thus, in order to calculate the WIMP relic density, one has to make assumptions about the pre-BBN Universe.

The standard computation of freeze-out assumes conserved entropy of both matter and radiation, thermal production of the WIMPs, that their decoupling occurred while the Universe was dominated by radiation and that they were in chemical- and thermal equilibrium before decoupling. Then, production and annihilations of WIMP pairs took place via SM particles:

$$\chi\bar{\chi} \leftrightarrow e^+e^-, \mu^+\mu^-, q\bar{q}, W^+W^-, ZZ, HH, \dots \quad (2.22)$$

Processes from right to left occurred as long as the SM particles in the plasma had enough energy to produce the DM candidate, e.g. $T \gg m_\chi$. The WIMP annihilation was in equilibrium with the production processes with common rate

$$\Gamma_{\text{ann}} = \langle \sigma_{\text{ann}} v \rangle n_{\text{eq}}, \quad (2.23)$$

where σ_{ann} is the WIMP cross section, v the relative velocity and n_{eq} the number density at chemical equilibrium. The angles $\langle \cdot \rangle$ is the average over the thermal distribution. As the Universe expanded, the number density of the interacting particles decreased, causing the annihilation- and production rates to decline accordingly. Then, when the annihilation rate Γ_{ann} became smaller than the Hubble rate,

$$\Gamma_{\text{ann}} < H, \quad (2.24)$$

chemical decoupling occurred and the number of comoving WIMPs attained a (approximately) constant value, viz. the number density decreased as $\sim 1/r^3$ with the expansion of the Universe. This is the *freeze-out mechanism*.

In many cases, the WIMP is assumed to be a Majorana fermion such that it coincides with its own antiparticle: $\chi = \bar{\chi}$. In particular this is the case for the models studied in this work.

The present WIMP density can be calculated via [12]

$$\frac{dn}{dt} = -3Hn - \langle \sigma_{\text{ann}} v \rangle (n^2 - n_{\text{eq}}^2), \quad (2.25a)$$

$$\frac{ds}{dt} = -3Hs. \quad (2.25b)$$

In eq. (2.25) time is denoted by t , the entropy densities by s and n (n_{eq}) stands for the number density (at equilibrium). The term $\sim H$ is responsible for the dilution due to the expansion, while the term $\sim \langle \sigma_{\text{ann}} v \rangle$ accounts for annihilations and inverse annihilations of the WIMP. Combining these two equations by introducing the new parameters $Y = n/s$ and $x = m/T$, where T denotes the temperature of the photon bath, one obtains

$$\frac{dY}{dx} = \frac{1}{3H} \frac{ds}{dx} \langle \sigma_{\text{ann}} v \rangle (Y^2 - Y_{\text{eq}}^2). \quad (2.26)$$

The energy- and entropy density can be related to the photon temperature via

$$\rho = \frac{\pi^2}{30} g_{\text{eff}}(T) T^4, \quad s = \frac{2\pi^2}{45} h_{\text{eff}}(T) T^3, \quad (2.27)$$

where g_{eff} (h_{eff}) stands for the effective degree of freedom of the energy (entropy) density. With

$$g_*^{1/2} = \frac{h_{\text{eff}}}{g_{\text{eff}}^{1/2}} \left(1 + \frac{1}{3} \frac{T}{h_{\text{eff}}} \frac{dh_{\text{eff}}}{dT} \right), \quad (2.28)$$

one can rewrite eq. (2.26) as

$$\frac{dY}{dx} = - \left(\frac{45}{\pi M_{\text{Pl}}^2} \right)^{-1/2} \frac{g_*^{1/2} m}{x^2} \langle \sigma_{\text{ann}} v \rangle (Y^2 - Y_{\text{eq}}^2). \quad (2.29)$$

where $M_{\text{Pl}} = 1/\sqrt{G} \approx 1.2 \times 10^{19}$ GeV is the Planck mass. This equation is most easily solved numerically with initial conditions $Y = Y_{\text{eq}}$ at $x \approx 1$ resulting in today's Y_0 . Then, one can calculate the WIMP relic density as

$$\Omega_\chi h^2 = \frac{\rho_\chi^0 h^2}{\rho_c^0} = \frac{m_\chi s_0 Y_0 h^2}{\rho_c^0}. \quad (2.30)$$

The zero as sub- or superscript denotes the present value of the respective quantity. One important feature of this framework is, that decreasing $\langle \sigma_{\text{ann}} v \rangle$ in eq. (2.26) leads to an increased WIMP number density and thus to an augmented relic abundance. Since the quantity $\langle \sigma_{\text{ann}} v \rangle$ depends on the interaction strength, it is expected that a weaker coupling leads to a higher relic density.

Irrespective of the production mechanism responsible for the relic density, the theoretical prediction has to be compared with observational data. For example the combined limit from the WMAP+eCMB+BAO+ H_0 data set gives a cold DM relic density [9, Table 17] of

$$\Omega_\chi h^2 \stackrel{\text{obs.}}{=} 0.1153 \pm 0.0019, \quad (2.31)$$

restricting possible DM models.

Chapter 3

Supersymmetry in a Nutshell

In this chapter the basics of supersymmetry as extension of the Standard Model of particle physics are introduced.

3.1 Symmetries in Particle Physics

The importance of symmetries can be found in probably every field in physics. Particularly in particle physics, symmetries can allow or forbid particles and interactions of a model. The mathematical description is formulated in terms of the action

$$S = \int d^4x \mathcal{L}, \quad (3.1)$$

where $\mathcal{L} = \mathcal{L}(\phi, A_\mu)$ is the Lagrangian being a function of the fields and interactions of the model. According to Noether's theorem, whenever the action remains unchanged under a transformation

$$S \rightarrow S' = S + \delta S = S, \quad (3.2)$$

there exists a corresponding conserved quantity. It is said, that the system possess the symmetry corresponding to the transformation. In classical physics, if a system is invariant under translations, the momentum is conserved etc. However this concept is more general and can be applied to any symmetry. The Lagrangian \mathcal{L} can be considered to be the building block of a theory¹ and encapsulates arguably all physical information about a system. From it, equation of motions, scattering amplitudes, decay widths and cross sections can be computed.

Since the laws of nature do not change with respect to Lorentz transformations, it is reasonable to demand that also \mathcal{L} should be invariant with respect to them. One example is the free scalar theory,

$$\mathcal{L}_{\text{free}} = \frac{1}{2} \partial_\mu \phi \partial^\mu \phi - \frac{1}{2} m^2 \phi^2, \quad (3.3)$$

¹Up to redefinitions and integration-by-part identities

in which the fields ϕ transform trivially under the Lorentz group and describe a spin-0 particle. Since ϕ transforms trivially, the Lagrangian is Lorentz invariant.

The free theory of a complex scalar,

$$\mathcal{L}_{\text{free}} = \partial_\mu \phi \partial^\mu \phi^* - m^2 \phi \phi^*, \quad (3.4)$$

is not only Lorentz invariant, but additionally invariant under the global $U(1)$ transformation

$$\phi \rightarrow e^{-i\alpha} \phi, \quad \alpha \in \mathbb{R}. \quad (3.5)$$

The corresponding Noether current,

$$J_\mu = \frac{\partial \mathcal{L}_{\text{free}}}{\partial(\partial_\mu \phi)} \frac{\delta \phi}{\delta \alpha} + \frac{\partial \mathcal{L}_{\text{free}}}{\partial(\partial_\mu \phi^*)} \frac{\delta \phi^*}{\delta \alpha} = -i(\phi \partial_\mu \phi^* - \phi^* \partial_\mu \phi) \quad (3.6)$$

and charge

$$Q = \int d^3x J_0 \quad (3.7)$$

are immediate consequence of Noether's theorem [13, Chapter 3.3]. If we allow the parameter in eq. (3.5) to be spacetime dependent, $\alpha = \alpha(x)$, the derivatives in eq. (3.4) have to be replaced by covariant derivatives for the Lagrangian to remain invariant:

$$\partial_\mu \rightarrow D_\mu \equiv \partial_\mu + ieA_\mu. \quad (3.8)$$

The gauge field A_μ can be identified with the photon field. The $U(1)$ symmetry with a spacetime dependent parametrization $\alpha(x)$ is now considered to be *local* (or *gauged*) and the Lagrangian reads

$$\mathcal{L} = D_\mu \phi D^\mu \phi^* - m^2 \phi \phi^*. \quad (3.9)$$

Note, that the covariant derivative introduces interactions between the charged scalar and the photon. Often, this gauge redundancy (or invariance) is referred to as *gauge symmetry*. Adding the kinetic term of a photon, a spin-1 vector field, leads to the model of scalar quantum electrodynamics (QED), in which a charged spin-zero particle interacts with photons:

$$\mathcal{L}_{\text{scalar QED}} = -\frac{1}{4} F_{\mu\nu} F^{\mu\nu} + D_\mu \phi (D^\mu \phi)^* - m^2 \phi \phi^*. \quad (3.10)$$

Here $F_{\mu\nu} = i/e [D_\mu, D_\nu]$ is the field strength tensor.

Similarly, the SM is a gauge theory whose group structure is determined by $SU(3)_c \times SU(2)_L \times U(1)_Y$, corresponding to the color, left and hypercharge symmetries respectively. The SM consists of gauge fields, three generations of fermions and an uncharged Higgs scalar. After the latter obtains a vacuum expectation value (vev), the SM gauge group is broken down to $SU(3)_c \times U(1)_{em}$ whereby the fermions and electroweak gauge bosons acquire masses.

3.2 Why Supersymmetry?

Although the Standard Model (SM) of high-energy physics allows us to study particles and their interactions in the Universe remarkably precisely, some phenomena are unexplained such that more physics remains to be discovered. Some examples showing our lack of understanding include [14, Chapter 1.4]

- We do not have a non-classical model of gravity describing phenomena at the quantum level. Our current best model, Einstein theory, is non renormalizable at very small length scales (equivalently at high energies $M_{\text{pl}} = 1/\sqrt{G} \approx 1.2 \times 10^{19}$ GeV).
- The hierarchy problem: Why are the electroweak- and Planck scale so different with $M_{\text{EW}}/M_{\text{pl}} \approx 10^{-15}$? Related is the necessity of fine tuning order by order in perturbation theory due to the sensitivity of the SM Higgs potential to UV physics.
- Strong CP problem: Ad hoc, no symmetry forbids a term $\theta F^{\mu\nu} \tilde{F}_{\mu\nu}$ in the QCD part of the SM Lagrangian, where $F_{\mu\nu}$ is the QCD field strength tensor and $\tilde{F}_{\mu\nu}$ its dual. Experimentally, this parameter is unnaturally small with $\theta < 10^{-8}$.
- Is there a reason for the internal structure of the SM (gauge group $SU(3)_c \times SU(2)_L \times U(1)_Y$, three generations of fermions, $3 + 1$ spacetime dimensions, origin of all SM parameters, ...)?
- What dark energy and dark matter is.

Since these (and other) problems cannot be solved or explained within the SM, extensions have to be made. Some of these add new particles and/or interactions to the Lagrangian, while others extend the symmetries. In the latter case, one can either modify internal symmetries, like embedding the SM gauge group $SU(3)_c \times SU(2)_L \times U(1)_Y$ into a more general grand unified theory (GUT), or modify spacetime symmetries themselves. In this regard, commonly studied ideas include adding extra dimensions or imposing a new symmetry relating matter and interaction fields: supersymmetry (SUSY).

SUSY solves some of the mentioned problems. In particular it unifies the gauge couplings of the SM, offers a DM candidate - usually the lightest neutralino - and resolves the hierarchy issue and the related sensitivity of the SM Higgs potential to a high energy scale. Its mass - in the SM - obtains quadratic divergent corrections from higher order loop diagrams proportional to the cut-off scale. For a cut-off at the Planck scale, these diagrams lead to corrections which are 30 orders of magnitudes larger than the Higgs mass itself [15]. In a supersymmetric extension however,

every SM loop diagram with fermions is matched with a similar diagram with the superpartner of the fermion running in the loop. In unbroken SUSY, these two terms cancel each other and protect the SM Higgs boson from quantum corrections.

While there are many of these useful consequences of SUSY, the idea itself seemed to be an academical curiosity first, and only later turned out to be useful for solving problem in the SM [16]. Apart from the SM, it also offers insights into different aspects of general quantum theories and general relativity.

3.3 Supersymmetric Lagrangians

3.3.1 The Supersymmetry Algebra

SUSY can be seen as naturally emerging from analyzing the scattering matrix S (S matrix) in a general way using group theoretical arguments. In this elegant and concise approach the so called no-go theorem, also known as Coleman-Mandula theorem, plays a central role [17, Chapter 1.2]. This theorem states that the only symmetries of the S matrix can be the direct product of the Poincaré group (e.g. Lorentz group + translations) with internal symmetries. Further symmetries would overconstrain the S matrix and would make it non-physical. For example in $2 \rightarrow 2$ scattering, the S matrix is only a function of the scattering angle, if only Poincaré is taken into account. A further symmetry would constrain this angle to a certain value which renders the S matrix non-analytical. However, extending the Lie algebra to a so called graded-Lie algebra allows for an additional symmetry between bosons and fermions, which does not violate the no-go theorem. As it turns out [18], this is indeed the only possibility to extend the Poincaré algebra in such a way that the Coleman-Mandula theorem is not violated. So not only does it circumvent the original theorem, but it also is the only way to do it. This means that the SM gauge group can be extended with an additional, non-internal symmetry. Except noted differently, only $D = 4$ and $\mathcal{N} = 1$ (one set of SUSY generators) SUSY is discussed here.

The SUSY algebra is a graded-Lie algebra, meaning that anticommutation relations and spinorial/Grassmannian generators Q_α and $Q_{\dot{\alpha}}^\dagger$ replace the usual commutation relations between bosonic-like generators for the extended part. Additionally to the Poincaré algebra, the SUSY algebra reads

$$\{Q_\alpha, Q_\beta\} = \{Q_{\dot{\alpha}}^\dagger, Q_{\dot{\beta}}^\dagger\} = 0, \quad (3.11a)$$

$$\{Q_\alpha, Q_{\dot{\alpha}}^\dagger\} = 2\sigma_{\alpha\dot{\alpha}}^\mu P_\mu, \quad (3.11b)$$

where the latter equation encapsulates the non-trivial extension of the Poincaré algebra (for the convention see section 3.3.2).

3.3.2 Chiral Supermultiplets: The Wess-Zumino Model

The arguably easiest example of a supersymmetric theory is the Wess-Zumino model [19]. Following [15, Chapter 3.2], Dirac spinors ψ_D are represented by left- and right-handed anti-commuting Weyl spinors ξ and χ^\dagger respectively:

$$\psi_D = \begin{pmatrix} \xi_\alpha \\ \chi^{\dagger\dot{\alpha}} \end{pmatrix}, \quad \bar{\psi}_D = \left(\chi^\alpha \quad \xi_{\dot{\alpha}}^\dagger \right) = \psi_D^\dagger \begin{pmatrix} & 1 \\ 1 & \end{pmatrix}, \quad (3.12)$$

with spinor space indices $\alpha, \dot{\alpha} = 1, 2$ for the left and right handed spinors respectively. These are raised and lowered with the ϵ -symbol, defined via

$$\epsilon^{12} = -\epsilon^{21} = \epsilon_{21} = -\epsilon_{12} = 1, \quad \epsilon^{11} = \epsilon^{22} = \epsilon_{11} = \epsilon_{22} = 0. \quad (3.13)$$

Such that for example $\xi_\alpha = \epsilon_{\alpha\beta}\xi^\beta$ and $\chi_{\dot{\alpha}}^\dagger = \epsilon_{\dot{\alpha}\dot{\beta}}\chi^{\dagger\dot{\beta}}$. The convention for contracting indices between different spinors is such that

$$\xi\chi \equiv \xi^\alpha\chi_\alpha \equiv \xi^\alpha\epsilon_{\alpha\beta}\chi^\beta = \dots = \chi\xi. \quad (3.14)$$

Note the position of the undotted indices, ${}^\alpha_\alpha$, while dotted indices are always contracted from bottom left to top right, ${}_{\dot{\alpha}}^{\dot{\alpha}}$. The Pauli matrices take the form

$$\sigma^0 = \bar{\sigma}^0 = \begin{pmatrix} 1 & \\ & 1 \end{pmatrix}, \quad \sigma^1 = -\bar{\sigma}^1 = \begin{pmatrix} & 1 \\ 1 & \end{pmatrix}, \quad (3.15a)$$

$$\sigma^2 = -\bar{\sigma}^2 = \begin{pmatrix} & -i \\ i & \end{pmatrix}, \quad \sigma^3 = -\bar{\sigma}^3 = \begin{pmatrix} 1 & \\ & -1 \end{pmatrix}. \quad (3.15b)$$

The basic ingredients needed to construct the Wess-Zumino model are:

1. The Lagrangian of a free, massless charged scalar
2. The Lagrangian of a free, massless left-handed fermion
3. Imposing SUSY-transformation: The scalar and fermion should transform into each other
4. The action should remain invariant under this transformation
5. SUSY algebra has to be close; in other words, we want to find a representation of the superalgebra
6. Find allowed interaction terms

The first two points are well known, the respective Lagrangians read

$$\mathcal{L}_{\text{scalar}} = \partial^\mu \phi^* \partial_\mu \phi \quad \text{and} \quad \mathcal{L}_{\text{fermion}} = i\psi^\dagger \bar{\sigma}^\mu \partial_\mu \psi \quad (3.16)$$

and together form the 3 + 1-dimensional action

$$S = \int d^4x (\mathcal{L}_{\text{scalar}} + \mathcal{L}_{\text{fermion}}). \quad (3.17)$$

The scalar and fermion are related to each other via their transformation behavior under SUSY. In fact, the boson ϕ (and ϕ^*) is imposed to transform into the fermion:

$$\delta\phi \sim \psi_\alpha \Rightarrow \delta\phi = \epsilon\psi \quad (\delta\phi^* = \epsilon^\dagger \psi^\dagger). \quad (3.18)$$

The equality after " \Rightarrow " is due to the spinor structure of ψ_α on the left hand side and holds up to an arbitrary factor. Note, that ϵ is an infinitesimal anti-commuting spinorial parameter of mass dimension $-1/2$. With that, the total scalar Lagrangian transforms as

$$\delta\mathcal{L}_{\text{scalar}} = \epsilon\partial^\mu \psi \partial_\mu \phi^* + \epsilon^\dagger \partial^\mu \psi^\dagger \partial_\mu \phi. \quad (3.19)$$

Since the action has to remain invariant, the corresponding transformed fermion Lagrangian has to cancel this contribution (up to a boundary term):

$$\delta\mathcal{L}_{\text{scalar}} + \delta\mathcal{L}_{\text{fermion}} \stackrel{!}{=} \partial_\mu(\dots), \quad (3.20)$$

Keeping in mind the mass dimensions as well as the respective Lorentz- and spinorial structure, the variation of the fermion is fixed to be of the form:

$$\delta\psi_\alpha \sim (\sigma^\mu \epsilon^\dagger)_\alpha \partial_\mu \phi, \quad \delta\psi^\dagger_{\dot{\alpha}} \sim (\epsilon \sigma^\mu)_{\dot{\alpha}} \partial_\mu \phi^*. \quad (3.21)$$

By plugging this transformation behavior into eq. (3.20) and applying the identities

$$i) [\bar{\sigma}^\mu \sigma^\nu + \bar{\sigma}^\nu \sigma^\mu]_{\dot{\beta}}^{\dot{\alpha}} = 2\eta^{\mu\nu} \delta_{\dot{\alpha}}^{\dot{\beta}}, \quad ii) [\sigma^\mu \bar{\sigma}^\nu + \sigma^\nu \bar{\sigma}^\mu]_{\alpha}^{\beta} = 2\eta^{\mu\nu} \delta_{\alpha}^{\beta}, \quad (3.22)$$

one finds the proportionality constants $-i$ and i respectively and obtains:

$$\delta\psi_\alpha = -i(\sigma^\mu \epsilon^\dagger)_\alpha \partial_\mu \phi, \quad \delta\psi^\dagger_{\dot{\alpha}} = i(\epsilon \sigma^\mu)_{\dot{\alpha}} \partial_\mu \phi^*. \quad (3.23)$$

Now, the only thing which has to be checked is if the SUSY algebra is closed, e.g. if the commutator of two SUSY transformations is another symmetry of the theory. Let ϵ_1 and ϵ_2 be the parameters characterizing the SUSY transformation of ϕ and ψ . Then one obtains

$$\delta_{\epsilon_1} \delta_{\epsilon_2} \phi = \delta_{\epsilon_2}(\epsilon_1) = \epsilon_1(-i)\sigma^\mu \epsilon_2^\dagger \partial_\mu \phi \quad (3.24)$$

and thus

$$(\delta_{\epsilon_1} \delta_{\epsilon_2} - \delta_{\epsilon_2} \delta_{\epsilon_1})\phi = i(-\epsilon_1 \sigma^\mu \epsilon_2^\dagger + \epsilon_2 \sigma^\mu \epsilon_1^\dagger) \partial_\mu \phi. \quad (3.25)$$

As apparent, the RHS is proportional to the generator of spacetime translation. However a similar calculation for the transformation of the fermion leads to

$$(\delta_{\epsilon_1} \delta_{\epsilon_2} - \delta_{\epsilon_2} \delta_{\epsilon_1})\psi_\alpha = i(-\epsilon_1 \sigma^\mu \epsilon_2^\dagger + \epsilon_2 \sigma^\mu \epsilon_1^\dagger) \partial_\mu \psi_\alpha + \text{non-zero}, \quad (3.26)$$

where the non-zero terms only vanish on-shell. This means, that SUSY is only satisfied in the on-shell limit. This problem can be circumvented by introducing an auxiliary field F to the Lagrangian

$$\mathcal{L}_{\text{aux}} = F^* F, \quad \text{with } [F] = 2 \quad (3.27)$$

which transforms under SUSY as

$$\delta F = -\epsilon^\dagger \bar{\sigma}^\mu \partial_\mu \psi, \quad \delta F^* = i \partial_\mu \psi^\dagger \bar{\sigma}^\mu \epsilon. \quad (3.28)$$

This auxiliary field is responsible for the cancellation of any off-shell part violation of the SUSY algebra as in eq. (3.26). Now, also the transformation behavior of ψ has to be altered accordingly,

$$\delta \psi_\alpha = -i(\sigma^\mu \epsilon^\dagger)_\alpha \partial_\mu \phi + \epsilon_\alpha F, \quad \delta \psi_\alpha^\dagger = i(\epsilon \sigma^\mu)_\alpha \partial_\mu \phi^* + \epsilon_\alpha^\dagger F^*. \quad (3.29)$$

such that indeed $\delta S = 0$ while also accommodating that the SUSY algebra closes off-shell. Indeed, one finds

$$(\delta_{\epsilon_1} \delta_{\epsilon_2} - \delta_{\epsilon_2} \delta_{\epsilon_1})X = i(-\epsilon_1 \sigma^\mu \epsilon_2^\dagger + \epsilon_2 \sigma^\mu \epsilon_1^\dagger) \partial_\mu X \quad (3.30)$$

for any $X = \phi, \phi^*, \psi, \psi^\dagger, F, F^*$. The triple (ϕ, ψ, F) is referred to as a chiral supermultiplet.

In order to derive the interactions between scalars and spinors, consider n ($i = 1, \dots, n$) copies of free Wess-Zumino Lagrangians:

$$\mathcal{L}_{\text{free}} = \partial^\mu \phi^{i*} \partial_\mu \phi_i + i \psi^{i\dagger} \bar{\sigma}^\mu \partial_\mu \psi_i + F^{i*} F_i. \quad (3.31)$$

The interaction Lagrangian also has to be invariant under SUSY transformations, such that the most general ansatz can be chosen to be

$$\mathcal{L}_{\text{int}} = \left(-\frac{1}{2} W^{ij} \psi_i \psi_j + W^i F_i \right) + \text{h.c.} \quad (3.32)$$

From

$$0 \stackrel{!}{=} \delta \mathcal{L}_{\text{int}} \Big|_{4 \text{ spinors}}, \quad (3.33)$$

one finds that

- $\delta W^{ij}/\delta\phi_k$ is totally symmetric in i, j, k ,
- $\delta W^{ij}/\delta\phi_k^* = 0$, e.g. W^{ij} is *holomorph* in ϕ_k ,

motivating the ansatz

$$W^{ij} = M^{ij} + y^{ijk}\phi_k \quad (3.34)$$

with y^{ijk} a totally symmetric Yukawa coupling and M^{ij} a symmetric mass matrix. Furthermore, this defines implicitly the *superpotential*

$$W = \frac{1}{2}M^{ij}\phi_i\phi_j + \frac{1}{6}y^{ijk}\phi_i\phi_j\phi_k, \quad (3.35)$$

such that

$$W^{ij} = \frac{\delta^2}{\delta\phi_i\delta\phi_j}W. \quad (3.36)$$

Note, that in general the superpotential can have a term of the type $L^i\phi_i$ with $[L] = 2$ if ϕ_i is a gauge singlet. Since in the SM no fermion is a gauge singlet, so is no corresponding superpartner. However this term plays a role in spontaneous SUSY-breaking. Similar proceeding for the condition $0 \stackrel{!}{=} \delta\mathcal{L}_{\text{int}}|_{\partial}$ shows that also W^i is related to the superpotential:

$$W^i = \frac{\delta W}{\delta\phi_i}. \quad (3.37)$$

Using the equation of motion for the auxiliary fields, they can be replaced in the Lagrangian in favor of the superpotential. Finally, in terms of the superpotential W , the Lagrangian reads

$$\mathcal{L} = \partial^\mu\phi^{i*}\partial_\mu\phi_i + i\psi^{i\dagger}\bar{\sigma}^\mu\partial_\mu\psi_i - \frac{1}{2}\left(W^{ij}\psi_i\psi_j + W_{ij}^*\psi^{\dagger i}\psi^{\dagger j}\right) - W^iW_i^*. \quad (3.38)$$

3.3.3 Gauge Supermultiplets

Following [15, Chapter 3.3], the supersymmetric partner of a gauge field A_μ^a is called a gaugino λ^a with index a running over the adjoint representation of the gauge group. The SUSY invariant Lagrangian reads

$$\mathcal{L} = -\frac{1}{4}F_{\mu\nu}^a F^{\mu\nu a} + i\lambda^{\dagger a}\bar{\sigma}^\mu\nabla_\mu\lambda^a + \frac{1}{2}D^a D^a \quad (3.39)$$

with the covariant derivative of the gaugino

$$\nabla_\mu\lambda^a = \partial_\mu\lambda^a + gf^{abc}A_\mu^b\lambda^c \quad (3.40)$$

and D^a is an auxiliary field and plays a similar role as F before. Interactions between a chiral supermultiplet and a gauge multiplet are introduced by replacing the ordinary derivatives with covariant derivatives. Since SUSY commutes with gauge transformations, all elements of a chiral supermultiplet are in the same representation of the gauge group. This means, that under an infinitesimal gauge transformation expressed by Λ^a ,

$$X_i \rightarrow X_i + ig\Lambda^a(T^a X)_i, \quad (3.41)$$

where the matrices T^a correspond to the representation to which all of the $X_i = \phi, \psi, F$ belong to. With the mentioned introduction of the covariant derivative, new terms including interactions between gauginos and matter fields are generated, which are not compatible with SUSY invariance. Thus, once again the transformation behavior in δF_i has to be altered. After all these steps have been taken, the scalar potential in $\mathcal{L}_{\text{total}}$ reads

$$V(\phi, \phi^*) = F^{*i}F_i + \frac{1}{2} \sum_a D^a D^a = W_i^* W^i + \frac{1}{2} \sum_a g_a^2 (\phi^* T^a \phi)^2 > 0. \quad (3.42)$$

The first and second term are called " F -term" and " D -term" contributions, respectively.

3.3.4 Superspace and Superfields

Following [15, Chapter 4], an alternative approach to the direct construction is based on objects called *superfields* living in *superspace* as introduced by Salam and Strathdee in 1974 [20]. This formalism is used to discuss supersymmetric theories in a more formal and theoretical way. Instead of working with spacetime only, the usual coordinates x^μ are extended with sets of complex, anti-commuting two component spinors θ^α and θ_α^\dagger whose components behave like Grassmann numbers. The coordinates $(x^\mu, \theta^\alpha, \theta_\alpha^\dagger)$ define the *superspace*. The integration- and differentiation behavior of the Grassmann coordinates allows manipulation- and projection techniques which are used to extract supersymmetry-respecting terms for the Lagrangian. For example, the following equations hold:

$$\frac{\partial}{\partial \theta^\alpha} (\psi \theta) \equiv \frac{\partial}{\partial \theta^\alpha} (\psi^\beta \theta_\beta) = \frac{\partial}{\partial \theta^\alpha} (\theta^\beta \psi_\beta) = \delta_\alpha^\beta \psi_\beta = \psi_\alpha, \quad (3.43a)$$

$$\frac{\partial}{\partial \theta^\alpha} (\theta \theta) \equiv \frac{\partial}{\partial \theta^\alpha} (\theta^\beta \theta^\gamma \epsilon_{\beta\gamma}) = \epsilon_{\alpha\gamma} \theta^\gamma - \epsilon_{\beta\alpha} \theta^\beta = 2\theta_\alpha, \quad (3.43b)$$

$$\int d^2\theta \theta \theta = 1, \quad \int d^2\theta^\dagger \theta^\dagger \theta^\dagger = 1. \quad (3.43c)$$

The integration measures are defined as

$$d^2\theta \equiv -\frac{1}{4} d\theta^\alpha d\theta^\alpha \epsilon_{\alpha\beta} \quad \text{and} \quad d^2\theta^\dagger \equiv -\frac{1}{4} d\theta_\alpha^\dagger d\theta_\beta^\dagger \epsilon^{\dot{\alpha}\dot{\beta}}. \quad (3.44)$$

Explicitly, the first integral in eq. (3.43c) reads:

$$\int d\theta^\alpha d\theta^\beta \epsilon_{\alpha\beta} \theta_\delta \theta_\gamma \epsilon^{\gamma\delta} = \epsilon_{\alpha\beta} \epsilon^{\gamma\delta} \int d\theta^\alpha \left(\delta_\delta^\beta \theta_\gamma - \theta_\delta \delta_\gamma^\beta \right) = 2\epsilon_{\alpha\beta} \epsilon^{\alpha\beta} = -4, \quad (3.45)$$

where the property of Grassmann numbers has been used to interchange integral and derivative.

A general superfield $S = S(x, \theta, \theta^\dagger)$ encapsulates all component-fields of a supermultiplet, e.g. the spin-0-, spin- $\frac{1}{2}$ - and auxiliary field of a chiral supermultiplet. Since it is a function of both bosonic spacetime coordinates x^μ and fermionic anticommuting coordinates θ^α and θ_α^\dagger , we can make the following expansion in coordinates:

$$\begin{aligned} S(x, \theta, \theta^\dagger) = & a + \theta\xi + \theta^\dagger\chi^\dagger + \theta\theta b + \theta^\dagger\theta^\dagger c + \theta^\dagger\bar{\sigma}^\mu\theta v_\mu + \\ & + \theta^\dagger\theta^\dagger\theta\eta + \theta\theta\theta^\dagger\zeta^\dagger + \theta\theta\theta^\dagger\theta^\dagger d. \end{aligned} \quad (3.46)$$

Latin characters represent scalar- or vector fields, while Greek characters stand for spinorial, anticommuting fields. Due to the Grassmann nature of the additional coordinates, all higher order terms vanish. Note

- The general superfield has 16 fermionic- and 16 bosonic degrees of freedom, while, for example, the chiral supermultiplet only contains $4 + 4 = 8$. This means, that the general superfield in eq. (3.46) is a reducible representation of supersymmetry.
- Using the integration measures as defined in eq. (3.44), one can project out certain components of $S(x, \theta, \theta^\dagger)$. This will be very important when constructing the invariant action later on. Some examples are:

$$\begin{aligned} \int d^2\theta S(x, \theta, \theta^\dagger) &= b(x) + \theta^\dagger\zeta^\dagger(x) + \theta^\dagger\theta^\dagger d(x) \\ \int d^2\theta^\dagger S(x, \theta, \theta^\dagger) &= c(x) + \theta\eta(x) + \theta\theta d(x) \\ \int d^2\theta d^2\theta^\dagger S(x, \theta, \theta^\dagger) &= d(x) \end{aligned}$$

- Dirac delta functions in superspace can be used for the same purpose. With respect to the fermionic integration measures they are:

$$\delta^2(\theta - \theta') = (\theta - \theta')(\theta - \theta'), \quad \delta^2(\theta^\dagger - \theta'^\dagger) = (\theta^\dagger - \theta'^\dagger)(\theta^\dagger - \theta'^\dagger).$$

- It is possible to conduct simplifications via integration-by-parts in Grassmann coordinates:

$$\int d^2\theta \frac{\partial}{\partial\theta^\alpha} = \int d^2\theta^\dagger \frac{\partial}{\partial\theta_\alpha^\dagger} = 0.$$

One appealing feature of this formalism is the observation, that SUSY transformations correspond to translations in superspace, e.g.

$$\sqrt{2}\delta_\epsilon S(x, \theta, \theta^\dagger) = -i(\epsilon\hat{Q} + \epsilon^\dagger\hat{Q}^\dagger)S(x, \theta, \theta^\dagger) \quad (3.47a)$$

$$= S(x^\mu + i\epsilon\sigma^\mu\theta^\dagger + i\epsilon^\dagger\bar{\sigma}^\mu\theta, \theta + \epsilon, \theta^\dagger + \epsilon^\dagger) - S(x^\mu, \theta, \theta^\dagger) \quad (3.47b)$$

with differential operators

$$\hat{Q}_\alpha = i\frac{\partial}{\partial\theta^\alpha} - (\sigma^\mu\theta^\dagger)_\alpha\partial_\mu, \quad \hat{Q}^{\dagger\dot{\alpha}} = i\frac{\partial}{\partial\theta^{\dot{\alpha}}} - (\bar{\sigma}^\mu\theta)^{\dot{\alpha}}\partial_\mu. \quad (3.48)$$

One can check that these differential operators satisfy the SUSY algebra and can use them to work out the transformation behavior of all fields in S .

As mentioned before, the general superfield S is a reducible representation of SUSY since the degrees of freedom (dof) do not match the field content of neither the chiral supermultiplet nor the vector supermultiplet. For the chiral supermultiplet the redundant dofs of a superfield $\Phi(x, \theta, \theta^\dagger)$ can be removed using the (anti-) chiral D_α ($\bar{D}_{\dot{\alpha}}$) covariant derivatives²

$$D_\alpha := \frac{\partial}{\partial\theta^\alpha} - i(\sigma^\mu\theta^\dagger)_\alpha\partial_\mu, \quad \bar{D}_{\dot{\alpha}} := -\frac{\partial}{\partial\theta^{\dot{\alpha}}} + i(\theta\sigma^\mu)_{\dot{\alpha}}\partial_\mu, \quad (3.49)$$

where the constrain defining the *left-chiral* (or *chiral*) superfield reads

$$\bar{D}_{\dot{\alpha}}\Phi = 0, \quad (3.50)$$

while the *right-chiral* (or *anti-chiral*) superfield is defined by

$$D_\alpha\Phi^* = 0. \quad (3.51)$$

One can solve these constraints by a shift $x^\mu \rightarrow y^\mu = x^\mu - i\theta\sigma^\mu\theta^\dagger$ and will find in terms of $(x, \theta, \theta^\dagger)$

$$\begin{aligned} \Phi(x, \theta, \theta^\dagger) &= \phi(x) - i\theta\sigma^\mu\theta^\dagger\partial_\mu\phi(x) - \frac{1}{4}\theta\theta\theta^\dagger\theta^\dagger\partial^2\phi(x) + \sqrt{2}\theta\psi(x) \\ &\quad - \frac{i}{\sqrt{2}}\theta\theta\theta^\dagger\bar{\sigma}^\mu\partial_\mu\psi(x) + \theta\theta F(x) \end{aligned} \quad (3.52)$$

and a similar expression for Φ^* . The fields (ϕ, ψ, F) appearing are identified with the elements of a chiral superfield behaving under SUSY transformations as derived in section 3.3.2.

The constraints for extracting a vector supermultiplet is comparably simple and reads

$$V = V^* \quad (3.53)$$

²This covariant derivative commutes with SUSY transformations

for a superfield V . Again, solving this equation leads to a superfield whose components are identified with the elements (A_μ, λ, D) of a vector supermultiplet;

$$\begin{aligned}
 V(x, \theta, \theta^\dagger) = & a + \theta\xi + \theta^\dagger\xi^\dagger + \theta\theta b + \theta^\dagger\theta^\dagger b^* + \theta\sigma^\mu\theta^\dagger A_\mu + \theta^\dagger\theta^\dagger\left(\lambda - \frac{i}{2}\sigma^\mu\partial_\mu\xi^\dagger\right) \\
 & + \theta\theta\theta^\dagger\left(\lambda^\dagger - \frac{i}{2}\bar{\sigma}^\mu\partial_\mu\xi\right) + \theta\theta\theta^\dagger\theta^\dagger\left(\frac{1}{2}D - \frac{1}{4}\partial^2 a\right). \quad (3.54)
 \end{aligned}$$

The fields a , ξ and b are additional auxiliary fields which can be removed via a "supergauge" transformation [15, Chapter 4.5].

With the field content of a chiral and vector supermultiplet identified, the question is how to find the corresponding Lagrangian using these superfields. As hinted at earlier, the Grassmann nature of the additional coordinates can be used for certain projections. Note that,

$$\int d^4x \int d^2\theta d^2\theta^\dagger \delta_\epsilon S \sim \int d^4x \int d^2\theta d^2\theta^\dagger \left(\epsilon\hat{Q} + \epsilon^\dagger\hat{Q}^\dagger\right) \stackrel{\text{IBP}}{=} 0. \quad (3.55)$$

Such that the action can have SUSY-invariant terms of the form $\int d^4x \int d^2\theta d^2\theta^\dagger S$. In particular, a vector superfield will contribute to the Lagrangian this way. This contribution is called *D-term*:

$$[V]_D \equiv \int d^2\theta d^2\theta^\dagger V(x, \theta, \theta^\dagger) = V(x, \theta, \theta^\dagger) \Big|_{\theta\theta\theta^\dagger\theta^\dagger} = \frac{1}{2}D - \frac{1}{4}\partial^2 a \quad (3.56)$$

where the term $\sim a$ vanishes under the integral $\int d^4x$. Another contribution arises from the chiral superfield. Noticing that $\delta_\epsilon F \sim \partial_\mu\psi$, the $\theta\theta$ - component of Φ is invariant under SUSY and thus may contribute. This term is called *F-term*:

$$[\Phi]_F \equiv \int d^2\theta d^2\theta^\dagger \delta^{(2)}(\theta^\dagger)\Phi = \int d^2\theta \Phi \Big|_{\theta^\dagger=0} = \Phi \Big|_{\theta\theta} = F. \quad (3.57)$$

Since the action has to be real, also its complex conjugate has to be included:

$$[\Phi]_F + \text{c.c.} = \int d^2\theta d^2\theta^\dagger \left[\delta^{(2)}(\theta^\dagger)\Phi + \delta^{(2)}(\theta)\Phi^*\right] \quad (3.58)$$

As it turns out, the D-term of a vector superfield and the F-term of a chiral superfield are the only possible ways of extracting a SUSY invariant contribution for a Lagrangian density. In general, the underlying superfields Φ and V are composite objects made of other superfields. For example, the superfield $S = \Phi^*\Phi$ with $\Phi = \Phi(x, \theta, \theta^\dagger)$ as in eq. (3.52), is a vector superfield whose *D-term* reproduces the free Wess-Zumino Lagrangian. In general, this function of superfields,

$$K(\Phi, \Phi^*) = c_{mn}\Phi^{*m}\Phi^n, \quad (3.59)$$

is called the *Kähler potential*. Interactions are deduced from any holomorphic function $W(\Phi_i)$ of the chiral superfields via its F-term. In fact, this coincides with the earlier derived superpotential. The superpotential

$$W = \frac{1}{2}M^{ij}\Phi_i\Phi_j + \frac{1}{6}y^{ijk}\Phi_i\Phi_j\Phi_k \quad (3.60)$$

replicates all interactions between the fields of n copies of Wess-Zumino models. It is also possible to describe (non-) Abelian gauge theories in this formalism which can be achieved by modifying the Kähler potential to be supergauge invariant [15, Chapter 4.8 f.]

It is noteworthy that SUSY can offer interesting theoretical insights in general QFT. For example, the fact that the superpotential is holomorph in the field Φ only, results in the observation that the (Wilsonian) effective action does not get quantum corrections [21]. Or, in other words, the superpotential is not renormalized [17, Chapter 8]. In more general SUSY theories a generalization of this observation is linked to the *non renormalization theorems*. One interesting example is the $\mathcal{N} = 4$ Super Yang-Mills theory, for which the Lagrangian does not get renormalized at all. Thus, also the β - function vanishes and the theory becomes scale invariant [22–24].

3.4 The Minimal Supersymmetric Standard Model

The minimal realization of SUSY in virtue of a model describing nature at our scale is the Minimal Supersymmetric Standard Model (MSSM) whose core features are summarized here. We assume conserved R - (or matter-) parity ensuring that the lightest supersymmetric particle (LSP) is stable.

3.4.1 Field Content

Each fermion and spin-1 gauge boson of the SM is respectively embedded into a chiral- or vector supermultiplet (following [25, Chapter 8.2]). Their bosonic (fermionic) counterparts are then called sfermion (gaugino). In the case of leptons (quarks), the supersymmetric spin-0 particles are called sleptons (squarks). The first generation of sfermions can be written as

$$\tilde{\ell}_{1L} = \begin{pmatrix} \tilde{\nu} \\ \tilde{e}^- \end{pmatrix}_L, \quad \tilde{e}_{1R}, \quad \tilde{q}_{1L} = \begin{pmatrix} \tilde{u} \\ \tilde{d} \end{pmatrix}_L, \quad \tilde{u}_{1R}, \quad \tilde{d}_{1R}. \quad (3.61)$$

Where the sfermions with left (right) label are the superpartners of the respective left (right) chiral fermion and do not carry themselves a chirality. The chiral superfields then read

$$L_1 = \begin{pmatrix} L_{\nu_e} \\ L_e \end{pmatrix}, \quad \bar{E}_1, \quad Q_1 = \begin{pmatrix} Q_u \\ Q_d \end{pmatrix}, \quad \bar{U}_1, \bar{D}_1, \quad (3.62)$$

where the unbarred fields L_1 and Q_1 are the left chiral fermion doublets while quantities with a bar are the antifermion singlet chiral superfields. Note that all quantum numbers of a multiplet are identical. The other generations are expressed similarly. Since the superpotential can only contain left chiral superfields, one has to take the charge conjugates of the $SU(2)$ singlet right chiral fermion fields and complex conjugates of the right sfermion fields as fundamental fields in the superfield formalism.

Each SM gauge boson is embedded into a vector supermultiplet. The superpartners of the $U(1)_Y$, $SU(2)_L$ and $SU(3)_c$ gauge bosons B_μ , W_μ^i and g_μ^a are four-component Majorana fermions $\tilde{\lambda}_0$, $\tilde{\lambda}^i$ and \tilde{g}^a respectively.

The Higgs sector of the MSSM differs from the SM case in that it needs two Higgs doublets. This is due to the fact that, while in the SM one Higgs doublet is responsible for the generation of masses for both left- and right chiral fields, the property of the superpotential $\mathcal{W}_{\text{MSSM}}$ forbids a similar framework. Because it is an analytic function of left chiral fields only, one needs one Higgs doublet (with hypercharges $Y = \mp 1$) for each set of fields with $T_{3L} = +\frac{1}{2}$ and $T_{3L} = -\frac{1}{2}$ each, called h_1 and h_2 . Together with their superpartners they form superfields H_1 and H_2 , see section 3.4.2.

Before going into more details of the different sectors, let's present the overall picture. The Lagrangian for the MSSM can be split into two contributions [25, Chapter 8.3]

$$\mathcal{L}_{\text{MSSM}} = \mathcal{L}_{\text{SUSY}} + \mathcal{L}_{\text{SOFT}}, \quad (3.63)$$

where $\mathcal{L}_{\text{SUSY}}$ contains the pure gauge \mathcal{L}_g , pure matter \mathcal{L}_M and Higgs-Yukawa part \mathcal{L}_H . The latter contains

$$\mathcal{L}_H \supset \int d^4\theta \left[\mathcal{W}_{\text{MSSM}} \delta^{(2)}(\bar{\theta}) + \mathcal{W}_{\text{MSSM}}^\dagger \delta^{(2)}(\theta) \right] \quad (3.64)$$

with the superpotential

$$\mathcal{W}_{\text{MSSM}} = \mu H_1 \cdot H_2 - f_{ij}^e H_1 \cdot L_i \bar{E}_j - f_{ij}^d H_1 \cdot Q_i \bar{D}_j - f_{ij}^u Q_i \cdot H_2 \bar{U}_j \quad (3.65)$$

Here, the indices i, j are family indices, $A \cdot B \equiv \epsilon_{cd} A^c B^d$ for $SU(2)$ superfields A and B . The f_{ij}^f are Yukawa couplings and μ is a free parameter.

The second term $\mathcal{L}_{\text{SOFT}}$ breaks SUSY explicitly and is needed since in the pure MSSM no spontaneous global SUSY-breaking can occur as can be shown using supertrace mass sum rules [25, ch. 9.1]. Effectively this allows the study of the MSSM irrespective of the exact source of SUSY-breaking. Some ideas about the origin are portrayed in section 3.5. The soft Lagrangian can be divided into two different contributions:

$$-\mathcal{L}_{\text{SOFT}} \equiv V_{\text{SOFT}} + \text{gaugino mass terms} \quad (3.66)$$

with the part containing no gaugino mass terms reading

$$\begin{aligned}
 V_{\text{SOFT}} &= \tilde{q}_{iL}^* (\mathcal{M}_{\tilde{q}_L}^2)_{ij} \tilde{q}_{jL} + \tilde{u}_{iR}^* (\mathcal{M}_{\tilde{u}_R}^2)_{ij} \tilde{u}_{jR} + \tilde{d}_{iR}^* (\mathcal{M}_{\tilde{d}_R}^2)_{ij} \tilde{d}_{jR} \\
 &\quad + \tilde{\ell}_{iL}^* (\mathcal{M}_{\tilde{\ell}_L}^2)_{ij} \tilde{\ell}_{jL} + \tilde{e}_{iR}^* (\mathcal{M}_{\tilde{e}_R}^2)_{ij} \tilde{e}_{jR} \\
 &\quad + h_1 \cdot \tilde{\ell}_{iL} (f^e A^e)_{ij} \tilde{e}_{jR}^* + h_1 \cdot \tilde{q}_{iL} (f^d A^d)_{ij} \tilde{d}_{jR}^* + \text{h.c.} \\
 &\quad + \tilde{q}_{iL} \cdot h_2 (f^u A^u)_{ij} \tilde{u}_{jR}^* + \text{h.c.} \\
 &\quad + m_1^2 |h_1|^2 + m_2^2 |h_2|^2 + (B\mu h_1 \cdot h_2 + \text{h.c.}).
 \end{aligned} \tag{3.67}$$

The gaugino mass terms read

$$-\mathcal{L}_{\text{gaugino mass}} = + \frac{1}{2} (M_1 \bar{\lambda}_0 P_L \tilde{\lambda}_0 + M_1^* \tilde{\lambda}_0 P_R \bar{\lambda}_0) \tag{3.68a}$$

$$+ \frac{1}{2} (M_2 \bar{\lambda}^i P_L \tilde{\lambda}^i + M_2^* \tilde{\lambda}^i P_R \bar{\lambda}^i) \tag{3.68b}$$

$$+ \frac{1}{2} (M_3 \bar{g}^a P_L \tilde{g}^a + M_3^* \tilde{g}^a P_R \bar{g}^a). \tag{3.68c}$$

The potential V_{SOFT} plays a role for the mass terms for sfermions as well as in the Higgs sector.

3.4.2 Higgs sector

As mentioned previously, the MSSM Higgs sector consists of two $SU(2)$ doublets h_1 and h_2 which together with their superpartners are part of the superfields H_1 and H_2 respectively. Writing out the suppressed $SU(2)$ indices of $h_{1,2}$ explicitly one gets

$$h_1 \equiv \begin{pmatrix} h_1^1 \\ h_1^2 \end{pmatrix} = \begin{pmatrix} h_1^0 \\ h_1^- \end{pmatrix}, \quad h_2 \equiv \begin{pmatrix} h_2^1 \\ h_2^2 \end{pmatrix} = \begin{pmatrix} h_2^+ \\ h_2^0 \end{pmatrix}, \tag{3.69}$$

contributing to the soft Lagrangian as

$$-\mathcal{L}_{\text{SOFT}} \supset m_1^2 |h_1|^2 + m_2^2 |h_2|^2 + (B\mu h_1 \cdot h_2 + \text{h.c.}) \tag{3.70}$$

where B is the soft SUSY-breaking bilinear and $|\mu|$ is the Higgs-higgsino mass parameter. Their left chiral supersymmetric partners, called *higgsinos*, are

$$\tilde{h}_{1L} \equiv \begin{pmatrix} \tilde{h}_1^1 \\ \tilde{h}_1^2 \end{pmatrix} = \begin{pmatrix} \tilde{h}_1^0 \\ \tilde{h}_1^- \end{pmatrix}_L, \quad \tilde{h}_{2L} \equiv \begin{pmatrix} \tilde{h}_2^1 \\ \tilde{h}_2^2 \end{pmatrix} = \begin{pmatrix} \tilde{h}_2^+ \\ \tilde{h}_2^0 \end{pmatrix}_L. \tag{3.71}$$

The Higgs and higgsino fields are contained in left chiral superfields

$$H_1 = \begin{pmatrix} H_1^1 \\ H_1^2 \end{pmatrix} \supset (h_1, \tilde{h}_{1L}), \quad H_2 = \begin{pmatrix} H_2^1 \\ H_2^2 \end{pmatrix} \supset (h_2, \tilde{h}_{2L}). \tag{3.72}$$

In the context of spontaneous symmetry breaking the Higgs fields obtain vacuum expectation values (vevs)

$$\langle h_1 \rangle = \frac{1}{\sqrt{2}} \begin{pmatrix} v_1 \\ 0 \end{pmatrix}, \quad \langle h_2 \rangle = \frac{1}{\sqrt{2}} \begin{pmatrix} 0 \\ v_2 \end{pmatrix}, \quad (3.73)$$

where $v_{1,2}$ can be chosen to be real and positive. Their ratio is defined as

$$\tan \beta \equiv \frac{v_2}{v_1}, \quad 0 \leq \beta \leq \pi/2 \quad (3.74)$$

and is a free parameter. Furthermore, assuming correct EWSB, they are related to the masses of the W and Z Bosons by

$$m_W = \frac{g}{2}(v_1^2 + v_2^2)^{1/2}, \quad m_Z = \frac{(g'^2 + g^2)^{1/2}}{2}(v_1^2 + v_2^2)^{1/2} \quad (3.75)$$

The Higgs potential reads

$$V_H = \frac{1}{8}(g'^2 + g^2)(|h_1|^2 - |h_2|^2)^2 + \frac{g^2}{2}|h_1^\dagger h_2|^2 \\ + m_{1h}^2|h_1|^2 + m_{2h}^2|h_2|^2 + (m_{12}^2 h_1 \cdot h_2 + \text{h.c.}) \quad (3.76)$$

with

$$|h|^2 \equiv h^\dagger h \quad (3.77a)$$

$$h_1 \cdot h_2 = \tilde{h}_1^\dagger h_2 \equiv i\tau_2 h_1^* h_2, \quad (3.77b)$$

$$m_{12}^2 \equiv B\mu \quad (3.77c)$$

$$m_{1,2h}^2 = m_{1,2}^2 + |\mu|^2. \quad (3.77d)$$

Replacing the Higgs field in the potential with their respective vevs one obtains

$$V_H^{\min} = \frac{1}{32}(g'^2 + g^2)(v_1^2 - v_2^2)^2 + \frac{1}{2}m_{1h}^2 v_1^2 + \frac{1}{2}m_{2h}^2 v_2^2 - m_{12}^2 v_1 v_2. \quad (3.78)$$

Demanding that $\partial V_H^{\min}/\partial v_i = 0$ for $i = 1, 2$ leads to the relations

$$m_{12}^2 = -\frac{1}{2}(m_1^2 - m_2^2) \tan(2\beta) - \frac{1}{2}m_Z^2 \sin(2\beta) \quad (3.79a)$$

$$|\mu|^2 = \frac{1}{\cos 2\beta}(m_2^2 \sin^2 \beta - m_1^2 \cos^2 \beta) - \frac{1}{2}m_Z^2. \quad (3.79b)$$

which can be recast into (see e.g. eq. (8.1.10) in [15])

$$\sin 2\beta = \frac{2m_{12}^2}{m_1^2 + m_2^2 + 2|\mu|^2}, \quad (3.80a)$$

$$m_Z^2 = \frac{|m_2^2 - m_1^2|}{\sqrt{1 - \sin^2(2\beta)}} - m_2^2 - m_1^2 - 2|\mu|^2, \quad (3.80b)$$

highlighting a fine tuning problem between the input parameters in order to obtain the physical Z -boson mass. Further, μ is a SUSY-respecting parameter, while the soft masses $m_{1,2}$ and B are SUSY-breaking, such that any fine tuned balancing between them seems unnatural. This potential lack of naturalness can be quantified via the naturalness c_a of a parameter a as

$$c_a \equiv \left| \frac{\partial \ln(m_Z^2)}{\partial \ln(a)} \right|. \quad (3.81)$$

and is explicitly calculated in SUSY spectrum generators like SOFTSUSY [26] and SUSPECT [27].

The mass matrix is given by

$$m_{ij}^2 = \left\langle \frac{\partial^2 V_H}{\partial \phi_i \partial \phi_j} \right\rangle \quad (3.82)$$

where ϕ_i stands for any component of any Higgs field involved. Investigating the mass diagonal fields one finds

$$H^\pm = \sin \beta h_1^\pm + \cos \beta h_2^\pm, \quad (3.83a)$$

$$G^\pm = -\cos \beta h_1^\pm + \sin \beta h_2^\pm, \quad (3.83b)$$

with masses

$$m_{H^\pm}^2 = m_A^2 + m_W^2, \quad m_{G^\pm}^2 = 0. \quad (3.84)$$

The massless Goldstone modes are eaten by the SM $SU(2)$ gauge bosons and combine to the massive W^\pm . The mass m_A^2 is the mass of the CP odd Higgs A :

$$\frac{A}{\sqrt{2}} = \text{Im } h_1^0 \sin \beta + \text{Im } h_2^0 \cos \beta, \quad (3.85a)$$

$$\frac{G^0}{\sqrt{2}} = -\text{Im } h_1^0 \cos \beta + \text{Im } h_2^0 \sin \beta. \quad (3.85b)$$

with

$$m_A^2 = \frac{2m_{12}^2}{\sin 2\beta}, \quad m_{G^0}^2 = 0. \quad (3.86)$$

As before, the neutral Goldstone is absorbed and gives mass to the Z Boson. Additionally there are two neutral CP even Higgs fields H and h in the spectrum, of which the latter is identified with the discovered signal at the LHC in 2012 [28, 29]. Since at tree level

$$m_h < m_Z |\cos(2\beta)|, \quad (3.87)$$

large radiative corrections are needed to explain the measured value of $m_h \approx 125$ GeV, where the biggest contribution comes from top and stop loops.

3.4.3 Neutralinos

The neutralinos emerge as mass eigenstates of the vector

$$(\psi^0)^T \equiv (\lambda_0, \lambda_3, \tilde{h}_1^1, \tilde{h}_2^2) \quad (3.88)$$

consisting of neutral gauginos λ_0 (bino) and λ_3 (neutral wino) and neutral Higgsinos \tilde{h}_1^1 and \tilde{h}_2^2 . The mass Lagrangian reads

$$-\mathcal{L} = \frac{1}{2}(\psi^0)^T \mathcal{M}^n (\psi^0) + \text{h.c.} \quad (3.89)$$

with explicit mass matrix

$$\mathcal{M}^n = \begin{pmatrix} M_1 & 0 & -m_Z c_\beta s_W & m_Z s_\beta s_W \\ 0 & M_2 & m_Z c_\beta c_W & -m_Z s_\beta c_W \\ -m_Z c_\beta s_W & m_Z c_\beta c_W & 0 & -\mu \\ m_Z s_\beta s_W & -m_Z s_\beta c_W & -\mu & 0 \end{pmatrix}, \quad (3.90)$$

using the notation $c_\alpha \equiv \cos(\alpha)$ and $s_\alpha \equiv \sin(\alpha)$ for $\alpha = \beta, \theta_W$. This matrix can be diagonalized with a unitary 4×4 matrix N such that

$$N^* \mathcal{M}^n N^{-1} = \text{diag}(m_{\tilde{\chi}_1^0}, m_{\tilde{\chi}_2^0}, m_{\tilde{\chi}_3^0}, m_{\tilde{\chi}_4^0}) \quad (3.91)$$

with ordering $m_{\tilde{\chi}_1^0} < m_{\tilde{\chi}_2^0} < m_{\tilde{\chi}_3^0} < m_{\tilde{\chi}_4^0}$ of the absolute values of the eigenvalues of \mathcal{M}^n . The corresponding mass eigenstates (neutralinos) then read

$$\tilde{\chi}_i^0 = N_{ik} \psi_k^0. \quad (3.92)$$

In particular, the lightest of these has the form

$$\tilde{\chi}_1^0 = N_{11} \lambda_0 + N_{12} \lambda_3 + N_{13} \tilde{h}_1^1 + N_{14} \tilde{h}_2^2 \equiv \chi \quad (3.93)$$

explicitly showing that the lightest neutralino consists of four different fields whose relative weights depend on the SUSY parameters M_1 , M_2 , μ and $\tan \beta$. Furthermore since N is unitary, the weights satisfy

$$\sum_i |N_{1i}|^2 = 1. \quad (3.94)$$

Although it is possible to obtain the matrix N analytically [15, 25], it is easier to diagonalize \mathcal{M}^n using numerical tools instead. In this case one has to manually sort the eigenvectors according to the absolute value of the eigenvalues in order to identify the lightest state.

3.4.4 Charginos

The chargino mass matrix is derived from the mass term of the fields

$$\psi^+ \equiv \begin{pmatrix} \lambda^+ \\ \tilde{h}_2^1 \end{pmatrix}, \quad \psi^- \equiv \begin{pmatrix} \lambda^- \\ \tilde{h}_1^2 \end{pmatrix} \quad (3.95)$$

which are four-component objects consisting of the charged gauginos (e.g. winos) $\lambda^\pm \equiv (\lambda_1 \mp i\lambda_3)/\sqrt{2}$ and spinorial higgsino fields \tilde{h}_1^2 and \tilde{h}_2^1 each having two components. The mass Lagrangian takes the form

$$-\mathcal{L} = (\psi^-)^T X \psi^+ + \text{h.c.} \quad (3.96)$$

with mass matrix

$$X = \begin{pmatrix} M_2 & \sqrt{2}m_W \sin \beta \\ \sqrt{2}m_W \cos \beta & \mu \end{pmatrix}. \quad (3.97)$$

The matrix X can be diagonalized with two unitary 2×2 matrices U and V such that

$$U^* X V^{-1} = M_c^D. \quad (3.98)$$

Equivalently one can take the transpose and obtain

$$(M_c^D)^T = (U^* X V^{-1})^T = V^* X^T U^\dagger \equiv O_R X^T O_L^T = M_c^D \quad (3.99)$$

with $O_R \equiv V^*$ and $O_L \equiv U^*$. Ignoring potential phases of M_2 and μ , thus making X purely real, one can parameterize the mixing matrices as

$$U = \begin{pmatrix} \cos \phi_u & \sin \phi_u \\ -\sin \phi_u & \cos \phi_u \end{pmatrix}, \quad V = \begin{pmatrix} \cos \phi_v & \sin \phi_v \\ -\epsilon_v \sin \phi_v & \epsilon_v \cos \phi_v \end{pmatrix} \quad (3.100)$$

with

$$\epsilon_v \equiv \text{sgn det } X = \text{sgn}(M_2 \mu - m_W^2 \sin(2\beta)) \quad (3.101)$$

and $(u, v) \rightarrow (L, R)$ in the notation in which $O_{L/R}$ instead of U/V have been chosen. With the matrix diagonalized, one can identify the mass eigenstates

$$\chi_k^+ = V_{km} \psi_m^+ \quad (3.102a)$$

$$\chi_k^- = U_{km} \psi_m^- \quad (3.102b)$$

and rewrite the mass Lagrangian as

$$-\mathcal{L} = \chi_k^- (M_c^D)_{km} \chi_m^+ + \text{h.c.} \quad (3.103)$$

with diagonal matrix

$$M_c^D = \text{diag}(m_{\chi_1^\pm}, m_{\chi_2^\pm}). \quad (3.104)$$

The masses

$$m_{\chi_{1,2}^\pm}^2 = \frac{1}{2} \left[|M_2^2| + |\mu^2| + 2m_W^2 \mp \left((|M_2^2| - |\mu^2|)^2 + 4m_W^4 \cos^2(2\beta) + 4m_W^2 (|M_2^2| + |\mu^2| + 2 \operatorname{Re}\{M_2\mu\} \sin(2\beta)) \right)^{1/2} \right] \quad (3.105)$$

are the eigenvalues of $X^\dagger X$ or XX^\dagger diagonalized by V or U respectively, e.g.

$$(M_c^D)^2 = VX^\dagger XV^{-1} = U^* XX^\dagger (U^*)^{-1}. \quad (3.106)$$

The angles $\phi_{L/R}$ of the mixing matrices satisfy

$$\tan 2\phi_L = \frac{2\sqrt{2}m_W(M_2 \cos \beta + \mu \sin \beta)}{M_2^2 - \mu^2 - 2m_W^2 \cos 2\beta} \quad (3.107a)$$

$$\tan 2\phi_R = \frac{2\sqrt{2}m_W(M_2 \sin \beta + \mu \cos \beta)}{M_2^2 - \mu^2 + 2m_W^2 \cos 2\beta}. \quad (3.107b)$$

As noted in [25], since eq. (3.107) is invariant under $\phi_{L/R} \rightarrow \phi_{L/R} + \pi/2$, one has to check which of the four solutions leads to eq. (3.98) being satisfied.

3.4.5 Sfermions

The masses of sfermions have different sources of origin (following [25, Section 9.4]): explicit mass terms and trilinear A -terms from V_{SOFT} , the contribution from F -terms due to $\mathcal{W}_{\text{MSSM}}$ and contributions from D -terms. The latter two are realized after EWSB while the first is invariant under $SU(2)_L \times U(1)_Y$ and thus in some sense more universal. A feature is, that left- and right sleptons can mix, but also mixing of charged sleptons between different generations is - in general - allowed. The last point however may often be disregarded due to current experimental bounds hinting at flavor conservation. The sfermion mass terms can be expressed in terms of six-component vectors

$$\tilde{\mathbf{f}} = \begin{pmatrix} \tilde{f}_L \\ \tilde{f}_R \end{pmatrix}, \quad (3.108)$$

where both \tilde{f}_L and \tilde{f}_R are three-component interaction eigenstates in generation space. For example for selectron type fields $\tilde{f} = \tilde{e}$ one obtains $\tilde{f}_{iL} = (\tilde{e}_L, \tilde{\mu}_L, \tilde{\tau}_L)^T$ and corresponding supersymmetric partners of the right handed leptons. Finally, the mass term for each $\tilde{\mathbf{f}}$ reads

$$-\mathcal{L}_{\text{sfermion mass}} = \tilde{\mathbf{f}}^\dagger \mathcal{M}_{\tilde{f}}^2 \tilde{\mathbf{f}}. \quad (3.109)$$

For the sneutrinos the block matrix (with 3×3 blocks) reads

$$\mathcal{M}_{\tilde{\nu}}^2 = \begin{pmatrix} \mathcal{M}_{\tilde{\ell}_L}^2 + m_Z^2 T_{3L}^{\tilde{\nu}} \cos 2\beta & 0 \\ 0 & 0 \end{pmatrix}, \quad (3.110)$$

while for the quarks and charged leptons the matrix is

$$\mathcal{M}_{\tilde{f}}^2 = \begin{pmatrix} \mathcal{M}_{\tilde{f}_{LL}}^2 & \mathcal{M}_{\tilde{f}_{LR}}^2 \\ \mathcal{M}_{\tilde{f}_{RL}}^2 & \mathcal{M}_{\tilde{f}_{RR}}^2 \end{pmatrix}, \quad (3.111)$$

with [30]

$$\mathcal{M}_{\tilde{f}_{LL}}^2 = \mathcal{M}_{\tilde{f}_L}^2 + m_Z^2 (T_{3L}^{\tilde{f}} - Q_f \sin^2 \theta_W) \cos 2\beta + m_f^2 \quad (3.112a)$$

$$\mathcal{M}_{\tilde{f}_{LR}}^2 = -m_f (A^{f*} + \mu \kappa) \quad (3.112b)$$

$$\mathcal{M}_{\tilde{f}_{RR}}^2 = \mathcal{M}_{\tilde{f}_R}^2 + m_Z^2 (T_{3L}^{\tilde{f}} - Q_f \sin^2 \theta_W) \cos 2\beta + m_f^2 \quad (3.112c)$$

$$\mathcal{M}_{\tilde{f}_{RL}}^2 = -m_f (A^f + \mu^* \kappa) \quad (3.112d)$$

where the matrices $\mathcal{M}_{\tilde{e}_L}^2 \equiv \mathcal{M}_{\tilde{\ell}_L}^2$ and $\mathcal{M}_{\tilde{u}_L, \tilde{d}_L}^2 \equiv \mathcal{M}_{\tilde{q}_L}^2$ appear in the soft breaking Lagrangian as mass of the left chiral fields, while $\mathcal{M}_{\tilde{e}_R}^2$ and $\mathcal{M}_{\tilde{u}_R, \tilde{d}_R}^2$ are the masses of the right chiral fields and A^f are the trilinear couplings, see eq. (3.67). The third component of the weak isospin of \tilde{f} is given by $T_{3L}^{\tilde{f}}$, while the charge and mass of the fermion f is given by Q_f and m_f respectively and finally $\kappa = \tan \beta$ for $f = e, d$ and $\kappa = \cot \beta$ for $f = u$.

The terms m_f and m_f^2 above are only approximations; in general one would have matrices \mathbf{m}_f and $\mathbf{m}_f \mathbf{m}_f^\dagger$ in generation space respectively in place, see [25, Chapter 9.4]. They are - in general and in particular in the SM - not diagonal and the corresponding gauge eigenstates have to be rotated into the mass eigenstates first. In the SM this is achieved as

$$(\mathbf{m}_e)_{ij} = m_{e_i} \delta_{ij}, \quad (U^{uL\dagger} \mathbf{m}_u U^{uR})_{ij} \equiv m_{u_i} \delta_{ij}, \quad (U^{dL\dagger} \mathbf{m}_d U^{dR})_{ij} \equiv m_{d_i} \delta_{ij}. \quad (3.113)$$

where the matrices U^{qL} and U^{qR} are unitary. However since the masses of the fermions in the first two generations are relative small compared to the masses of fermions in the third generation, as well as the mixing of the third generation with the first two generations is rather small, it is fair to make the simplification of diagonal mixing matrices, e.g. assume that mass and gauge eigenstates are identical:

$$(\mathbf{m}_{u,d})_{ij} = m_{u_i, d_i} \delta_{ij} \quad (3.114)$$

Another way to put it is, that since the masses of the first two generations are comparably small, approximately, the only non-vanishing elements of the Yukawa

matrices generating the masses after EWSB can be taken to be [31, Section 12 and Section 17.4]

$$y_u^{33} = y_t; \quad y_d^{33} = y_b; \quad y_e^{33} = y_\tau. \quad (3.115)$$

3.5 SUSY-Breaking Scenarios

Since current experiments did not find mass-degenerate supersymmetric partners of SM particles, SUSY has to be broken spontaneously at a scale M_{SUSY} [15]. There are multiple ways this can be achieved and usually involve the introduction of new fields and/or sectors. From a practical point of view, it makes sense to simply parameterize the effect of any spontaneous SUSY-breaking mechanism implicitly in the form of the soft breaking $\mathcal{L}_{\text{SOFT}}$ we introduced in eq. (3.66). Some ways, in which these soft terms can be generated, are introduced here.

3.5.1 SUGRA

As first model lets discuss the minimal Supergravity³ (mSUGRA) model [25, Chapter 12]; in which the universal soft breaking terms are due to flavor blind supergravity interactions mediating SUSY-breaking from a hidden sector to the visible. At the GUT scale $M_{\text{GUT}} \sim 2 \cdot 10^{16}$ GeV unification of the unbroken SM gauge couplings are assumed. The free parameters (at the GUT scale) are the unified scalar mass m_0 , unified gaugino mass $m_{1/2}$, the universal trilinear coupling A_0 and the Higgs sector parameters which in the presence of correct EWSB reduce to $\tan\beta$ and $\text{sgn}\mu$.

3.5.2 AMSB

Another scenario for the transmission of SUSY-breaking is the anomaly mediated supersymmetry breaking (AMSB) scheme [15, Chapter 7.8]. The setup here involves extra spatial dimensions such that there exists a physical separation between the hidden- and visible sector. In many cases it is assumed that only one extra dimension exists whose size R_5 (in units of fundamental Planck scale M_5) is relatively larger than the remaining four dimensions. This is required in order to explain the suppression of flavor violating terms rather naturally not relying on any fine tuning, e.g. they are suppressed exponentially $\sim \exp(-R_5 M_5)$. The MSSM chiral supermultiplets are confined to the visible four dimensional brane which are separated from the fifth dimension by a 5D bulk. One type of model assumes that the gauge multiplets propagate in the bulk and thus transmit the breaking of SUSY from the extra dimension. This is often referred to as *gaugino mediated* SUSY-breaking.

³A theory with local super-Poincaré invariance, similarly to the interpretation of Einstein gravity as gauge theory of local Lorentz invariance, see [17, Chapter 15]

In the case that the gauge multiplets are also confined to the MSSM brane, the SUSY-breaking is entirely governed by supergravity effects leading to AMSB. The name originates from the fact the MSSM soft terms are linked to the violation of a local superconformal invariance (extension of scale - invariance). In certain formulations of supergravity, Newton's - or Planck's - constant is obtained from the vev of a non-dynamical scalar field ϕ , also known as *conformal compensator*. In the presence of spontaneous SUSY-breaking, the auxiliary field F_ϕ of the supermultiplet of ϕ also obtains a vev $\langle F_\phi \rangle \sim m_{3/2}$. Now, there is an anomalous symmetry breaking due to the non-vanishing beta functions and anomalous dimensions which break the superconformal invariance and ultimately lead to the soft breaking terms in the MSSM.

The free parameters are then the universal scalar mass m_0 (necessary in order to prevent tachyonic sleptons), the gravitino mass $m_{3/2}$, $\tan \beta$ and $\text{sgn} \mu$.

3.5.3 GMSB

In the gauge mediated supersymmetry breaking (GMSB) scenario, SUSY-breaking is mediated via gauge interactions from the hidden sector to the observable. Thus scalars with the same quantum numbers obtain the same soft mass in $\mathcal{L}_{\text{SOFT}}$ irrespective of their flavor. The minimal version assumes that the messenger (super-) fields form complete representations of $SU(5)$ which is the simple Lie group with lowest rank containing all SM fields. Since in GMSB the LSP is usually the gravitino, this model is not considered here.

Chapter 4

The Anapole Moment

This chapter focuses on the one-loop induced anapole moment, characterizing the only allowed interaction between a Majorana fermion and a photon.

Many calculations in this chapter have been done with the help of (semi-) automatic computational tools in the MATHEMATICA environment. For the SM, diagram generation has been done using FEYNARTS [32] and further analyzed using FEYN-CALC [33–35]. The expressions have been translated into Passarino-Veltman functions and then analytically simplified using PACKAGE-X [36] which can be linked to the previously mentioned packages using FEYNHELPERS [37]. Feynman diagrams are mostly drawn with the help of TIKZ-FEYNMAN [38].

4.1 Electromagnetic Interactions of Fermions

The effective interaction between fermions ψ_i, ψ_j and a photon γ can schematically be expressed via the diagram in fig. 4.1. In this sense also off-diagonal (transition) interactions are allowed in which $\psi_i \neq \psi_j$. In this work however, after discussing the general case briefly, we will assume diagonal interactions with $\psi_i = \psi_j$.

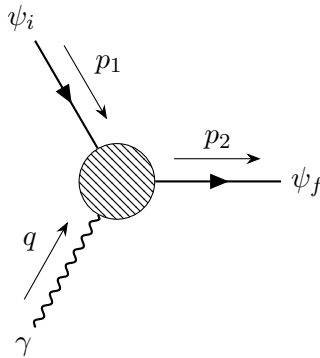


Figure 4.1: Schematic representation of the effective interaction between a fermion and photon

For now, let's assume that ψ_i and ψ_f are massive Dirac fermions, and discuss the Majorana case later. The corresponding effective interaction is described by the matrix element [39]

$$\langle \psi_i | j_\mu^{\text{eff}}(0) | \psi_f \rangle = \bar{u}_f(p_f) M_\mu^{fi}(p_i, p_f) u_i(p_i) \quad (4.1)$$

where $j_\mu^{\text{eff}}(x)$ is the effective current and

$$M_\mu^{fi}(q) = (\gamma_\mu - q_\mu \not{q}/q^2) \left[f_Q^{fi}(q^2) + f_A^{fi}(q^2) q^2 \gamma_5 \right] - i \sigma_{\mu\nu} q^\nu \left[f_M^{fi}(q^2) + i f_E^{fi}(q^2) \gamma_5 \right] \quad (4.2)$$

is the only decomposition of linearly independent terms in the basis

$$\Gamma_i = \{1, \gamma_\mu, i\gamma_5, \gamma_\mu \gamma_5, \sigma_{\mu\nu} \equiv i[\gamma_\mu, \gamma_\nu]/2\} \quad (4.3)$$

for which

$$\Gamma_i^\dagger = \gamma^0 \Gamma_i \gamma^0. \quad (4.4)$$

Additionally the matrix element satisfies the hermitian condition

$$M_\mu^{fi}(q) = \gamma^0 [M_\mu^{if}(-q)]^\dagger \gamma^0. \quad (4.5)$$

The coefficients $f_Q(q^2)$, $f_M(q^2)$, $f_E(q^2)$ and $f_A(q^2)$ are the charge-, dipole magnetic-, dipole electric- and anapole form factor respectively. In the limit of an on-shell photon, $q^2 \equiv (p_f - p_i)^2 \rightarrow 0$, these form factors reduce to the following quantities:

$$\begin{aligned} f_Q^{fi}(0) &= q_{fi} && \text{charge,} \\ f_M^{fi}(0) &= \mu_{fi} && \text{magnetic moment,} \\ f_E^{fi}(0) &= \epsilon_{fi} && \text{electric moment,} \\ f_A^{fi}(0) &= a_{fi} && \text{anapole moment.} \end{aligned}$$

Due to the hermitian property of the matrix element in eq. (4.1), also the form factors have to be hermitian, e.g. $f_\Omega^{fi} = (f_\Omega^{if})^*$ for $\Omega = Q, M, E, A$. Assuming, that the theory is invariant under a CP transformation, one obtains further constraints on the form factors, namely

$$f_\Omega^{fi} = f_\Omega^{if} = (f_\Omega^{fi})^* \quad \text{for } \Omega = Q, M, A \quad (4.6a)$$

$$f_E^{fi} = -f_E^{if} = -(f_E^{fi})^*. \quad (4.6b)$$

In the presence of an external electromagnetic field the non-relativistic Hamiltonian for the diagonal interaction reads (see also appendix A)

$$\mathcal{H} \sim -\boldsymbol{\mu}(\boldsymbol{\sigma} \cdot \mathbf{B}) - \boldsymbol{\epsilon}(\boldsymbol{\sigma} \cdot \mathbf{E}) - a(\boldsymbol{\sigma} \cdot \nabla \times \mathbf{B}). \quad (4.7)$$

Note that the form factors in eq. (4.2) do not necessarily correspond to the coefficients in the classical multipole expansion. In particular the anapole moment does not have a classical counterpart, but coincides with the toroidal moment in the on-shell limit with $m_i = m_f$ instead, see appendix A.

If the particles ψ_i and ψ_f are not Dirac fermions, but Majorana fermions instead, even more constraints on the amplitude M_μ^{if} emerge. The Majorana nature manifests itself in the condition

$$\psi_k = \psi_k^c \equiv \mathcal{C}\bar{\psi}_k^T, \quad (4.8)$$

viz. the particle is its own anti-particle. Here \mathcal{C} is the charge conjugation matrix satisfying

$$\mathcal{C}^\dagger = \mathcal{C}^{-1}, \quad \mathcal{C}^T = -\mathcal{C}, \quad \mathcal{C}^{-1}\Gamma_i\mathcal{C} = \eta_i\Gamma_i^T, \quad (4.9)$$

with

$$\eta_i = \begin{cases} +1 & \text{for } \Gamma_i = 1, i\gamma_5, \gamma_\mu\gamma_5 \\ -1 & \text{for } \Gamma_i = \gamma_\mu, \sigma_{\mu\nu}. \end{cases} \quad (4.10)$$

In this case, the matrix element takes the form

$$\langle \psi_f | j_\mu^{\text{eff}}(0) | \psi_i \rangle = \bar{u}_f(p_f) M_\mu^{fi}(p_i, p_f) u_i(p_i) - \bar{v}_i(p_i) M_\mu^{if}(p_f, p_i) v_f(p_f) \quad (4.11a)$$

$$= \bar{u}_f(p_f) \left[M_\mu^{fi}(p_i, p_f) + \mathcal{C}[M_\mu^{if}(p_i, p_f)]^T \mathcal{C}^\dagger \right] u_i(p_i), \quad (4.11b)$$

where the second term in eq. (4.11a) originates from the antifermion contribution. With

$$\widetilde{M}_\mu^{fi} := M_\mu^{fi} + \mathcal{C}[M_\mu^{if}(p_i, p_f)]^T \mathcal{C}^\dagger \quad (4.12)$$

one obtains the matrix for the effective Majorana vertex interaction

$$\widetilde{M}_\mu = (\gamma_\mu - q_\mu \not{q} / q^2) \left[\widetilde{f}_Q(q^2) + \widetilde{f}_A(q^2) q^2 \gamma_5 \right] - i\sigma_{\mu\nu} q^\nu \left[\widetilde{f}_M(q^2) + i\widetilde{f}_E(q^2) \gamma_5 \right] \quad (4.13)$$

with matrices \widetilde{f}_Ω satisfying

$$\widetilde{f}_\Omega = -\widetilde{f}_\Omega^T = -\widetilde{f}_\Omega^* \quad \text{for } \Omega = Q, M, E \quad (4.14a)$$

$$\widetilde{f}_A = \widetilde{f}_A^T = \widetilde{f}_A^*. \quad (4.14b)$$

In particular this means that for a Majorana fermion the only non-vanishing diagonal form factor is the anapole form factor. Since in this work we are mainly interested in the diagonal form factors, we will only consider $i = f$ from now on.

In order to obtain a certain form factor from a given amplitude, it is useful to make use of the fact that the Γ_i make up a basis. For this, we follow the vertex

conventions of [36, 40] and reparameterize eq. (4.2) in terms of the dimensionless coefficients F_i and G_i as

$$M_\mu(q) = F_1(q^2\gamma_\mu - \gamma_\mu\not{q}) + F_2\frac{iq_\nu\sigma^{\mu\nu}}{2m} + F_3\frac{2q_\mu}{2m} + G_1(q^2\gamma_\mu - \gamma_\mu\not{q})\gamma_5 + G_2\frac{iq_\nu\sigma^{\mu\nu}\gamma_5}{2m} + G_3\frac{2q_\mu\gamma_5}{2m}, \quad (4.15)$$

where p_1 (p_2) is the momentum of the incoming (outgoing) fermion and m is their mass. Comparing this equation to eq. (4.1), note that the anapole form factor is given by

$$f_A(q^2) \equiv G_1. \quad (4.16)$$

We can define a projection operator

$$\mathcal{P}^\mu := (\not{p}_1 + m) \left((f_1 + g_1\gamma_5)\gamma^\mu + (f_2 + g_2\gamma_5)\frac{(p_1 + p_2)^\mu}{2m} + (f_3 + g_3\gamma_5)\frac{q^\mu}{m} \right) (\not{p}_2 + m). \quad (4.17)$$

where the brackets $(\not{p}_i + m)$ on the left- and right side substitute for the spinors $\bar{u}(p_f)$ and $u(p_i)$ respectively, enforcing e.g. $\not{p}u(p, s) = mu(p, s)$. In order to obtain the coefficients f_i and g_i , we calculate

$$\text{tr}[\mathcal{P}^\mu M_\mu] \stackrel{!}{=} \{a F_i \text{ or } G_i\}. \quad (4.18)$$

and solve the resulting set of equations. For the anapole moment we obtain

$$\mathcal{P}_{G_1}^\mu = (\not{p}_1 + m) \left(-\frac{mq^\mu\gamma_5}{(D-2)q^4(4m^2 - q^2)} - \frac{\gamma^\mu\gamma_5}{2(D-2)q^2(4m^2 - q^2)} \right) (\not{p}_2 + m). \quad (4.19)$$

Since we work with dimensional regularization in $D = 4 - 2\epsilon$ dimensions, the trace technique requires a scheme for the treatment of the γ_5 appearing. Here, we mostly used naive dimensional regularization, and checked the expressions with both the Breitenlohner-Maison-t'Hooft-Veltman scheme (BMHV) [41, 42] and the Larin scheme [43]. The surrounding problematic and some schemes are discussed in appendix B.

4.2 The SM Neutrino Charge Radius and Anapole Moment

Historically the calculation of the neutrino charge radius has been faced with various serious problems regarding its finiteness and gauge independence [44–46]. Before we address a solution in the context of the Pinch-Technique/Background Field Method in section 4.3, we will revisit the origin of the issue at hand briefly.

The electromagnetic vertex of the (massless) SM Dirac neutrino can be parameterized using the single Dirac form factor $f_D(q^2)$ the following way [39, 47, 48]

$$M_\mu(q) = f_D(q^2)\gamma_\mu(1 + \gamma_5) \quad (4.20)$$

Comparing this expression with eq. (4.2), we can infer for the charge- and anapole form factor that

$$f_Q(q^2) = f_D(q^2), \quad f_A(q^2) = f_D(q^2)/q^2. \quad (4.21)$$

Alternatively, we can write down the EM vertex directly [49] as

$$M_\mu(q) = (\gamma_\mu q^2 - q_\mu \not{q}) [f_Q(q^2)/q^2 + f_A(q^2)\gamma_5], \quad (4.22)$$

and not introduce the Dirac form factor.

The charge form factor can be associated with the charge density in momentum space. In particular, in the Breit frame for which $q_0 = 0$ and $|\mathbf{q}| = \sqrt{-q^2}$, the following relationship holds [46, 47]

$$f_Q(q^2) = \int d^3r \rho(r) e^{-i\mathbf{q}\cdot\mathbf{r}} = \int d^3r \rho(r) \frac{\sin(|\mathbf{q}|r)}{|\mathbf{q}|r}. \quad (4.23)$$

Taking the derivative and subsequently the limit $q^2 \rightarrow 0$ we find

$$\lim_{q^2 \rightarrow 0} \frac{df_Q(q^2)}{dq^2} = \int d^3x \rho(r) \frac{r^2}{6} =: \frac{\langle r^2 \rangle}{6}. \quad (4.24)$$

This means, that the charge radius of the neutrino is expressed in terms of the electric form factor $f_Q(q)$ as follows

$$\langle r_{\nu_i}^2 \rangle = 6 \left. \frac{df_Q(q^2)}{dq^2} \right|_{q^2=0}, \quad (4.25)$$

and parallels the calculation of the anapole moment, since

$$a_{\nu_i} = \left. \frac{f_Q(q^2)}{q^2} \right|_{q^2=0} = \left. \frac{df_Q(q^2)}{dq^2} \right|_{q^2=0} \quad (4.26)$$

and thus

$$\langle r_{\nu_i}^2 \rangle = 6a_{\nu_i}. \quad (4.27)$$

Naively speaking, one would project out the Lorentz structure corresponding to the Dirac form factor from the vertex $\nu_i \gamma \rightarrow \nu_k$ at e.g. one loop level and then extract the charge radius. The contributing diagrams are shown in fig. 4.2. For the sake of simplicity we will only look at the diagonal case $i = k$ from now on.

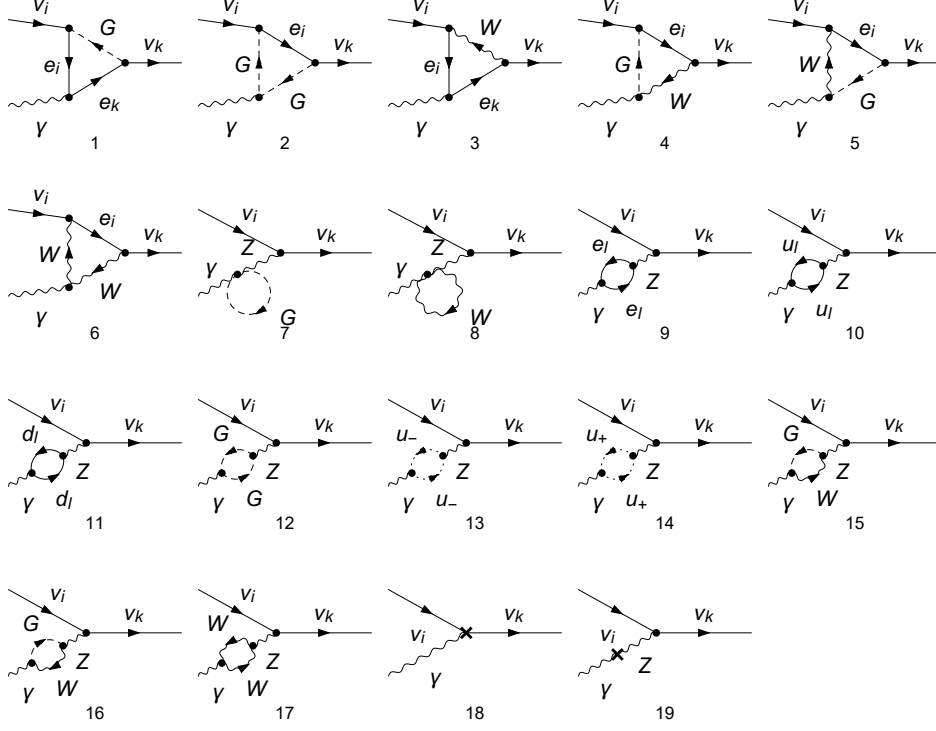


Figure 4.2: Diagrams used for the naive calculation of the SM neutrino anapole moment

The counterterms appearing in diagram 18 and 19 of fig. 4.2 are needed in order to render the amplitude UV-finite when all particles are taken to be on-shell. One way this can be achieved is by using the on-shell renormalization scheme, which is mathematically formulated in terms of certain renormalization conditions [50]. In the case here, the field renormalization constants δZ_{AZ} and δZ_{ZA} appear, which are the off diagonal elements in the renormalization matrix of the neutral gauge bosons,

$$\begin{pmatrix} Z_0 \\ A_0 \end{pmatrix} = \begin{pmatrix} Z_{ZZ}^{1/2} & Z_{ZA}^{1/2} \\ Z_{AZ}^{1/2} & Z_{AA}^{1/2} \end{pmatrix} \begin{pmatrix} Z \\ A \end{pmatrix} = \begin{pmatrix} 1 + \frac{1}{2}\delta Z_{ZZ} & \frac{1}{2}\delta Z_{ZA} \\ \frac{1}{2}\delta Z_{AZ} & 1 + \frac{1}{2}\delta Z_{AA} \end{pmatrix} \begin{pmatrix} Z \\ A \end{pmatrix}, \quad (4.28)$$

connecting the bare fields Z_0 and A_0 to their renormalized counterparts Z and A respectively. The on-shell renormalization conditions involving δZ_{AZ} and δZ_{ZA} read

$$\text{Re} \hat{\Gamma}_{\mu\nu}^{AZ}(k) \varepsilon^\nu(k) \Big|_{k^2=m_Z^2} = 0, \quad \hat{\Gamma}_{\mu\nu}^{AZ}(k) \varepsilon^\nu(k) \Big|_{k^2=0} = 0, \quad (4.29)$$

or, equivalently

$$\text{Re} \hat{\Sigma}_T^{AZ}(M_Z^2) = 0, \quad \hat{\Sigma}_T^{AZ}(0) = 0. \quad (4.30)$$

Here, Σ_T^{AZ} is the transverse part in the renormalized (hatted quantities) irreducible two point function, e.g.

$$\begin{aligned}
 A_\mu \xrightarrow{k} \text{---} \text{---} \text{---} \text{---} Z_\nu &\equiv \hat{\Gamma}_{\mu\nu}^{AZ}(k) \\
 &= -i \left(g_{\mu\nu} - \frac{k_\mu k_\nu}{k^2} \right) \hat{\Sigma}_T^{AZ}(k^2) - i \frac{k_\mu k_\nu}{k^2} \hat{\Sigma}_L^{AZ}(k^2). \quad (4.31)
 \end{aligned}$$

Then the renormalization constants can be calculated in terms of the unrenormalized (unhatted) self energies as

$$\delta Z_{AZ} = -2 \operatorname{Re} \frac{\Sigma_T^{AZ}(M_Z^2)}{M_Z^2}, \quad \delta Z_{ZA} = 2 \frac{\Sigma_T^{AZ}(0)}{M_Z^2}. \quad (4.32)$$

With these renormalization constants the amplitude corresponding to the sum of the diagrams in fig. 4.2 is indeed finite and well defined in the on-shell limit. Explicitly the counterterm diagrams evaluate to

$$(\text{CTs}) = e \frac{q^\mu \not{q} P_L [(q^2 - \xi_Z m_Z^2) \delta Z_{AZ} + (q^2 - m_Z^2) \delta Z_{ZA}] + \gamma_\mu P_L q^2 (m_Z^2 - q^2) \delta Z_{AZ}}{4c_w s_w (q^2 - m_Z^2)(q^2 - \xi_Z m_Z^2)}, \quad (4.33)$$

While the UV-part of of the amplitude $M_{\nu \rightarrow \gamma \nu}^\mu$ is vanishing in the on-shell limit, the appearing Lorentz structure allows for a non-zero contribution to the anapole moment:

$$f_A(0) \Big|_{\text{UV}} = e^3 \frac{(27\xi_w - 185) m_W^2 - 85m_Z^2}{3456\pi^2 c_w^2 s_w^4 m_Z^4} \frac{1}{\epsilon_{\text{UV}}}. \quad (4.34)$$

This inevitable means that the anapole moment is not physical and not measurable since it is not only explicitly gauge parameter dependent, but also UV-divergent; both non-physical properties. This has also been realized in the literature and lead to many attempts to solve the issue of an unphysical neutrino anapole moment/charge radius [45, 51–57]. In particular it was discovered that similar UV-divergent and gauge dependent expression are found when embedding the vertex into a $\psi_1 \psi_2 \rightarrow \psi_1 \psi_2$ process (e.g. neutrino-electron scattering) and looking at other topologically distinct diagrams, e.g. box diagrams. Since the overall amplitude does behave physical, the question was if this cancellation between vertex- and box diagrams can be formalized and ultimately if proper, physical off-shell vertex functions can be defined in a non ad-hoc manner. The answer turns out to be yes and the fundamentals are going to be addressed in the next section.

4.3 The Pinch-Technique and the Background Field Method

Before we examine the anapole form factor and anapole moment further, it is important to investigate the Pinch-Technique (PT) and the Background Field Method

(BFM) in order to understand the historical issues surrounding the calculation of the anapole moment [45, 51–60]. In particular the calculation of the neutrino charge radius (and thus the anapole moment) within the Standard Model lead to serious issues finding a subamplitude satisfying simultaneously gauge-invariance, finiteness and target-independence as demonstrated in the previous section.

Following the arguments of [58], it is well known that in the standard QFT procedure, one starts with a quantized Lagrangian including a gauge fixing term to remove redundant degrees of freedom. This gauge fixing term allows a proper mathematical treatment of the theory, in the sense, that Feynman rules can be derived consistently. However, this method introduces new redundancies, e.g. individual off-shell Green functions may explicitly depend on the gauge fixing parameter, have unphysical thresholds etc. It is clear however from the Becchi-Rouet-Stora-Tyutin (BRST) invariance that for physical quantities, like the S matrix, these unphysical effects will eventually be absent due to internal cancellations. A related topic are the relatively recent developments in the context of on-shell scattering amplitudes [61], in which the calculation of Feynman diagrams can be avoided altogether. Thus intermediate cancellations of unphysical terms stemming from different contributions are absent to begin with. Nevertheless for the calculation of individual sub-amplitudes and form factor one has to deal with unphysical redundancies.

The PT is a diagrammatic algorithm which allows the construction of off-shell Green functions in non-Abelian gauge theories which are gauge-invariant and independent of the gauge-fixing parameters [58, 62]. Furthermore, these Green functions satisfy ghost-free Ward identities similar to Green functions in Abelian theories. The PT makes use of certain longitudinal momenta inside box- and vertex diagrams whose structure is propagator-like and thus can be reassigned to self-energy diagrams. It was noticed that effective Green functions satisfying QED-like Ward identities can also be constructed in the context of the Background Field Method (BFM). In fact, the PT coincides with the BFM for a special choice of the quantum gauge fixing parameter: $\xi_Q = 1$ [58, 59, 63, 64]. Thus, it is not necessary to use the diagrammatic algorithm of rearranging certain terms, and can work with the BFM instead in order to calculate gauge invariant off-shell quantities. In particular, for the calculation of the anapole moment in a non-Abelian theory, only a minimal alternation of the standard Feynman rules has to be carried out, see appendix C.2.

4.4 General Anapole Moment for Majorana Fermions

In this section we will derive two contributions to the anapole moment stemming from scalar and vector fields present in the one-loop Feynman diagrams. Subsequently, this general result will be applied to the SM neutrino anapole moment in section 4.5 and we will find a gauge independent and finite expression. A further

numerical evaluation is presented in chapter 6. For the calculation, the conventions of [25, 65] are used, supplemented by the treatment of Feynman rules involving fermion-number-violating interactions by Denner et. al. [66, 67] which are summarized in appendix C.1.

For a generic Majorana fermion, all diagrams as shown in fig. 4.3 may contribute to the anapole form factor. Note that $\hat{\gamma}$ is the background field photon due to the fact that we work in the background field gauge with quantum gauge parameter $\xi_Q = 1$. The Majorana fermion interaction vertices are parameterized via the Lagrangians

$$\mathcal{L}_{\text{FFS}} = \bar{\chi} [c_L P_L + c_R P_R] \tilde{f}^* f + \text{h.c.}, \quad (4.35a)$$

$$\mathcal{L}_{\text{FFV}} = V_\mu^- \bar{\chi} \gamma_\mu [v_L P_L + v_R P_R] \chi^+ + \text{h.c.}, \quad (4.35b)$$

where χ is a neutralino-like Majorana fermion, f and χ^+ are Dirac fermions, \tilde{f} is a scalar and V_μ^- is a vector field. The symbols are chosen in accordance to the later application within the MSSM, in which χ is the lightest neutralino, serving as DM candidate, f are SM fermions, \tilde{f} their respective supersymmetric spin-0 partners and $V_\mu^- = W_\mu^-$ is the weak gauge boson. The field χ^+ is identified with the chargino, the mass eigenstate of the mixed charged gauge- and Higgs bosons, see chapter 3.

As mentioned before, since the underlying theory may be non-Abelian, one has to either use the PT or the BFM replacing the quantum photon with the background photon in the background Feynman gauge. Here, the latter approach is used rendering the form factor gauge independent and finite. Effectively, the triple gauge vertex and the neutralino - Goldstone - gauge boson vertex are replaced by their respective background counterparts. The Feynman rules are listed in appendix C.2 and are based on the BFM SM rules by Denner et. al. [60]

Applying the Feynman rules to the diagrams in fig. 4.3 and using the momentum assignment of fig. 4.1, we obtain for the scalar contributions

$$(a) = i^6 \int \frac{(c_L P_L + c_R P_R) [\not{k} + \not{p}_2 + m_f] [-e Q_f \gamma_\mu] [\not{k} + \not{p}_1 + m_f] [c_L^* P_R + c_R^* P_L]}{\left((k + p_2)^2 - m_f^2 \right) \left((k + p_1)^2 - m_f^2 \right) (k^2 - M_{\tilde{f}}^2)} + \text{rev.} \quad (4.36)$$

$$(b) = i^6 \int \frac{(c_L P_L + c_R P_R) [\not{k} + \not{p}_2 + m_f] [c_L^* P_R + c_R^* P_L] [-e Q_{\tilde{f}} (2k + q)_\mu]}{\left((k + p_2)^2 - m_f^2 \right) \left((k + q)^2 - M_{\tilde{f}}^2 \right) (k^2 - M_{\tilde{f}}^2)} + \text{rev.} \quad (4.37)$$

and similarly for the vector contributions

$$(c) = i^6 \int \frac{\gamma_\beta [v_L P_L + v_R P_R] [\not{k} + \not{p}_2 + m_f] [-e \gamma_\mu]}{\left((k + p_2)^2 - m_{\chi^+}^2 \right) \left((k + p_1)^2 - m_{\chi^+}^2 \right) (k^2 - m_V^2)} \times \\ \times [\not{k} + \not{p}_1 + m_{\chi^+}] \gamma_\alpha [v_L^* P_L + v_R^* P_R] [-g^{\alpha\beta}] + \text{rev.} \quad (4.38)$$

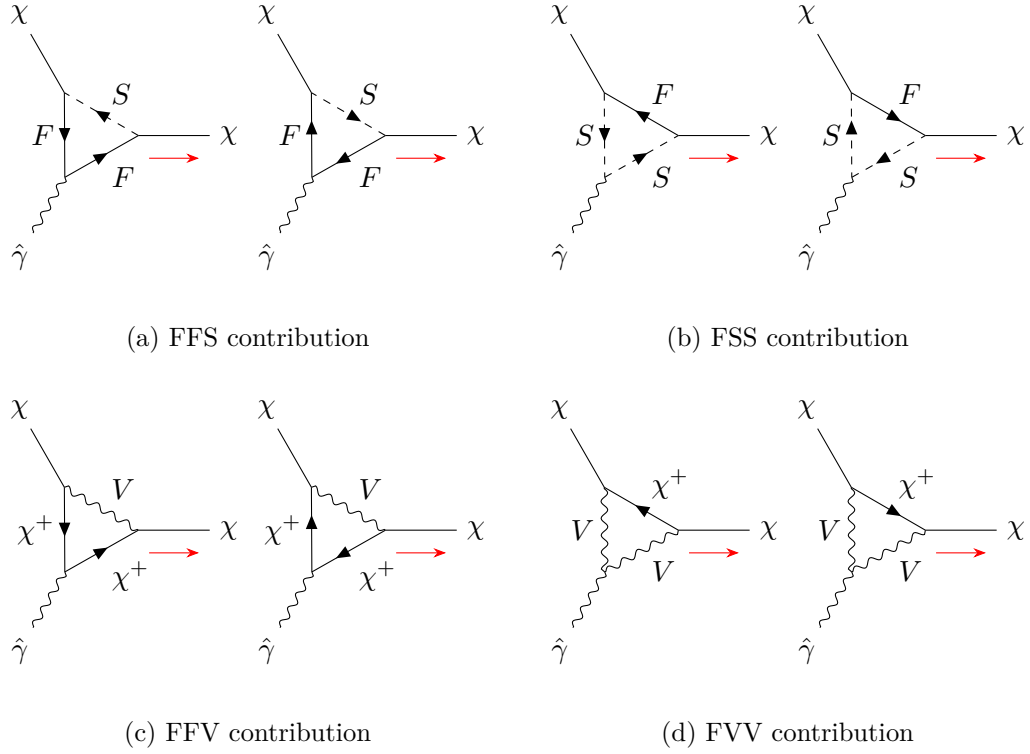


Figure 4.3: Fermion-Fermion-Scalar (FFS), Fermion-Scalar-Scalar (FSS), Fermion-Fermion-Vector (FFV) and Fermion-Vector-Vector (FVV) contributions to the anapole form factor. The red arrow defines the fermion flow. **01.02.2022: the fermions in the scalar diagrams also have to be positively charged to be consistent with the defined fermion flow**

and

$$\begin{aligned}
 (d) = i^6 \int \frac{\gamma_\beta [v_L P_L + v_R P_R] [\not{k} + \not{p}_2 + m_{\chi^+}] \gamma_\alpha [v_L^* P_L + v_R^* P_R] [-g^{\alpha\rho}]}{((k+q)^2 - m_V^2)((k+p_2)^2 - m_{\chi^+}^2)(k^2 - m_V^2)} \times \\
 \times [-e] [g_{\nu\rho}(-2k-q)_\mu - 2g_{\mu\nu}q_\rho + 2g_{\rho\mu}q_\nu] [-g^{\nu\beta}] + rev. \quad (4.39)
 \end{aligned}$$

where *rev.* symbolizes the respective second diagram in fig. 4.3 which has *reversed* propagators and vertices due to the fact that the fermion flow has opposite direction to the charge flow. The integration sign is shorthand for $\int \equiv \int \frac{d^4 k}{(2\pi)^4}$. Then, after multiplication with the anapole projector, taking the trace, setting $Q_{\tilde{f}} = Q_f$ and $q^2 \rightarrow 0$, we obtain the following scalar- and vector contribution to the anapole moment: **20.12.2022 this is in accordance with Ryo's result; compare the definition**

of \mathcal{F}_S in the resulting paper of this thesis: here \mathcal{F}_S was redefined. This however gives the opposite sign compared to Kopp et al. Sandick's notation is a little weird though (additional factor of i ?)

$$A_S \equiv a_{(a)+(b)} = \frac{e}{96\pi^2 m_\chi^2} Q_f \left[|c_L|^2 - |c_R|^2 \right] \mathcal{F}_S(\mu, \eta) \quad (4.40a)$$

$$A_V \equiv a_{(c)+(d)} = -\frac{e}{48\pi^2 m_\chi^2} \left[|v_L|^2 - |v_R|^2 \right] \mathcal{F}_V(\mu, \eta_V) \quad (4.40b)$$

where the functions $\mathcal{F}_{S/V}$ are defined as

$$\mathcal{F}_S(\mu, \eta) = \frac{3}{2} \log\left(\frac{\eta^2}{\mu^2}\right) - (3\eta^2 - 3\mu^2 + 1)f(\mu, \eta), \quad (4.41a)$$

$$\mathcal{F}_V(\mu, \eta_V) = \frac{3}{2} \log\left(\frac{\mu^2}{\eta_V^2}\right) + (3\eta_V^2 - 3\mu^2 - 7)f(\mu, \eta_V), \quad (4.41b)$$

with $\mu = m_f/m_\chi$, $\eta = M_{\tilde{f}}/m_\chi$, $\eta_V = m_V/m_\chi$ and

$$\begin{aligned} f(\mu, \eta) &= \frac{1}{2} \int_0^1 \frac{dx}{x\eta^2 + (1-x)\mu^2 - x(1-x)} \\ &= \begin{cases} \frac{1}{\sqrt{\Delta}} \operatorname{arctanh}\left(\frac{\sqrt{\Delta}}{\mu^2 + \eta^2 - 1}\right) & \Delta > 0 \\ \frac{1}{\sqrt{|\Delta|}} \operatorname{arctan}\left(\frac{\sqrt{|\Delta|}}{\mu^2 + \eta^2 - 1}\right) & \Delta < 0 \\ \frac{2}{(\mu^2 - \eta^2)^2 - 1} & \Delta = 0 \end{cases} \end{aligned} \quad (4.42)$$

with $\Delta \equiv \Delta(\mu, \eta) = (\mu^2 + \eta^2 - 1)^2 - 4\mu^2\eta^2$. The mass m_f is understood to be the mass of the circulating fermion, e.g. SM fermion-like for the scalar- and chargino-like for the vector contribution respectively. Note that the limit $q^2 \rightarrow 0$ is only applicable if $q^2 \ll m_f^2$. In particular for direct detection experiments in which the typical momentum transfer from DM to nucleus is $\sqrt{|q^2|} \approx 50$ MeV and the mediator couples to the light fermions such as electrons, this limit is not justified [68].

For cases, in which the incoming Majorana fermion is massless, we can expand eqs. (4.40a) and (4.40b) around $m_\chi = 0$ and obtain in leading order

$$A_S(m_f, M_{\tilde{f}}) = eQ_f \left(|c_L|^2 - |c_R|^2 \right) \frac{(m_f^2 + 2M_{\tilde{f}}^2) \log\left(m_f^2/M_{\tilde{f}}^2\right) + 3(M_{\tilde{f}}^2 - m_f^2)}{96\pi^2(m_f^2 - M_{\tilde{f}}^2)^2}, \quad (4.43a)$$

$$A_V(m_f, m_V) = e \left(|v_L|^2 - |v_R|^2 \right) \frac{(5m_f^2 - 2m_V^2) \log\left(m_f^2/m_V^2\right) + 3(m_V^2 - m_f^2)}{48\pi^2(m_f^2 - m_V^2)^2}. \quad (4.43b)$$

As before, for A_V the fermion mass is given by the chargino-like particle $m_f = m_{\chi^+}$. Further, we can take the limit in which the fermion and boson are mass-degenerate (MR 2021/09/13 there seems to be a factor of 7 missing):

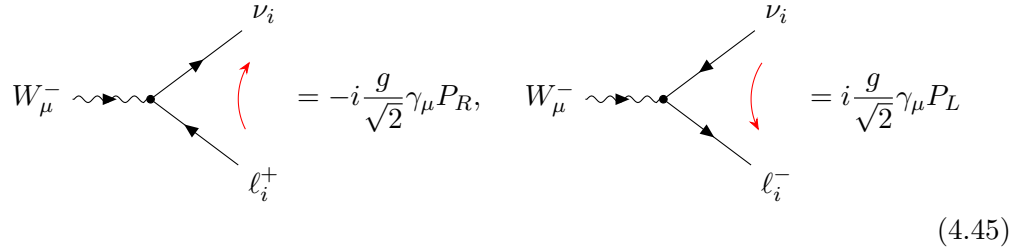
$$\lim_{M_{\tilde{f}} \rightarrow m_f} A_S(m_f, M_{\tilde{f}}) = -eQ_f \left(|c_L|^2 - |c_R|^2 \right) \frac{1}{192\pi^2 m_f^2}, \quad (4.44a)$$

$$\lim_{m_V \rightarrow m_f} A_V(m_f, m_V) = e \left(|v_L|^2 - |v_R|^2 \right) \frac{1}{96\pi^2 m_f^2}. \quad (4.44b)$$

Although this limit does not play a role for the studies of DM, it is relevant for checking the supersymmetric limit of the MSSM, in which the anapole moment is expected to vanish.

4.5 The SM Neutrino Charge Radius: Revisited

With the general results for the anapole moment of a Majorana fermion with (non-Abelian) vector- and scalar couplings derived in the last section, we can revisit the calculation of the neutrino charge radius of section 4.2. Note that the anapole moment of a Dirac fermion can be calculated using the previous results due to the fact that $a_{\text{Dirac}} = \frac{1}{2}a_{\text{Majorana}}$ [69]. For this, we set χ (χ^+) to be the SM neutrino ν_i (lepton ℓ_i) with $i = e, \mu, \tau$ and vanishing mass. $V_\mu = W_\mu$ is identified with the weak gauge Boson, G^+ the charged Nambu-Goldstone Boson and $\hat{\gamma}$ is the (background) photon. In the BFM framework, most of the diagrams in fig. 4.2 do not contribute. In particular, only diagrams of the type shown in fig. 4.3 have to be calculated which are inherently UV-finite. The necessary interactions are inferred from [50, 70] and read



$$\begin{aligned} W_\mu^- \text{ vertex } (\nu_i, \ell_i^+) &= -i \frac{g}{\sqrt{2}} \gamma_\mu P_R, & W_\mu^- \text{ vertex } (\nu_i, \ell_i^-) &= i \frac{g}{\sqrt{2}} \gamma_\mu P_L \end{aligned} \quad (4.45)$$

with Goldstone vertex similarly. The left vertex shows the interaction as used in the derivation for the anapole expression, while the right vertex is typically used in the literature. Thus the left/right couplings read:

$$W^+ \bar{\nu}_i \ell_j : v_L = 0, \quad v_R = -\frac{g}{\sqrt{2}} \delta_{ij} \quad (4.46a)$$

$$G^+ \bar{\nu}_i \ell_j : c_L = 0, \quad c_R = -\frac{g}{\sqrt{2}} \frac{m_{\ell_i}}{m_W} \delta_{ij} \quad (4.46b)$$

where $g = e/\sin\theta_W$. As apparent, it is expected that the Goldstone diagrams are phenomenologically suppressed¹ due to the $\sim m_{\ell_i}/m_W$ dependency of the coupling.

The vector contribution to the anapole moment reads

$$A_V^i = -\frac{eg^2}{96\pi(m_{\ell_i}^2 - m_W^2)^2} \left[3(m_W^2 - m_{\ell_i}^2) - (2m_W^2 - 5m_{\ell_i}^2) \log \frac{m_{\ell_i}^2}{m_W^2} \right] \quad (4.47a)$$

$$= -\frac{eg^2}{96\pi^2 m_W^2} \left[3 - 2 \log \frac{m_{\ell_i}^2}{m_W^2} \right] + \mathcal{O}\left(\frac{m_{\ell_i}^2}{m_W^2}\right) \quad (4.47b)$$

$$= -\frac{eG_F}{12\sqrt{2}\pi^2} \left[3 - 2 \log \frac{m_{\ell_i}^2}{m_W^2} \right] + \mathcal{O}\left(\frac{m_{\ell_i}^2}{m_W^2}\right) \quad (4.47c)$$

while the Goldstone (scalar) contribution reads

$$A_S^i = -\frac{eg^2}{192\pi(m_{\ell_i}^2 - m_W^2)^2} \frac{m_{\ell_i}^2}{m_W^2} \left[3(m_W^2 - m_{\ell_i}^2) + (2m_W^2 + m_{\ell_i}^2) \log \frac{m_{\ell_i}^2}{m_W^2} \right] \quad (4.48a)$$

$$= -\frac{eg^2}{198\pi^2} \frac{m_{\ell_i}^2}{m_W^4} \left[3 + 2 \log \frac{m_{\ell_i}^2}{m_W^2} \right] + \mathcal{O}\left(\frac{m_{\ell_i}^4}{m_W^4}\right) \quad (4.48b)$$

$$= -\frac{eG_F}{24\sqrt{2}\pi^2} \frac{m_{\ell_i}^2}{m_W^2} \left[3 + 2 \log \frac{m_{\ell_i}^2}{m_W^2} \right] + \mathcal{O}\left(\frac{m_{\ell_i}^4}{m_W^4}\right) \quad (4.48c)$$

with Fermi constant $G_F = \frac{\sqrt{2}g^2}{8m_W^2}$. The anapole moment of the (massless) SM neutrino is the sum of these contributions,

$$A_{\nu_i} = A_V^i + A_S^i \quad (4.49a)$$

$$= -\frac{eG_F}{12\sqrt{2}\pi^2} \left[3 - 2 \log \frac{m_{\ell_i}^2}{m_W^2} \right] + \mathcal{O}\left(\frac{m_{\ell_i}^2}{m_W^2}\right) \quad (4.49b)$$

This result has been crosschecked with the semi-automatic calculation using the MATHEMATICA packages FEYNARTS [32], FEYN CALC [33–35], PACKAGE-X [36] and FEYNHELPERS [37] using the distributed Background SM model file for FeynArts which is based on [60]. The result is in full agreement with the literature (e.g. [39]), taking into account the factor of 2 due to the Dirac nature of the neutrino, the conversion factor between charge radius and anapole moment as in eq. (4.27), and lastly a factor of $-e$ due to a different vertex parametrization. Then, the anapole moment in terms of charge radius reads

$$A_{\nu_i} = 2 \times \frac{1}{6} \times (-e) \times \langle r_{\nu_i}^2 \rangle_{\text{lit}}. \quad (4.50)$$

¹Note that this is model-dependent

The relative sign between anapole moment and charge radius varies in the literature, since the definition of the interaction vertex is ambiguous. In particular, the relative position of γ_μ and γ_5 and thus indirectly the definition/sign of the anapole form factor can alter.

Coincidentally, this non-standard interaction has recently been studied in the context of the low-energy recoil excess of the XENON1T experiment [71]. Based on this excess, bounds for the magnetic moment, charge radius, milicharge and anapole moment have been derived [72] under the assumption, that only one of the multipoles is present at a time.

Chapter 5

Connection to Direct Detection Experiments

In this section an introduction to direct detection (DD) experiments is given and the connection to the anapole moment is drawn.

5.1 Experiments and Constraints

There are several different approaches and environments where properties of a DM particle can be probed. Apart from indirect searches like gamma-ray and neutrino detection of the Large Area Telescope (LAT) [73] and IceCube [74] respectively, earth based experiments have been build to directly probe traces of DM particles scattering with nuclei. These type of experiments are called direct detection (DD) experiments. Searches at colliders like the Large Hadron Collider (LHC) look for missing energy in the spectrum, hinting at states escaping the detector.

Some current- and next-generation DD experiments include PandaX-II [75], LUX [76–78], LUX-ZEPLIN (LZ) [79] and XENONnT [80–83], of which the latter recently observed an excess in the low energy recoil spectrum [71], whose origin is still under debate (see for example [72, 84, 85]).

Baker and Thamm analyzed simplified models of WIMPs on the relic surface with n uncolored slepton-like coannihilation partners η_i with magnetic dipole and anapole couplings to the nuclei and found that for both direct- and indirect detection experiments the limits on the parameter space depend strongly on whether the WIMP is a Dirac- or Majorana fermion [69]. In contrast to the Dirac WIMP scenario, whose parameter space is excluded for $m_\chi < 2 \text{ TeV}$ and separately for $m_\eta/m_\chi - 1 < 0.1$ by XENON1T and can be tested fully with DARWIN [86] prospects, the parameter space for the Majorana WIMP is unconstrained and only $\sim 10\%$ is expected to be probed by DARWIN. However, these estimates strongly dependent on the coannihilation process, both via the number of partners η_i and the mass splitting between the DM particle and η_i . Enhancing coannihilations either by increasing the number of partners or by decreasing the splitting makes DD a favorable framework for probing the parameter space particularly for small mass splittings.

Current indirect detection experiments are sensitive to Dirac WIMPs only due to velocity suppression of the Majorana annihilation cross section. The strongest constraints are expected from CTA [87] probing masses $m_\chi \lesssim 5 \text{ TeV}$ for $0 \lesssim m_\eta/m_\chi - 1 \lesssim 0.4$.

Future collider searches (like the HE-LHC with $\sqrt{s} = 27 \text{ TeV}$) on the other hand are insensitive to the nature of the WIMP and can probe a significant part of parameter space for $m_\chi \sim 1 \text{ TeV}$ and comparably large mass splittings $0.2 \lesssim m_\eta/m_\chi - 1 \lesssim 0.4$ (see also [88]).

The work by Baker and Thamm focuses on scalar mediators generating the necessary electromagnetic interactions for DD experiments in the form of dipole and anapole moments. For additional vector couplings, the anapole moment may get sizeably enhanced via the novel calculation of A_V in this work such that the prospects of future direct detection experiments become stronger, particularly for Majorana WIMPs.

5.2 Basics of Direct Detection Experiments

As discussed in chapter 2, there is numerous evidence that DM exists on many different scales; in particular on the scale of galaxies. Thus, we can expect that DM also surrounds us and - if it interacts with visible matter in some way - should be detectable. Since we are studying the interactions between a WIMP and the nucleus, we need local information about the WIMP: the local DM density and velocity distribution.

On the scale of galaxies, there are several different models describing the DM halo, including the Navarro-Frenk-White (NFW) profile [89]

$$\rho(r) = \frac{4\rho_s}{(r/r_s)[1 + (r/r_s)]^2} \quad (5.1)$$

and the Einasto profile [90]

$$\rho(r) = \rho_s \exp\left(-\frac{2}{\alpha} \left[\left(\frac{r}{r_s}\right)^\alpha - 1\right]\right), \quad (5.2)$$

where r_s is a scale radius (defined as being the radius, at which the the density profile has a logarithmic slope of -2 [91]), $\rho_s = \rho(r = r_s)$ and for the latter α is the shape in the region $r \approx r_s$.

There are roughly two approaches to determine the local density [92]: (a) local measurements, where the kinematics of nearby stars are taken into account, and (b) global measurements, where the DM density profile is extracted from measurements of galactic rotation curves, and then extrapolated to the earth's location in the Milky

Way. We will work with the well motivated value for the local DM density of [93]

$$\rho_0 = 0.4 \text{ GeV/cm}^3. \quad (5.3)$$

The DM velocity distribution is typically assumed to follow a Maxwell-Boltzmann shape [91]

$$f(\mathbf{v}) = \begin{cases} N^{-1}(\pi v_0^2)^{-3/2} \exp(-|\mathbf{v}|^2/v_0^2) & |\mathbf{v}| < v_{\text{esc}} \\ 0 & |\mathbf{v}| > v_{\text{esc}} \end{cases} \quad (5.4)$$

where $v_0 \approx 220\text{km/s}$ is the most probable speed, e.g. the speed of objects following circular orbits in the Galactic center, $v_{\text{esc}} \approx 550\text{km/s}$ is the escape velocity of the Milky Way: WIMPs with higher velocities are not expected to appear in DD experiments. The normalization constant reads

$$N = \text{erf}\left(\frac{v_{\text{esc}}}{v_0}\right) - \frac{2v_{\text{esc}}}{\sqrt{\pi}v_0} \exp\left(-\frac{v_{\text{esc}}^2}{v_0^2}\right). \quad (5.5)$$

Then, from the perspective of the earth, the velocity distribution reads

$$f_{\oplus}(\mathbf{v}, t) = f(\mathbf{v}_{\text{obs}}(t) + \mathbf{v}), \quad (5.6)$$

with the velocity of the earth with respect to the halo reading [94]

$$\mathbf{v}_{\text{obs}}(t) = \mathbf{v}_{\text{LSR}} + \mathbf{v}_{\odot, \text{pec}} + \mathbf{V}_{\oplus}(t) \quad (5.7)$$

where $\mathbf{v}_{\odot, \text{pec}} \approx (11, 12, 7)\text{km/s}$ denotes the peculiar velocity of the sun [95], $\mathbf{v}_{\text{LSR}} = (0, v_{\text{rot}}, 0) \approx (0, 220\text{km/s}, 0)$ is the Local Standard of Rest and $\mathbf{V}_{\oplus}(t)$ is the velocity of the earth with respect to the sun with magnitude $V_{\oplus} \approx 30\text{km/s}$ [94]. The latter is expected to inherit an annual modulation due to earth's movement, which gives corrections of $\sim 3\%$ to the rate [96] and is here not considered.

The typical set-up of a DD experiment involves the measurement of the recoil energy of heavy nuclei caused by elastic scatterings $\chi N \rightarrow \chi N$ with corresponding differential rate of scattering events [97]

$$\frac{dR}{dE_R} = \frac{\rho_0}{m_{\chi}m_N} \int_{v_{\text{min}}}^{\infty} d^3v \frac{d\sigma_{\chi N}}{dE_R} v f_{\oplus}(\mathbf{v}, t), \quad (5.8)$$

where $\frac{d\sigma_{\chi N}}{dE_R}$ is the differential cross section. The scattering rate is usually given in terms of counts per day, per kg of target material, per keV recoil energy. The overall expected events are then given by [98],

$$N_p = MT \int_0^{\infty} dE_R \phi(E_R) \frac{dR}{dE_R}, \quad (5.9)$$

where M , T and $\phi(E_R)$ are respectively the detector mass, exposure time and detector response function and depend on the experiment.

The (differential) cross section is usually classified by a combination of a spin dependent (SD) and a spin independent contribution (SI) corresponding to the type of effective WIMP-nucleus interaction vertex. Subsequently the differential cross section in terms of $q^2 = 2m_A E_R$ can be written as [97]

$$\frac{d\sigma_{\chi N}}{dq^2}(v, q^2) = \frac{d\sigma_{\chi N}^{\text{SD}}}{dq^2}(v, q^2) + \frac{d\sigma_{\chi N}^{\text{SI}}}{dq^2}(v, q^2). \quad (5.10)$$

Here we will focus on elastic scattering only.

5.3 Standard SI and SD Contributions

Typical types of interaction models are the axial-vector coupling $\chi\gamma_\mu\chi\bar{q}\gamma^\mu q$ and scalar coupling $\bar{\chi}\chi\bar{q}q$ representing a SD and SI cross section respectively (see [99] for a full list and [100] for a selection of differential cross sections).

For the scalar- and axial-vector coupling the differential cross section for elastic scattering can be separated into a spin-independent (SI) and spin-dependent (SD) part [101, 102],

$$\frac{d\sigma_{\chi N}}{dE_R} = \frac{m_N}{2\mu_A^2 v^2} \left(\sigma_0^{\text{SI}} \cdot F_{\text{SI}}^2(E_R) + \sigma_0^{\text{SD}} \cdot F_{\text{SD}}^2(E_R) \right), \quad (5.11)$$

where μ_A is the reduced mass of the WIMP-nucleus system, m_N the nucleus mass and $\sigma_0^{\text{SI/SD}}$ is the cross section at zero momentum transfer. For the SI contribution, this cross section reads

$$\sigma_0^{\text{SI}} = \sigma_p \frac{\mu_A^2}{\mu_p^2} [Z \cdot f^p + (A - Z) \cdot f^n]^2, \quad (5.12)$$

where $f^{p(n)}$ are the relative couplings to the proton (neutron) of the nucleus and μ_p is the reduced mass of the WIMP-nucleon system. In many cases, the scalar coupling to the neutron and proton are very similar, viz. $f^n \approx f^p$ is often assumed (sometimes called *isospin conservation*). Then, the SI cross section reads

$$\sigma_0^{\text{SI}} = \sigma_p \frac{\mu_A^2}{\mu_p^2} A^2. \quad (5.13)$$

As evident, the SI cross section scales with the square of the number of nucleons A , such that heavier target materials like $^{129,131}\text{Xe}$ are expected to have comparatively high cross sections. The SI form factor can be taken to be the Helm form factor [96, 101, 102]

$$F_{\text{SI}}(E_R) = 3e^{-q^2 s^2/2} [\sin(qr) - qr \cos(qr)] / (qr)^3, \quad (5.14)$$

with $q = \sqrt{2m_N E_R}$, $s = 1$ fm, $r = \sqrt{R^2 - 5s^2}$, $R = 1.2A^{1/2}$ fm with A the nuclear mass number.

The SD cross section on the other hand can be expressed as

$$\sigma_0^{\text{SD}} = \frac{32\mu_A^2 G_F^2}{\pi} \frac{J+1}{J} \cdot [a_p \langle S^p \rangle + a_n \langle S^n \rangle]^2 \quad (5.15)$$

with the Fermi constant G_F , the coupling to the proton (neutron) a_p (a_n), the total nuclear spin J and $\langle S^{p(n)} \rangle$ being the average spin contributions due to the proton (neutron). The SD form factor $F_{\text{SD}}(E_R)$ is given by [103]

$$F_{\text{SD}}(E_R) = \begin{cases} \sin(qR_s)/(qR_s), & qR_s < 2.55, \quad qR_s > 4.5 \\ 0.217, & \text{otherwise} \end{cases} \quad (5.16)$$

with $R_s = A^{1/3}$.

The current experimental limits on the SI cross section σ_p and SD cross sections σ_n and σ_p with a 90% confidence level (C.L.) are obtained using *DDCalc v2.2.0* [98, 104] and shown in fig. 5.1. The experiment and the respective data set used can be inferred from the legend; the LZ data corresponds to a projection.

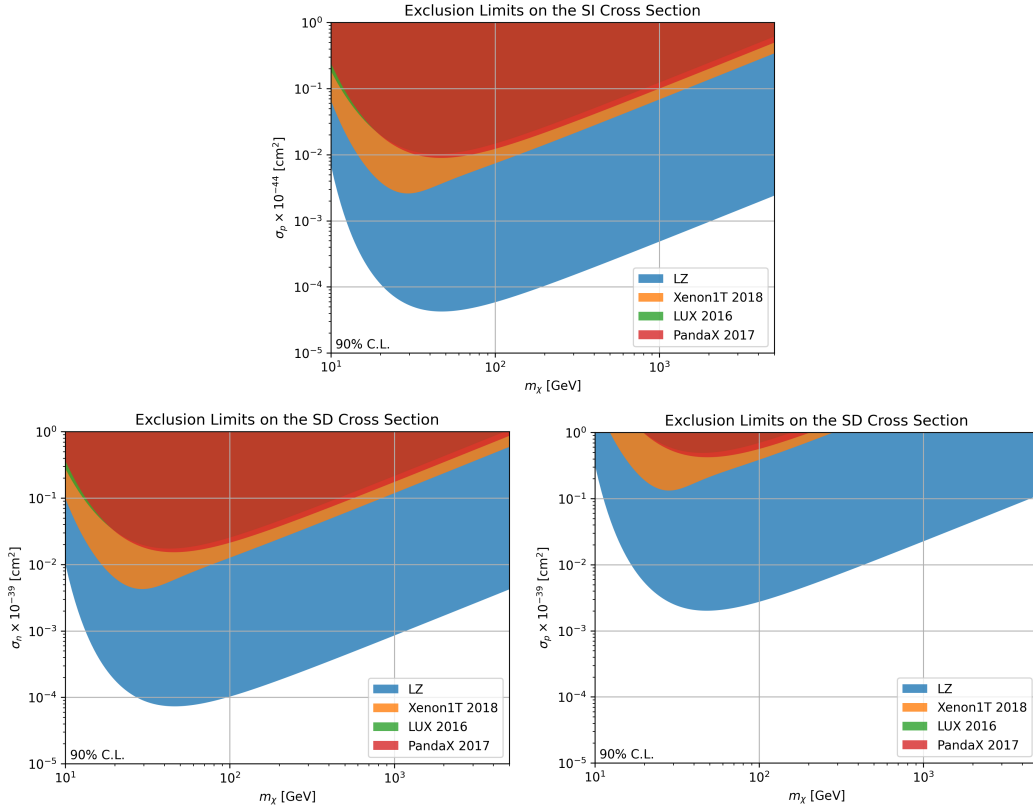


Figure 5.1: Experimental limits on the spin independent cross section σ_p (top) and spin dependent cross sections σ_n (bottom left) and σ_p (bottom right) of WIMP-nucleon scattering on a 90% confidence level

5.4 Magnetic Dipole Interaction

One class of studied interaction models is that of a loop induced electromagnetic dipole interaction between a Dirac WIMP and the nucleus [103, 105, 106]. The magnetic dipole coupling is described by the effective Lagrangian

$$\mathcal{L}_{\text{eff}} = \frac{d}{2} \bar{\chi} \sigma^{\mu\nu} \chi F_{\mu\nu}, \quad (5.17)$$

where μ is the magnetic dipole moment. This dimension five interaction is expected to dominate over a dimension six anapole operator with a differential rate ~ 5 orders of magnitudes larger [69] and thus drives the phenomenology. The differential cross

section reads [103, 107–109]

$$\frac{d\sigma_{\chi N}^d}{dE_R} = \frac{\alpha_{\text{em}} Z^2 F_Z^2(E_R) d^2}{E_R} \left[1 - \frac{E_R}{2m_N v^2} \left(1 + 2 \frac{m_N}{m_\chi} \right) \right] \quad (5.18a)$$

$$+ d^2 d_A^2 F_s^2(E_R) \left(\frac{J+1}{3J} \right) \frac{m_N}{\pi v^2}, \quad (5.18b)$$

where E_R is the recoil energy, Z is the nuclear charge, d_A the nuclear dipole moment, m_N the nuclear mass and v the velocity of the incoming DM candidate. Furthermore, $F_Z(E_R)$ is the nuclear charge form factor and can be taken as the Helm form factor [68, 102]. This form factor corresponds to the previously encountered spin independent form factor $F_{\text{SI}}(E_R)$, while $F_s(E_R)$ is the SD form factor $F_{\text{SD}}(E_R)$ [68].

5.5 Anapole Interaction

Another interaction of this type is given by the anapole moment, which is the only allowed electromagnetic interaction for a Majorana fermion, see chapter 4. Since we are mainly interested in Majorana fermion WIMPs like the MSSM LSP neutralino, this interaction may allow an experimental probe of this candidate and was studied by various authors in the context of direct- and indirect detection experiments and collider searches [68, 108, 110–115].

The effective Lagrangian for the WIMP-nucleus interaction reads [68, 110, 113, 115]

$$\mathcal{L}_{\text{eff}} = \frac{\mathcal{A}}{2} \bar{\chi} \gamma^\mu \gamma_5 \chi \partial^\nu F_{\mu\nu} + e A_\mu J^\mu, \quad (5.19)$$

where J^μ is the nuclear current operator. Then, neglecting the q^2 dependency of the anapole moment \mathcal{A} , the differential cross section of the scattering event involving the DM candidate and the nucleus reads [68, 110, 113]

$$\frac{d\sigma_{\chi N}^A}{dE_R} = 4\alpha_{\text{em}} \mathcal{A}^2 Z^2 F_Z^2(E_R) \left[2m_N - \left(1 + \frac{m_N}{m_\chi} \right)^2 \frac{E_R}{v^2} \right] \quad (5.20a)$$

$$+ 4\mathcal{A}^2 d_A^2 F_s^2(E_R) \left(\frac{J+1}{3J} \right) \frac{2E_R m_N^2}{\pi v^2}, \quad (5.20b)$$

Since for many target nuclei - including xenon - the dipole moment is comparably small, it can be neglected and one can focus on the spin-independent interaction $\sim F_Z^2(E_R)$ only.

Due to the fact that the velocity dependency of eq. (5.20) differs from the standard SI and SD cross sections as in eq. (5.11), the limits for the anapole moment have to be obtained using fits on the event level and can not be inferred from the

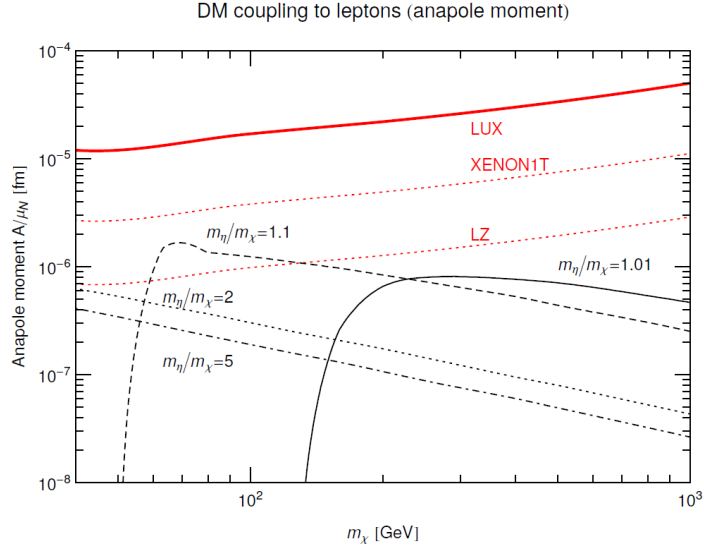


Figure 5.2: Experimental limit from LUX and projections from XENON1T and LZ on the anapole moment (red) and expected values for thermally produced DM coupled to right-handed muons (black) via a scalar η on a 90% confidence limit, from Garny et. al. [112]

standard SI/SD exclusion curves. For this, one needs to account for the detector specifics like the response function and detector mass/time as in eq. (5.9) and carry out the integrals (see for example [116, Appendix B] and [117, Appendix D]). The resulting experimental limit from LUX and projections from XENON1T and LZ by Garny et. al. [112] are shown in fig. 5.2, together with predicted anapole moments stemming from scalar contributions with couplings such that the relic density constraints are satisfied. As apparent, LUX excludes values $\mathcal{A}/\mu_N \gtrsim 10^{-5}$ fm for $m_\chi \approx (40 - 1000)$ GeV at a 90% confidence level, while current generation experiments - particularly LZ projections - are expected to be even stronger and can test theoretically predicted values of $\mathcal{A}/\mu_N \sim (10^{-6} - 10^{-5})$ fm soon.

Chapter 6

Numerical Analysis

In this chapter we will discuss the numerical analysis of the anapole moment in both a model-independent fashion and in the context of the MSSM. Most figures here were created using the PYTHON library MATPLOTLIB [118].

The anapole expression as derived in chapter 4 has units of $[\text{GeV}^{-2}]$. In order to relate the obtained values to results found in the literature, the anapole moment is multiplied with the inverse of the nuclear magneton $\mu_N = e/(2m_p)$, with m_p being the proton mass, and the conversion $\text{GeV}^{-1} \approx 197.3 \times 10^{-3} \text{ fm}$ is applied. Then, the anapole moment is expressed as A/μ_N in units of [fm].

Note however that for the anapole moment as calculated here the limit $q^2 \rightarrow 0$ was taken, such that the results here cannot directly be applied to direct detection experiments. This is the case if a mass is smaller than the DM-nucleus momentum transfer, e.g. if $m < \sqrt{|q^2|} \approx 40 \text{ MeV}$ [68].

6.1 Model-Independent Analysis

For the sake of convenience we repeat the final results of section 4.4, where the analytic expressions for the scalar- and vector contribution read respectively

$$A_S \equiv a_{(a)+(b)} = \frac{e}{96\pi^2 m_\chi^2} Q_f \left[|c_L|^2 - |c_R|^2 \right] \mathcal{F}_S(\mu, \eta), \quad (6.1a)$$

$$A_V \equiv a_{(c)+(d)} = -\frac{e}{48\pi^2 m_\chi^2} \left[|v_L|^2 - |v_R|^2 \right] \mathcal{F}_V(\mu, \eta_V), \quad (6.1b)$$

with the functions $\mathcal{F}_{S/V}$ defined as

$$\mathcal{F}_S(\mu, \eta) = \frac{3}{2} \log\left(\frac{\eta^2}{\mu^2}\right) - (3\eta^2 - 3\mu^2 + 1)f(\mu, \eta), \quad (6.2a)$$

$$\mathcal{F}_V(\mu, \eta_V) = \frac{3}{2} \log\left(\frac{\mu^2}{\eta_V^2}\right) + (3\eta_V^2 - 3\mu^2 - 7)f(\mu, \eta_V), \quad (6.2b)$$

where $\mu = m_f/m_\chi$, $\eta = M_{\tilde{f}}/m_\chi$, $\eta_V = m_V/m_\chi$ and

$$\begin{aligned}
 f(\mu, \eta) &= \frac{1}{2} \int_0^1 \frac{dx}{x\eta^2 + (1-x)\mu^2 - x(1-x)} \\
 &= \begin{cases} \frac{1}{\sqrt{\Delta}} \operatorname{arctanh} \left(\frac{\sqrt{\Delta}}{\mu^2 + \eta^2 - 1} \right) & \Delta > 0 \\ \frac{1}{\sqrt{|\Delta|}} \operatorname{arctan} \left(\frac{\sqrt{|\Delta|}}{\mu^2 + \eta^2 - 1} \right) & \Delta < 0 \\ \frac{2}{(\mu^2 - \eta^2)^2 - 1} & \Delta = 0 \end{cases} \quad (6.3)
 \end{aligned}$$

with $\Delta \equiv \Delta(\mu, \eta) = (\mu^2 + \eta^2 - 1)^2 - 4\mu^2\eta^2$. We may assume $\mu > 1$ or $\eta > 1$ in order to circumvent the discontinuity in the $\operatorname{arctan}(\text{h})$ function. This assumption is phenomenologically well motivated since the LSP DM candidate is usually $m_\chi \sim \mathcal{O}(100)$ GeV and thus automatically prevents crossing of the discontinuity in supersymmetric models. However, for more general cases, the condition

$$\mu^2 + \eta^2 \geq 1 \quad (6.4)$$

prevents the discontinuity being crossed.

As apparent from eqs. (6.1a) and (6.1b), the anapole moment is strongly dependent on the functions $\mathcal{F}_{S/V}(\mu, \eta)$. For this reason, a contour plot of these functions is given in fig. 6.1. The minimal values μ_{\min}, η_{\min} have been chosen such that points like $(\mu, \eta) \approx (1, 0)$ do not lead to a (numerical) singularity of the $\operatorname{arctan}(\text{h})$ function. Nevertheless it is apparent, especially in figs. 6.1a and 6.1b, that around this point $\mathcal{F}_{S/V}$ diverges. The characteristic circular separation in the lower left corner is due to the discontinuity of the $\operatorname{arctan}(\text{h})$ function whose radius is defined by eq. (6.4). Note that the coloring in figs. 6.1a and 6.1b and figs. 6.1c and 6.1d differs.

The anapole functions themselves are shown in figs. 6.2 to 6.4. The couplings have been set to $c_L = 0$, $c_R = 1$ for the scalar case and $v_L = 0$, $v_R = 1$ for the vector contribution. Also, in the scalar case, a colorless fermion with $Q_f = -1$ has been assumed. As apparent from these plots, the size of the anapole moment depends strongly on the masses involved. In particular the value of the anapole moment is enhanced if one mass is comparable to the DM mass, while the other is small, e.g. $m_1 \approx m_\chi$ and $m_2 \ll m_\chi$. This becomes even more noticeable in fig. 6.4, where the masses of the fermion is chosen as small as $m_f \sim 1$ MeV. Then, strong resonances are formed around the vicinity of $m_\chi \approx m_{S/V}$. The vertical green dashed line highlights the position of the W boson, such that in this case, for DM masses of $m_\chi \sim (50 - 150)$ GeV, the anapole moment is $|A|/\mu_N \sim (10^{-6} - 10^{-4})$ fm. It is noteworthy that related studies of the scalar anapole moment A_S have been conducted in [68, 111] with similar results.

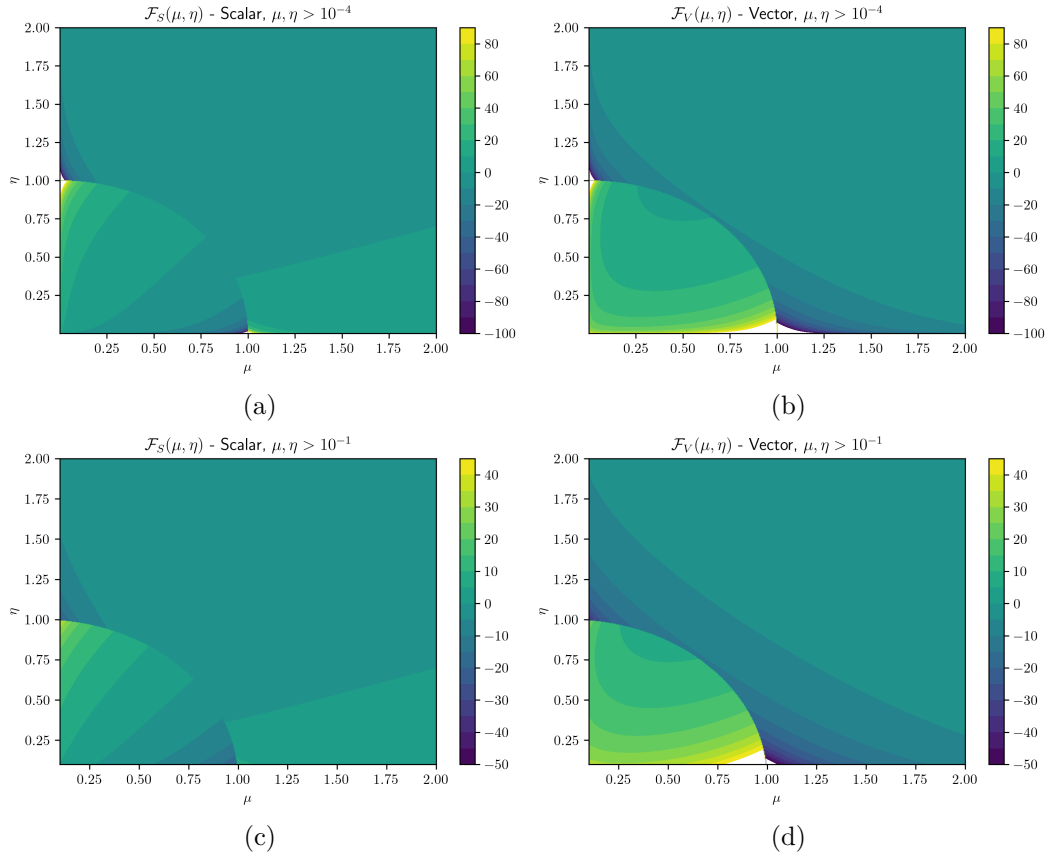


Figure 6.1: Contour plot of $\mathcal{F}_S(\mu, \eta)$ (left) and $\mathcal{F}_V(\mu, \eta)$ (right) for $\mu, \eta > 10^{-4}$ (top) and $\mu, \eta > 10^{-1}$ (bottom)

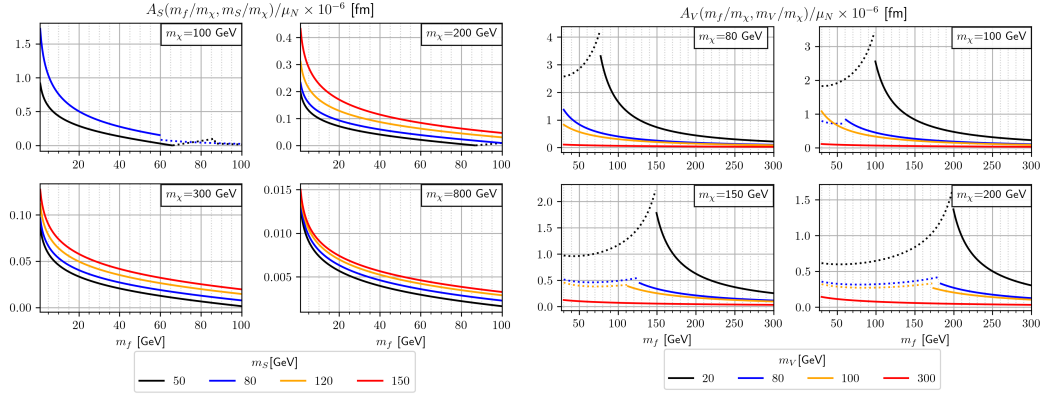


Figure 6.2: Scalar (left) and vector (right) anapole functions for some chosen masses of bosonic particles and DM candidates. The dotted lines correspond to negative values.

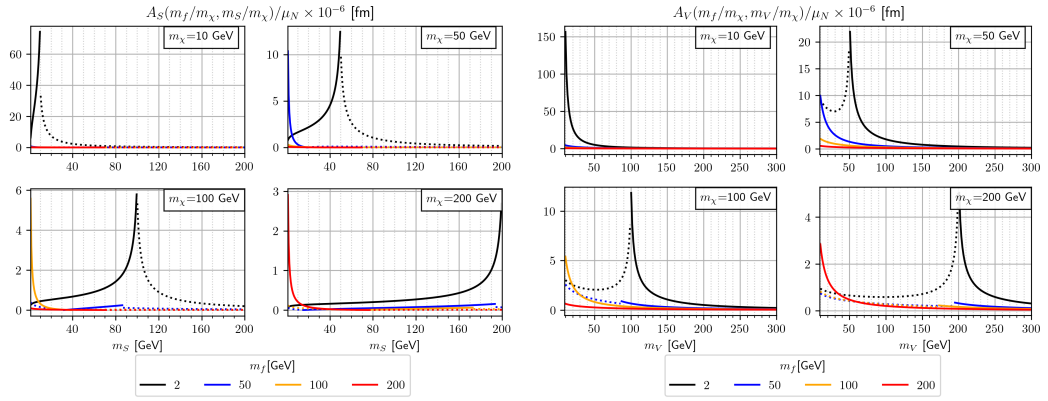


Figure 6.3: Scalar (left) and vector (right) anapole functions for some chosen masses of fermions and DM candidates. The dotted lines correspond to negative values.

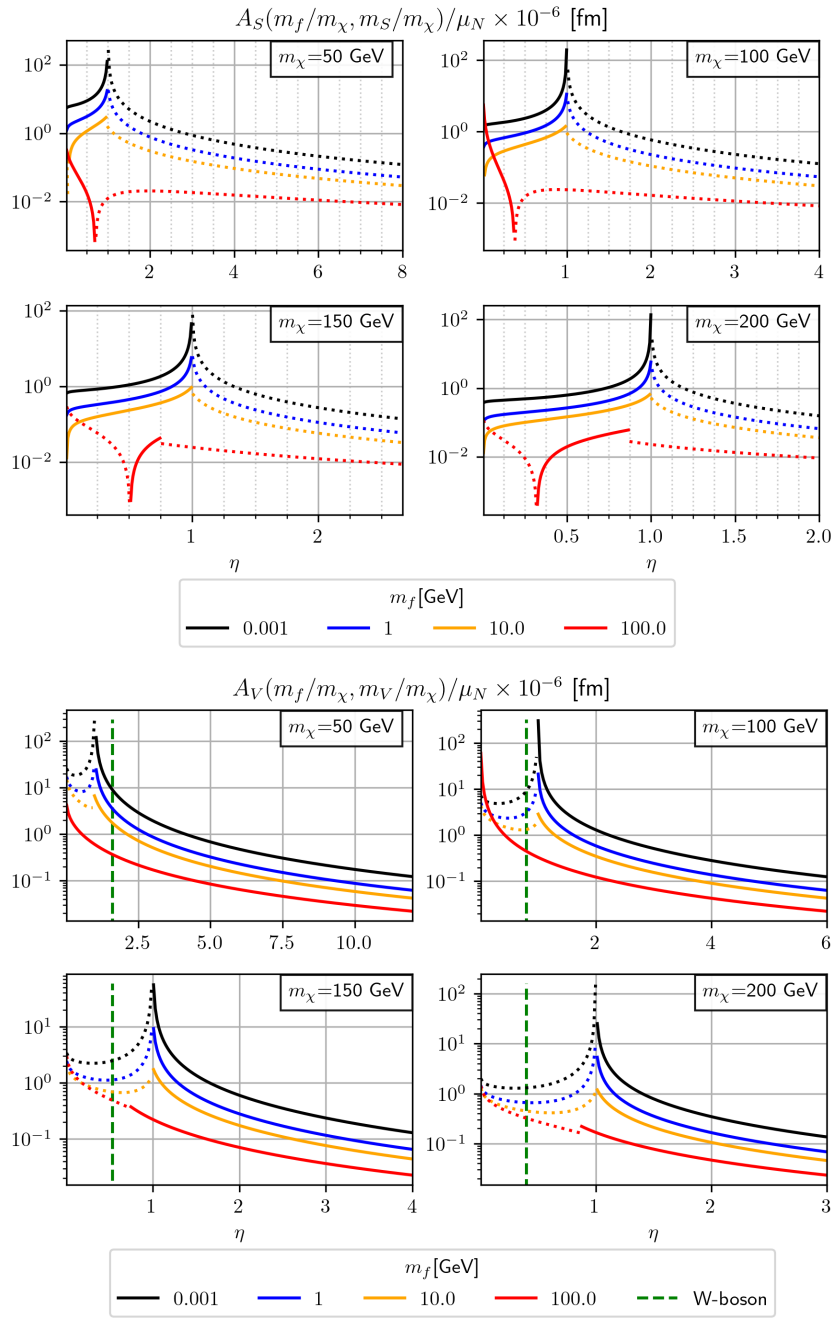


Figure 6.4: Scalar (top) and vector (bottom) anapole moment in terms of η for $c_{L/R} = 0, 1$ and $v_{L/R} = 0, 1$ on a logarithmic y-axis. The vertical green dashed line in the bottom diagrams stands for the W boson. Dotted lines correspond to negative values of the anapole moment. The $m_f \sim 1$ MeV fermion contributes the most.

6.2 MSSM: General Framework

The numerical part is slightly wrong: a bug in the code caused a factor of 10 enhancement in the sfermion contribution to the anapole moment. For the calculation of the anapole moment of the lightest neutralino χ_1^0 , all charged fermions and the two charginos appear in the diagrams of the type shown in fig. 4.3 and thus contribute to its anapole moment. The scalar- and vector contribution to the anapole moment are given as

$$A_S = \frac{e}{96\pi^2 m_\chi^2} \sum_{i,a} N_c^i Q_i [|c_L^{ia}|^2 - |c_R^{ia}|^2] \mathcal{F}_S(\mu_i, \eta_a) \quad (6.5)$$

$$A_W = -\frac{e}{48\pi^2 m_\chi^2} \sum_j [|v_L^j|^2 - |v_R^j|^2] \mathcal{F}_W(\mu_j, \eta_W) \quad (6.6)$$

Here, the indices $i(j)$ are labeling the SM fermions (charginos) and N_c^i is the color factor of the fermion, e.g. $N_c = 3$ if $f = q$ and $N_c = 1$ if $f = e$. Further, $\mu_i = m_{f_i}/m_\chi$, $\eta_a = M_{\tilde{f}_a}/m_\chi$, $\mu_j = m_{\chi_j^\pm}/m_\chi$ and $\eta_W = m_W/m_\chi$, with the SM W-boson mass m_W .

The couplings used and some required SM input parameters are summarized in appendix C.4. Note, that L/R mixing of the third generation only is included. In order to calculate quantities in the MSSM one inevitable has to use a spectrum generator to calculate masses and mixing elements appearing in the model. Commonly used ones include SUSPECT [119], SPHENO [120] and SOFTSUSY [26]. In this work, mainly SOFTSUSY 4.1.10 was used since it is easily callable via command-line input. The spectrum generator writes out in the widely used SLHA format [121] which then can be imported into the anapole code via PYSLHA [122]. The spectrum generator assumes certain boundary conditions at the GUT scale and calculates all masses and couplings via renormalization group evolution under the assumption of correct EWSB (models which do not incorporate correct EWSB are ruled out and flagged accordingly). All parameter ranges shown here satisfy all internal 'physical' checks of SOFTSUSY if not noted differently. Explicitly flags for tachyonic particles, incorrect EWSB and models in which $\tilde{\chi}_1^0$ is not the LSP, are inherited from SOFTSUSY and used in the code here. Furthermore, all masses appearing in the numerical analysis satisfy

$$\mu^2 + \eta^2 > 1, \quad (6.7)$$

preventing the anapole functions to cross the discontinuity of the arctan(h) function. This is simply due to the fact, that in all models considered here $\tilde{\chi}_1^0$ is the LSP.

To the commonly studied and already introduced models belong SUGRA and AMSB. While the anapole moment may obtain a sizeable value, it is important to also include current experimental bounds. In particular the LSP neutralino serves as

a DM candidate whose relic abundance can be calculated using the MICROMEAS code [123, 124] using SUSPECT as spectrum generator. The result can be checked against the literature, e.g. the 9-year data from the WMAP project [9]. The combined limit from the WMAP+eCMB+BAO+ H_0 data set gives a cold DM relic density [9, Table 17] of

$$\Omega_\chi h^2 = 0.1153 \pm 0.0019 \quad (6.8)$$

Here, we will assume that the neutralino is the LSP and is responsible for the measured DM relic abundance alone.

As further experimental constrain the mass of the light neutral CP even Higgs h has been extracted. Its current averaged experimental value according to the PDG [125] is

$$m_h = 125.10 \pm 0.14, \quad (6.9)$$

giving strong limits on SUSY models as we will discuss in the next sections.

We checked explicitly that the anapole moment of the lightest neutralino vanishes in the exact SUSY limit, as it should.

As a side note, a conceptually similar work has been carried out by Cabral-Rosetti et. al. [126], although they do not employ the BFM (or PT) framework and thus work with a gauge dependent quantity.

6.3 SUGRA

As first SUSY model lets discuss SUGRA. Unfortunately most of the parameter space in SUGRA has been ruled out by the discovery of the mass of the scalar Higgs boson [127–129] under the assumption that the neutralino is the single DM particle. Nevertheless, for large A_0 , there is a small strip of allowed parameter space as can be seen exemplarily in fig. 6.7a. Furthermore, the only region which satisfies all constraints and is predicted to be detectable at the LHC is the stop co-annihilation region occurring for some values of A_0 [129].

Some masses and the mixing elements of $\tilde{\chi}_1^0$ and the charginos are shown in fig. 6.5. For lower $m_{1/2} \lesssim 2.6$ TeV, the lightest neutralino is Higgsino-like while for $m_{1/2} \gtrsim 2.6$ TeV it becomes bino-like. The anapole moment in this model is shown in fig. 6.6. Note that the contribution from sfermions exhibits comparably large numeric noise. Within the sfermion sector, the largest contribution stems from the lightest fermions, e.g. electrons and light quarks. For lower $m_{1/2}$, the neutralino is mass degenerate with the lightest chargino, which leads to an amplification of the chargino-W contribution, since then $\mu = m_{\tilde{\chi}_1^\pm}/m_\chi \approx 1$. However, at the same time, the chargino mixing angles exhibit $\phi_L \approx \phi_R$, leading to a cancellation between v_L and v_R , suppressing the anapole moment (see appendix C.4 for the couplings) simultaneously.

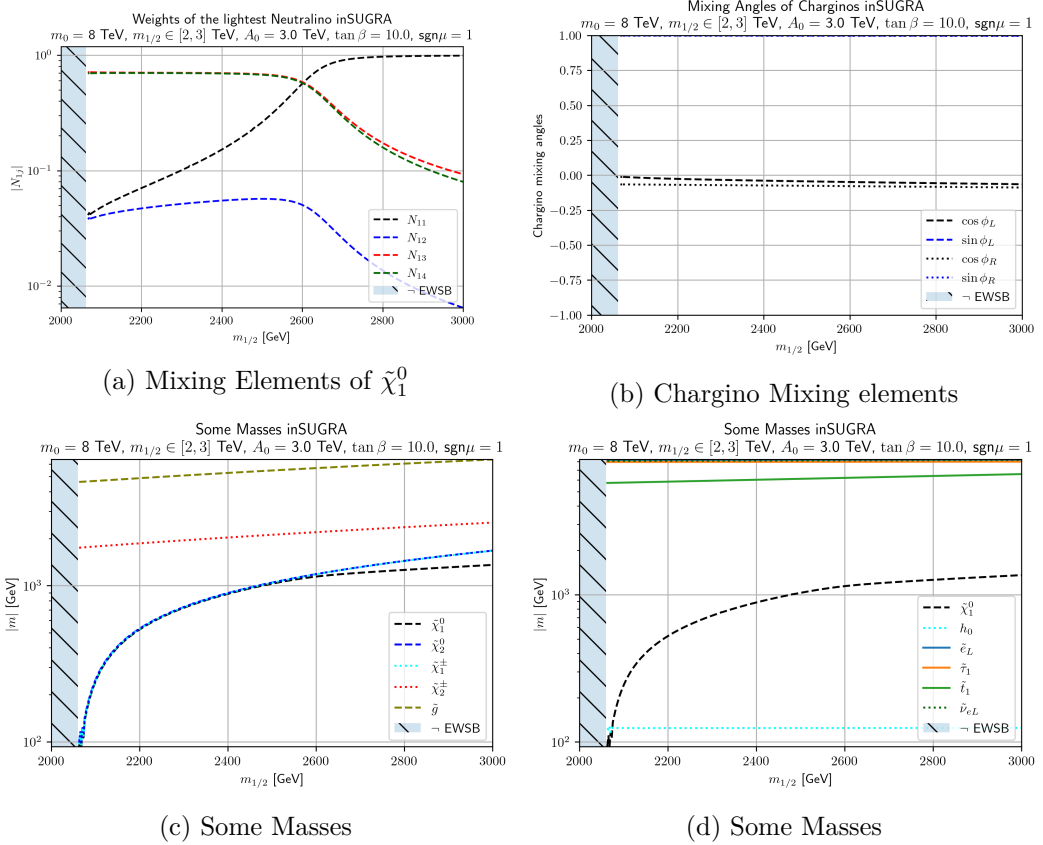


Figure 6.5: Mixing elements of the neutralinos (a), charginos (b) and masses in SUGRA with parameters $m_0 = 8 \text{ TeV}$, $m_{1/2} \in [2, 3] \text{ TeV}$, $A_0 = 3 \text{ TeV}$, $\tan \beta = 10$, $\text{sgn} \mu = +1$

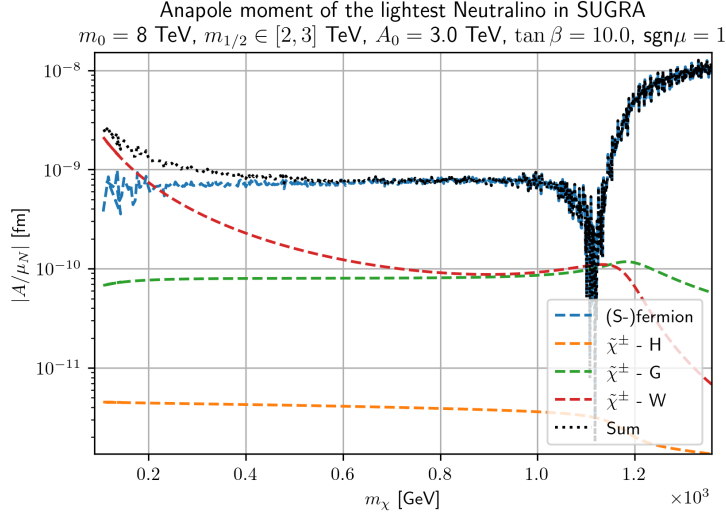


Figure 6.6: Anapole moment in SUGRA

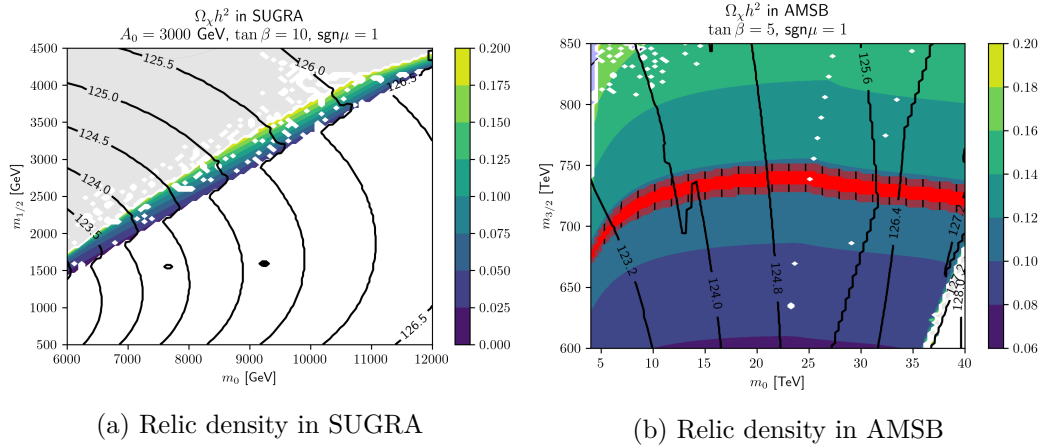


Figure 6.7: Relic density for 100×100 points in $m_0 \times m_{1/2}/m_{3/2}$ space. The black contours are showing m_h , while the red shaded area highlights the experimental bounds of $\Omega_\chi h^2 = 0.1153 \pm 0.0019$. The striped red area corresponds $\Omega_\chi h^2 = 0.1153 \pm 0.0038$. In the gray area, $\Omega_\chi h^2 > 0.2$, and white areas correspond to models without correct EWSB.

6.4 AMSB

The second SUSY model discussed here is AMSB. The compelling aspect of this particular realization of SUSY breaking is, that the neutralino is usually wino-like. Furthermore, it is mass-degenerate with the lighter chargino χ_1^\pm , such that a resonance as discussed in section 6.1, for the vector anapole contribution may be expected. Similar to the previous case, the relic abundance of the neutralino as well as the model's predicted Higgs mass is shown in fig. 6.7b. The chosen parameter range is motivated by the likelihood analysis of Bagnaschi et. al. [130, Table 2]. However, our $m_{3/2}$ is approximately 100 TeV smaller compared to their best-fit value. As visible, m_0 is hardly constrained by the WMAP data, while the Higgs measurement restricts its value to $m_0 \approx 25$ TeV. The mass of the neutralino is mainly determined by $m_{3/2}$, whose large value drives the DM mass to be in the TeV range. The mixing elements of $\tilde{\chi}_1^0$ and the charginos as well as some masses in this model are shown in fig. 6.8. Similar to the SUGRA case, the anapole moment is dominated by the sfermion contribution; in particular the light fermions contribute the most. The chargino contributions are suppressed due to $\phi_L \approx \phi_R$.

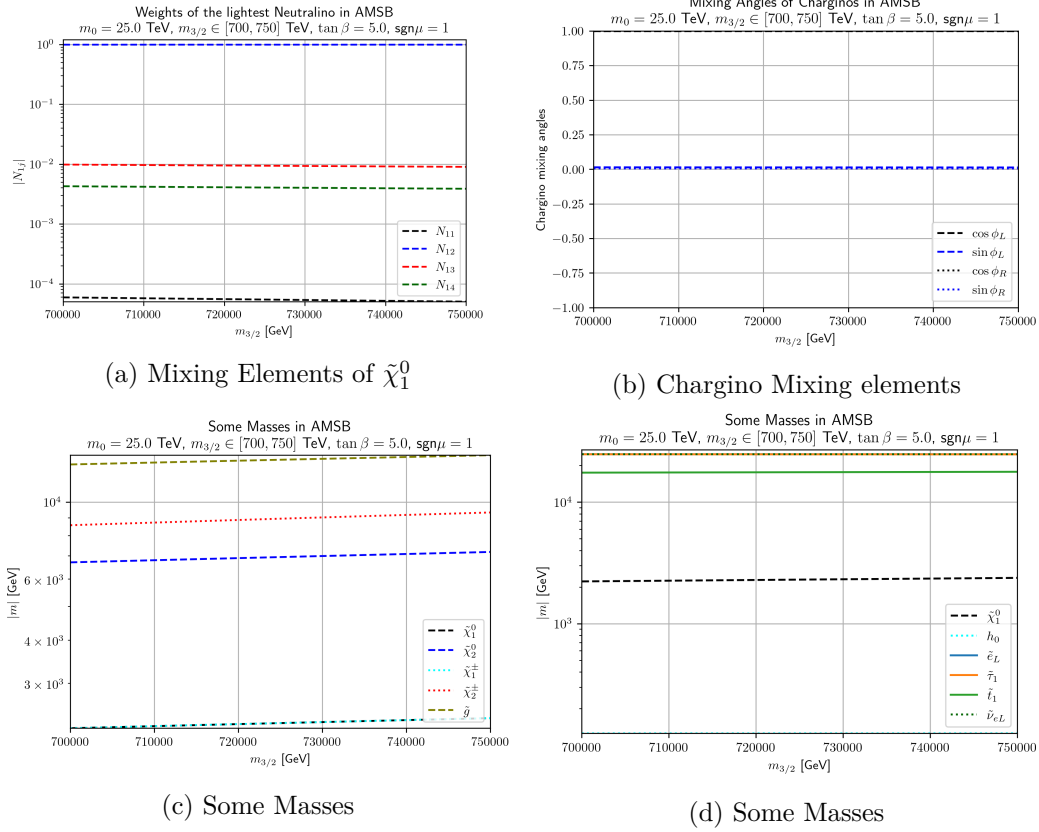


Figure 6.8: Mixing elements of the neutralinos (a), charginos (b) and masses (c,d) in AMSB with parameters $m_0 = 25$ TeV, $m_{3/2} \in [700, 750]$ TeV, $\tan \beta = 5$, $\text{sgn} \mu = +1$

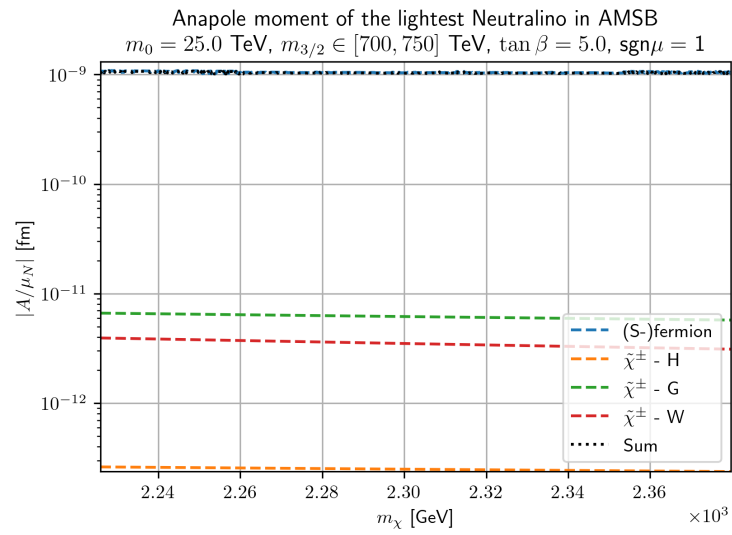


Figure 6.9: Anapole moment in AMSB

Chapter 7

Summary and Outlook

Summary

Dark matter is one of the biggest unsolved mysteries of particle physics and cosmology and plays a major role in the understanding of both the history of our Universe and the world surrounding us. Much effort is put into gaining knowledge about its nature and properties both experimentally and theoretically. While there is strong evidence towards the existence of this additional source of matter, so far no conclusive signal for it was found.

In this work the anapole moment of a generic Majorana fermion has been calculated in a model-independent fashion allowing a wide range of applications. For this, the important issue related to the charge radius of the neutrino has been recapitulated to highlight the non-trivial steps involved in the calculation of the vector contribution.

Finally, the anapole moment was studied numerically, both in a naive model-independent fashion and in the context of the MSSM, in which the lightest neutralino can serve as a DM candidate. The results have to be considered in the light of DD experiments and collider searches, where future experiments are expected to be sensitive enough to probe this loop induced coupling over a wide range in parameter space. Although the model-independent analysis allows comparatively high values for the anapole moment, it has to be noted, that the respective couplings $c_{L/R}$ and $v_{L/R}$ have been set to zero/unity; in general they are strongly model dependent. This dependency can be directly seen in the MSSM, where the parameters and masses have common origin and are not independent. There, the scenarios of SUGRA and AMSB have been considered under the experimental and observational constraints from the Higgs mass and the relic density (assuming the LSP is the single DM particle). It was found that for both SUGRA and AMSB, the anapole moment of the LSP neutralino is not expected to have a sizeable value. While for SUGRA most of the parameter space considered here is excluded already, the relic density constraints on AMSB are comparably lenient.

Outlook

The results and frameworks developed in this work can be used and extended in many different ways.

The model-independent expressions for the anapole moment obtained here are not only applicable to DM searches, but also serve as a basis to calculate the anapole moment of generic Dirac- and Majorana fermions in both the SM, MSSM and all BSM extensions.

For example, there are applications in neutrino phenomenology. The anapole and dipole moment can lead to signals in low energy neutrino-electron scattering [131] and neutrino-nucleus scattering [72]. Furthermore these higher order electromagnetic moments can have an effect on the solar neutrino flux due to solar flares and can lead to a depletion of the electron neutrino flux as measured on earth [132].

In the light of DM searches, the results here could be used to calculate up-to-date experimental limits on the anapole moment for both scalar and vector contributions. For direct detection experiments where the DM candidate interacts with the nucleus, one has to account for the fact, that the spin independent cross section appearing in the interaction via the anapole moment exhibits a different velocity dependency compared to the conventionally used one, such that the analysis has to be carried out on the level of expected events instead of cross section.

Higher electromagnetic moments can also induce interactions between sub-GeV DM and electrons in the detector material, and can help to probe whether DM is a Majorana- or Dirac fermion [133].

There are also expected consequences for the imprints of DM on cosmological scales. If the candidate couples via the anapole moment to the visible sector, the couplings of the scalar- and vector contributions can be related to the relic density via the thermal production mechanism and is not a free parameter anymore [69, 110, 112]. Furthermore, the non-standard electromagnetic moments can distort the CMB spectrum due to DM annihilating into fermion pairs during the recombination epoch [134]. This is particularly important for sub-GeV DM, since direct detection experiments where DM scatters with a nucleus are not sensitive in this regime [101].

In particularly dense regions of DM, e.g. in the Galactic Center or dwarf spheroidal galaxies, the same annihilation mechanism can influence the flux of gamma-rays, cosmic-rays and neutrinos due to the production of high energetic leptons and mono-energetic photons [69, 112]. Indirect detection experiments may observe signals of this type depending on whether the DM is a Majorana- or Dirac fermion. For heavy dark matter, only the latter case is expected to be detectable this way, since the Majorana annihilation cross section is velocity suppressed [69].

The analysis in the MSSM could be extended such that more experimental constraints, like limits on the branching ratio $\text{Br}(b \rightarrow s\gamma)$, are included. Also, the anapole moment of the LSP neutralino in particular can be investigated further:

-
1. In more general terms within the MSSM without relying on the SUGRA or AMSB scenario, like the phenomenological MSSM (pMSSM) [135].
 2. Giving up the assumption that the LSP neutralino makes up all of the DM would relax the rather strong constraints from WMAP and PLANCK. That is, the DM can (partly) be realized in a separate process or model.
 3. Scanning over a wider range of the SUGRA/AMSB parameter space, in particular the stop co-annihilation region of SUGRA may be of interest [129].

Appendix A

Classical Multipole Expansion and Toroid Moment

In this section the classical multipole expansion in electrodynamics is discussed and subsequently related to the anapole moment of relativistic fermions.

In classical electrodynamics the properties of spatially distributed sources can be described by their moments. Following the review by Dubovik and Tugushev [136], suppose that the charge density of the system is described by

$$\rho(\mathbf{r}, t) = \int d^3\xi \rho(\boldsymbol{\xi}, t) \delta^{(3)}(\boldsymbol{\xi} - \mathbf{r}). \quad (\text{A.1})$$

Expanding the delta distribution formally

$$\delta^{(3)}(\boldsymbol{\xi} - \mathbf{r}) = \sum_{\ell=0}^{\infty} \frac{(-1)^\ell}{\ell!} \underbrace{\xi_i \cdots \xi_k}_\ell \nabla_i \cdots \nabla_k \delta(\mathbf{r}), \quad (\text{A.2})$$

results in

$$\rho(\mathbf{r}, t) = \sum_{\ell=0}^{\infty} \frac{(-1)^\ell}{\ell!} A_{i \dots k}^{(\ell)} \partial_i \cdots \partial_k \delta(\mathbf{r}), \quad (\text{A.3})$$

where

$$A_{i \dots k}^{(\ell)} := \int d^3\xi \rho(\boldsymbol{\xi}, t) \xi_i \cdots \xi_k \quad (\text{A.4})$$

are the moments with $A^{(0)}$ being the charge and $A_i^{(1)}$ being the charge dipole moment etc. In many cases it is convenient to express these moments in terms of irreducible tensors of the rotation group $SO(3)$, e.g. in terms of spherical harmonics $Y_{\ell m}$.

Similarly the spatial components of the current density $\mathbf{j}(\mathbf{r}, t)$ can be described using a multipole expansion with coefficients

$$B_{ij \dots k}^{(\ell)} := \frac{(-1)^{\ell-1}}{(\ell-1)!} \int d^3\xi j_i \underbrace{\xi_j \cdots \xi_k}_{\ell-1}. \quad (\text{A.5})$$

Note, that the current density is related to the charge density due the the conservation law

$$\nabla \cdot \mathbf{j} = -\dot{\rho}, \quad (\text{A.6})$$

such that a relationship between $A_{i\dots k}^{(\ell)}$ and $B_{ij\dots k}^{(\ell)}$ is expected. According to the Helmholtz theorem, the current can be separated into a longitudinal \mathbf{j}_{\parallel} and a transversal part \mathbf{j}_{\perp} as

$$\mathbf{j} = \mathbf{j}_{\parallel} + \mathbf{j}_{\perp} \quad (\text{A.7})$$

with

$$\mathbf{j}_{\parallel} = \nabla\phi, \quad \mathbf{j}_{\perp} = \nabla \times \mathbf{f} \quad (\text{A.8})$$

where \mathbf{f} satisfies the gauge condition $\nabla \cdot \mathbf{f} = 0$ and ϕ is a scalar function. Then eq. (A.6) reduces to

$$\nabla \cdot \mathbf{j}_{\parallel} = -\dot{\rho}, \quad (\text{A.9})$$

showing that the multipole expansion of the longitudinal charge current is characterized by the multipole expansion of the charge density only. The transversal current on the other hand has two degrees of freedom remaining, whose expansions are independent of the charge moments. They can be expressed via the scalar- and pseudoscalar functions ψ and χ respectively as

$$\mathbf{j}_{\perp}(\mathbf{r}) = \mathcal{M}\psi(r, \theta, \varphi) + \nabla \times \mathcal{M}\chi(r, \theta, \varphi), \quad (\text{A.10})$$

describing toroidal currents flowing parallel on a sphere (first term) and poloidal currents flowing along the meridian on a torus (second term) respectively. The vector \mathcal{M} is defined as

$$\mathcal{M} \equiv -\mathbf{r} \times \nabla = i\mathbf{L}. \quad (\text{A.11})$$

Then one can rewrite the current as

$$\mathbf{j} = \nabla\phi + \nabla \times (\mathbf{r}\psi) + \nabla \times (\nabla \times (\mathbf{r}\chi)), \quad (\text{A.12})$$

reducing the problem to the multipole expansion of three scalar functions ϕ , ψ and χ satisfying the gauge constraints.

The interaction energy of a non-relativistic system of point charges with an external electric field is described by

$$W = \int d^3r (\rho\phi - \mathbf{j} \cdot \mathbf{A}) \quad (\text{A.13a})$$

$$\equiv W^{\text{ch}} + W^{\text{cur}} \quad (\text{A.13b})$$

with charge- and current density

$$\rho(\mathbf{r}, t) = \sum_{\alpha} e^{(\alpha)} \delta^{(3)}(\mathbf{r} - \boldsymbol{\xi}^{(\alpha)}(t)) = \sum_{\alpha} e^{(\alpha)} \exp(-\boldsymbol{\xi}^{(\alpha)} \cdot \nabla) \delta^{(3)}(\mathbf{r}), \quad (\text{A.14a})$$

$$\mathbf{j}(\mathbf{r}, t) = \sum_{\alpha} e^{(\alpha)} \dot{\boldsymbol{\xi}}^{(\alpha)} \delta^{(3)}(\mathbf{r} - \boldsymbol{\xi}^{(\alpha)}(t)) = \sum_{\alpha} e^{(\alpha)} \dot{\boldsymbol{\xi}}^{(\alpha)} \exp(-\boldsymbol{\xi}^{(\alpha)} \cdot \nabla) \delta^{(3)}(\mathbf{r}) \quad (\text{A.14b})$$

with $\boldsymbol{\xi}^{(\alpha)}(t)$ being the position of the charged particle α . After replacing the exponential with its Taylor series, the interaction energy becomes

$$W = - \sum_{\alpha} \sum_{n=0}^{\infty} \frac{e^{(\alpha)}}{(n+1)!} (\boldsymbol{\xi}^{(\alpha)} \cdot \nabla)^n \left(\boldsymbol{\xi}^{(\alpha)} \cdot \mathbf{E}(0) + 2 \frac{n+1}{n+2} \boldsymbol{\mu}^{(\alpha)} \cdot \mathbf{B}(0) \right) \quad (\text{A.15})$$

with magnetic dipole moment $\boldsymbol{\mu} = \frac{1}{2} \boldsymbol{\xi} \times \dot{\boldsymbol{\xi}}$. Then, one can decompose the terms at any order according to their symmetry property.

Alternatively, the expansion of the energy corresponding to the charge density only reads

$$W^{\text{ch}} = q\phi + \mathbf{d} \cdot \nabla\phi + Q_{ij} \nabla_i \nabla_j \phi + \frac{1}{6} r_q^{(2)} \Delta\phi + Q_{ijk} \nabla_i \nabla_j \nabla_k \phi + \dots \Big|_{r=0}. \quad (\text{A.16})$$

with the total charge $q = \int d^3\xi \rho$, charge dipole moment $\mathbf{d} = \int d^3\xi \boldsymbol{\xi} \rho$, charge quadrupole moment

$$Q_{ij} = \frac{1}{2} \int d^3\xi (\xi_i \xi_j - \frac{1}{3} \xi^2 \delta_{ij}) \rho, \quad (\text{A.17})$$

octupole moment

$$Q_{ijk} = \frac{1}{6} \int d^3\xi [\xi_i \xi_j \xi_k - \frac{1}{5} (\xi_i \delta_{jk} + \xi_j \delta_{ik} + \xi_k \delta_{ij})] \rho \quad (\text{A.18})$$

and $r_q^{(2)} = \int d^3\xi \xi^2 \rho$ being the mean-square radius of the charge density. The energy contribution due to the current reads

$$\begin{aligned} W^{\text{cur}} = & - \dot{\mathbf{d}} \cdot \mathbf{A} - \mathbf{M} \cdot (\nabla \cdot \mathbf{A}) - \frac{1}{2} \cdot Q_{ij} (\nabla_i A_j + \nabla_j A_i) - \frac{1}{6} \overline{r_q^{(2)}} \nabla \cdot \mathbf{A} \\ & - \dot{Q}_{ijk} \nabla_j \nabla_k A_i - M_{ij} \nabla_i (\nabla \cdot \mathbf{A})_j - \frac{1}{10} \overline{r_d^{(2)}} \cdot \nabla (\nabla \cdot \mathbf{A}) \\ & - \mathbf{T} \cdot (\nabla \times (\nabla \times \mathbf{A})) - \dots \Big|_{r=0}, \end{aligned} \quad (\text{A.19})$$

with the system's magnetic dipole moment

$$\mathbf{M} = \frac{1}{2} \int d^3\xi \boldsymbol{\xi} \times \mathbf{j}, \quad (\text{A.20})$$

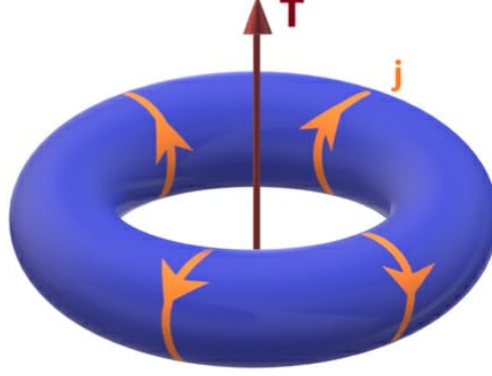


Figure A.1: Toroid dipole moment \mathbf{T} generated by a current \mathbf{j} along the surface of a torus, from [137]

magnetic quadrupole moment

$$\dot{\mathbf{Q}}^{(2)} = \frac{1}{10} \overline{\dot{\mathbf{r}}_d^{(2)}} = \frac{1}{10} \int d^3\xi (2\xi(\xi \cdot \mathbf{j}) + \xi^2 \mathbf{j}), \quad (\text{A.21})$$

with mean-square radius of the dipole density $\mathbf{r}_d^{(2)} = \int d^3\xi \xi \xi^2 \rho$. Finally, the toroid dipole moment (TDM) is given by

$$\mathbf{T} = \frac{1}{10} \int d^3\xi (\xi(\xi \cdot \mathbf{j}) - 2\xi^2 \mathbf{j}) \quad (\text{A.22})$$

This toroid moment can classically be generating using a solenoid folded into a torus, see fig. A.1.

There is no classical analog to the anapole moment as being part of a multipole expansion. Instead, it is related to the toroid dipole moment T . The axial part of the electromagnetic interaction vertex of chapter 4, eq. (4.2) can be rewritten as [138]

$$\Gamma_\mu(q) \sim i\epsilon_{\mu\nu\rho\sigma} P^\nu q^\lambda \gamma^\sigma \gamma_5 T(q^2) + \sigma_{\mu\nu} q^\nu D(\Delta m^2) \quad (\text{A.23})$$

$$- \frac{q^2 P_\mu - (q \cdot P) q_\mu}{q^2 - \Delta m^2} [D(q^2) - D(\Delta m^2)] \quad (\text{A.24})$$

with $P_\mu := p'_\mu + p_\mu$, $\Delta m = m_i - m_f$ and $D(\Delta m^2)$, $D(q^2)$ and $T(q^2)$ the charge dipole moment, charge dipole and toroid dipole form factor respectively for which a one-to-one correspondence to their counterparts in the multipole expansion exists.

Then, the anapole form factor can be identified as

$$A(q^2) = T(q^2) + \frac{m_i^2 - m_f^2}{q^2 - \Delta m^2} [D(q^2) - D(\Delta m^2)], \quad (\text{A.25})$$

coinciding with the toroid moment for $m_i = m_f$ on the mass-shell. For a Majorana field, the toroid moment in the rest frame is proportional to the spin direction (there is no other vector quantity characterizing the system) and can be defined as

$$T_\mu = eT(0)\bar{u}(0)\gamma_\mu\gamma_5u(0), \quad \mathbf{T} = eT(0)\varphi^\dagger\boldsymbol{\sigma}\varphi \quad (\text{A.26})$$

with the Pauli spinor φ and \mathbf{T} as in eq. (A.22) and $T(0)$ its magnitude. The interaction Hamiltonian reads

$$\mathcal{H}_{\text{int}} = eT(q^2)\bar{\psi}\gamma_\mu\gamma_5\psi \partial_\nu F^{\mu\nu} \quad (\text{A.27})$$

and in the non-relativistic limit in the rest frame

$$\mathcal{H}_{\text{int}} = -\mathbf{T} \cdot \mathbf{J}_{\text{ext}} \quad (\text{A.28})$$

$$= -T(0)\varphi^\dagger\boldsymbol{\sigma}\varphi \cdot (\nabla \times \mathbf{B} - \dot{\mathbf{E}}) \quad (\text{A.29})$$

which is invariant under time reversal \mathcal{T} , but not under parity \mathcal{P} and charge conjugation \mathcal{C} separately [139].

Appendix B

Treatment of γ_5

Since the anapole moment itself is characterized by the Lorentz structure $\gamma_\mu\gamma_5$ in the vertex, the discussed projection technique inevitably will lead to traces over a number of regular γ -matrices accompanied by γ_5 . In dimensional regularization, the appearance of γ_5 in $D \neq 4$ dimensions leads to inconsistencies [140] and one needs to pay special attention. In particular, a γ_5 in $D = 4 - 2\epsilon$ dimensions satisfying both the anticommutativity property,

$$\{\gamma_5, \gamma_\mu\} = 0, \quad (\text{B.1})$$

and the cyclicity of the trace,

$$\text{tr}(\gamma_\mu\gamma_\nu\gamma_\rho\gamma_\sigma\gamma_5) = 4i\epsilon_{\mu\nu\rho\sigma}, \quad (\text{B.2})$$

cannot exist and calculations assuming both of these conditions simultaneously may be plagued with inconsistencies.

Many different approaches have been investigated and different schemes have been developed to solve this problem [141–146]. However, up to today, there is no "one size fits all" solution, and one has to decide on a case-by-case basis which scheme is appropriate [35, and references within]. Some commonly used schemes include: Naive Dimensional Regularization (NDR), Dimensional Reduction (DRed) [145], Breitenlohner-Maison-t'Hooft-Veltman scheme (BMHV) [41, 42] and the Larin scheme [43]. Following Buras and Weisz [147], we will describe some of them here briefly.

The arguably easiest treatment is the NDR, in which it is assumed, that a γ_5 exists satisfying both conditions above. In particular, one introduces the D-dimensional metric tensor with

$$g_{\mu\nu} = g_{\nu\mu}, \quad g_{\mu\rho}g^\rho{}_\nu = g_{\mu\nu}, \quad g^\mu{}_\mu = D, \quad (\text{B.3})$$

and γ -matrices satisfying the Clifford algebra

$$\{\gamma_\mu, \gamma_\nu\} = 2g_{\mu\nu}. \quad (\text{B.4})$$

The γ_5 appearing in calculations satisfies

$$\{\gamma_\mu, \gamma_5\} = 0. \quad (\text{B.5})$$

In many cases, this does lead to correct results, while in other cases, things like the axial anomaly cannot be reproduced [147]. In particular expressions like $\text{tr}(\gamma_\mu \gamma_\nu \gamma_\rho \gamma_\sigma \gamma_5)$ can not be evaluated.

Regularization by DRed is an interesting scheme, since it does not only manage to offer a treatment for the γ_5 issue, but also preserves global SUSY [145]. Here, the γ -matrices are not extended to D dimensions but kept 4-dimensional instead. These 4-dimensional Dirac matrices are written as $\tilde{\gamma}$ and satisfy

$$\{\tilde{\gamma}_\mu, \tilde{\gamma}_\nu\} = 2\tilde{g}_{\mu\nu}. \quad (\text{B.6})$$

The 4-dimensional metric tensor satisfies

$$\tilde{g}_{\mu\nu} = \tilde{g}_{\nu\mu}, \quad \tilde{g}_{\mu\rho} \tilde{g}^\rho{}_\nu = \tilde{g}_{\mu\nu}, \quad \tilde{g}^\mu{}_\mu = 4, \quad (\text{B.7})$$

and its contraction with the D -dimensional metric tensor $g_{\mu\nu}$ follows the rule

$$\tilde{g}_{\mu\rho} g^\rho{}_\nu = g_{\mu\nu}. \quad (\text{B.8})$$

While this scheme involves some field theoretical subtleties [148] and has some algebraic inconsistencies, it still has led to correct results [147].

The BMHV scheme leads to an algebraic consistent treatment of the diagrams. Here, the metric tensors come in three separate copies g , \tilde{g} and \hat{g} , living in D -, 4- and -2ϵ - dimensions respectively. The D - and 4 dimensional metric tensor satisfy eq. (B.3) and eq. (B.7) respectively. The -2ϵ dimensional metric satisfies

$$\hat{g}_{\mu\nu} = \hat{g}_{\nu\mu}, \quad \hat{g}_{\mu\rho} \hat{g}^\rho{}_\nu = \hat{g}_{\mu\nu}, \quad \hat{g}^\mu{}_\mu = -2\epsilon. \quad (\text{B.9})$$

However, contrary to before, the contraction between metric tensors of different dimensions is given by

$$\tilde{g}_{\mu\rho} g^\rho{}_\nu = \tilde{g}_{\mu\nu}, \quad \hat{g}_{\mu\rho} g^\rho{}_\nu = \hat{g}_{\mu\nu}, \quad \hat{g}_{\mu\rho} \tilde{g}^\rho{}_\nu = 0. \quad (\text{B.10})$$

Also, the D -dimensional Dirac matrices γ_μ are split into pieces $\gamma_\mu = \tilde{\gamma}_\mu + \hat{\gamma}_\mu$ living in 4- and -2ϵ - dimensions respectively. The γ_μ and $\tilde{\gamma}_\mu$ satisfy Clifford algebras as introduced previously in the context of NDR and DRed, while for $\hat{\gamma}_\mu$ the relation

$$\{\hat{\gamma}_\mu, \hat{\gamma}_\nu\} = 2\hat{g}_{\mu\nu} \quad (\text{B.11})$$

holds. Furthermore,

$$\{\hat{\gamma}_\mu, \tilde{\gamma}_\nu\} = 0. \quad (\text{B.12})$$

In this scheme, γ_5 is introduced satisfying

$$\gamma_5^2 = 1, \quad \{\gamma_5, \tilde{\gamma}_\nu\} = 0, \quad [\gamma_5, \hat{\gamma}_\nu] = 0. \quad (\text{B.13})$$

This scheme, although algebraic consistent, leads to rather cumbersome calculations, and more importantly, some results may suffer from non-conservation of currents.

Finally, in Larin's scheme, before evaluating any traces, the substitution

$$\gamma_\mu \gamma_5 \longrightarrow -\frac{i}{6} \epsilon_{\mu\nu\rho\sigma} \gamma_\nu \gamma_\rho \gamma_\sigma \quad (\text{B.14})$$

is made. All indices are D dimensional.

In the context here, terms involving four Dirac matrices and a γ_5 can always be reduced to be of the form

$$p_1^\mu p_2^\nu q^\rho p_{1,2}^\sigma \text{tr}(\gamma_\mu \gamma_\nu \gamma_\rho \gamma_\sigma \gamma_5), \quad (\text{B.15})$$

which vanishes in both BMHV and Larin's scheme, since

$$p_{1,2}^\mu p_{1,2}^\nu \text{tr}(\gamma_\mu \gamma_\nu \gamma_\alpha \gamma_\beta \gamma_5) \stackrel{\text{anti sym.}}{=} 0, \quad (\text{B.16})$$

due to the antisymmetry of the trace in any pair of Lorentz indices, here $\nu \leftrightarrow \mu$.

Appendix C

Feynman Rules

C.1 Majorana Fermion Interactions

Following the treatment of Majorana fermions in [66, 67], we summarize the Feynman rules for interactions involving Majorana fermions. Without loss of generality the interaction Lagrangian between Majorana fermions χ_a , Dirac fermions ψ_b and bosonic fields Φ_c can be written as

$$\mathcal{L} \supset \frac{1}{2} g_{abc}^i \bar{\chi}_a \Gamma_i \chi_b \Phi_c + k_{abc}^i \bar{\chi}_a \Gamma_i \psi_b \Phi_c^* + k_{abc}^{i*} \bar{\psi}_b \Gamma_i \chi_a \Phi_c + h_{abc}^i \bar{\psi}_a \Gamma_i \psi_b \Phi_c, \quad (\text{C.1})$$

where g_{abc}^i , k_{abc}^i and h_{abc}^i are couplings and the Dirac matrices Γ_i are as introduced in section 4.1. Fermion chains are assigned a *fermion flow*, diagrammatically represented by red arrows, which resolves the usual sign ambiguities arising in Majorana rules. The resulting vertices and propagators are shown in eqs. (C.5) to (C.10). This fermion flow is set globally for a given amplitude and fixes the relative signs between diagrams. The Feynman rules for interaction vertices in eq. (C.5) are formulated using the shorthand notation for the interactions in eq. (C.1), in which e.g.

$$\bar{\chi} \Gamma \psi \equiv k_{abc}^i \bar{\chi}_a \Gamma_i \psi_b \Phi_c^*, \quad (\text{C.2})$$

suppressing the bosonic field. In this notation, one defines the *reversed vertex*

$$\Gamma' := \mathcal{C} \Gamma^T \mathcal{C}^{-1}, \quad (\text{C.3})$$

which replaces the ordinary vertex whenever the fermion flow - represented by the red arrow - is opposite to the charge flow of a Dirac fermion. The *reversed propagator* is defined similarly as

$$S'(p) := \mathcal{C} S_{\psi}^T(p) \mathcal{C}^{-1} = \frac{1}{-\not{p} - m} = S_{\psi}(-p). \quad (\text{C.4})$$

The application of the Feynman rules works as in the normal case, apart from setting this (arbitrary) fermion flow for each fermion chain. Thus one starts at an external

leg or - for loops - at any propagator and applies the rules in opposite to the fermion flow.

$$\begin{array}{c}
 \chi \\
 \nearrow \\
 \Phi \text{ ---} \bullet \\
 \searrow \\
 \chi
 \end{array}
 \begin{array}{c}
 \text{red arrow} \\
 \curvearrowright
 \end{array}
 = i\Gamma
 \qquad
 \begin{array}{c}
 \chi \\
 \nearrow \\
 \Phi \text{ ---} \bullet \\
 \searrow \\
 \chi
 \end{array}
 \begin{array}{c}
 \text{red arrow} \\
 \curvearrowleft
 \end{array}
 = i\Gamma
 \qquad (C.5)$$

$$\begin{array}{c}
 \chi \\
 \nearrow \\
 \Phi \text{ ---} \bullet \\
 \searrow \\
 \psi
 \end{array}
 \begin{array}{c}
 \text{red arrow} \\
 \curvearrowright
 \end{array}
 = i\Gamma
 \qquad
 \begin{array}{c}
 \chi \\
 \nearrow \\
 \Phi \text{ ---} \bullet \\
 \searrow \\
 \psi
 \end{array}
 \begin{array}{c}
 \text{red arrow} \\
 \curvearrowleft
 \end{array}
 = i\Gamma'
 \qquad (C.6)$$

$$\begin{array}{c}
 \psi \\
 \nearrow \\
 \Phi \text{ ---} \bullet \\
 \searrow \\
 \chi
 \end{array}
 \begin{array}{c}
 \text{red arrow} \\
 \curvearrowright
 \end{array}
 = i\Gamma
 \qquad
 \begin{array}{c}
 \psi \\
 \nearrow \\
 \Phi \text{ ---} \bullet \\
 \searrow \\
 \chi
 \end{array}
 \begin{array}{c}
 \text{red arrow} \\
 \curvearrowleft
 \end{array}
 = i\Gamma'
 \qquad (C.7)$$

$$\begin{array}{c}
 \psi \\
 \nearrow \\
 \Phi \text{ ---} \bullet \\
 \searrow \\
 \psi
 \end{array}
 \begin{array}{c}
 \text{red arrow} \\
 \curvearrowright
 \end{array}
 = i\Gamma
 \qquad
 \begin{array}{c}
 \psi \\
 \nearrow \\
 \Phi \text{ ---} \bullet \\
 \searrow \\
 \psi
 \end{array}
 \begin{array}{c}
 \text{red arrow} \\
 \curvearrowleft
 \end{array}
 = i\Gamma'
 \qquad (C.8)$$

$$\begin{array}{c}
 \text{red arrow} \\
 \longrightarrow
 \end{array}
 \bullet \longrightarrow \bullet = iS_\psi(p), \quad
 \begin{array}{c}
 \text{red arrow} \\
 \longleftarrow
 \end{array}
 \bullet \longrightarrow \bullet = iS_\psi(-p), \quad
 \begin{array}{c}
 \text{red arrow} \\
 \longrightarrow
 \end{array}
 \bullet \longleftarrow \bullet = iS_\psi(p) \qquad (C.9)$$

Although only indirectly relevant in this work, for the sake of completeness the rules for the external states are shown in eq. (C.10).

$$\begin{aligned}
 \begin{array}{ccc} \bullet \xrightarrow{\text{red}} & \bullet \xleftarrow{\text{red}} & \bullet \xrightarrow{\text{red}} \\ \bullet \xrightarrow{\text{black}} & \bullet \xleftarrow{\text{black}} & \bullet \xrightarrow{\text{black}} \end{array} &= \bar{u}(p, s) \\
 \begin{array}{ccc} \bullet \xleftarrow{\text{red}} & \bullet \xleftarrow{\text{red}} & \bullet \xleftarrow{\text{red}} \\ \bullet \xrightarrow{\text{black}} & \bullet \xleftarrow{\text{black}} & \bullet \xrightarrow{\text{black}} \end{array} &= v(p, s) \\
 \begin{array}{ccc} \xrightarrow{\text{red}} \bullet & \xrightarrow{\text{red}} \bullet & \xrightarrow{\text{red}} \bullet \\ \xrightarrow{\text{black}} \bullet & \xleftarrow{\text{black}} \bullet & \xrightarrow{\text{black}} \bullet \end{array} &= u(p, s) \\
 \begin{array}{ccc} \xleftarrow{\text{red}} \bullet & \xleftarrow{\text{red}} \bullet & \xleftarrow{\text{red}} \bullet \\ \xrightarrow{\text{black}} \bullet & \xleftarrow{\text{black}} \bullet & \xrightarrow{\text{black}} \bullet \end{array} &= \bar{v}(p, s)
 \end{aligned} \tag{C.10}$$

C.2 Background Field Vertices

In the calculation of the anapole moment the background field versions of the triple gauge vertex $\hat{\Gamma}_{AWW}^{\mu\nu\rho}$ and the gauge-gauge-Goldstone vertex $\hat{\Gamma}_{AWG}^{\mu\nu}$ appear. Their Feynman rules are shown in eq. (C.11) with explicit values in the BFM Feynman gauge (e.g. with $\xi_Q = 1$) given in eqs. (C.12) and (C.13).

$$\begin{array}{ccc}
 \begin{array}{c} \hat{A}_\mu \xrightarrow{k_1} \bullet \\ \begin{array}{l} \nearrow^{k_2} W_\nu^+ \\ \searrow_{k_3} W_\rho^- \end{array} \end{array} & = i\hat{\Gamma}_{AWW}^{\mu\nu\rho}, & \begin{array}{c} \hat{A}_\mu \xrightarrow{k_1} \bullet \\ \begin{array}{l} \nearrow^{k_2} W_\nu^+ \\ \searrow_{k_3} G^- \end{array} \end{array} & = i\hat{\Gamma}_{AWG}^{\mu\nu}
 \end{array} \tag{C.11}$$

Explicitly, the triple gauge vertex reads

$$i\hat{\Gamma}_{AWW}^{\mu\nu\rho}(k_1, k_2, k_3) = -ie [g_{\nu\rho}(k_3 - k_2)_\mu + g_{\mu\nu}(k_2 - k_1 + k_3)_\rho + g_{\rho\mu}(k_1 - k_3 - k_2)_\nu] \tag{C.12}$$

and the gauge-gauge-Goldstone vertex reads

$$i\hat{\Gamma}_{AWG}^{\mu\nu}(k_1, k_2, k_3) = 0. \tag{C.13}$$

The other vertices do not differ from the conventional rules [60].

C.3 Supersymmetric Vertices

The Feynman rules used for the calculation of the anapole moment in the MSSM are based on the notation and conventions of [25]. Furthermore, since we are only interested in the lightest neutralino in this work, the abbreviation $\chi \equiv \tilde{\chi}_1^0$ is used. The interaction Lagrangian can be split into two "prototypes", in which the exact couplings and fields depend on the exact scenario at hand. The sfermion-fermion-neutralino interaction can be written as

$$\mathcal{L}_{\tilde{f}f\chi} = \bar{\chi} (c_L P_L + c_R P_R) f \tilde{f}^* + \text{h.c.}, \quad (\text{C.14})$$

whereas the W-neutralino-chargino Lagrangian reads

$$\mathcal{L}_{W\chi\chi^+} = W_\mu^- \bar{\chi} g_k^j \Gamma_\mu^j \chi_k^+ + \text{h.c.}, \quad (\text{C.15})$$

with

$$g_k^j \Gamma_\mu^j = \gamma_\mu \left[v_L^k P_L + v_R^k P_R \right]. \quad (\text{C.16})$$

The corresponding Feynman rules, taking into account the special treatment introduced in appendix C.1, are summarized in fig. C.1.

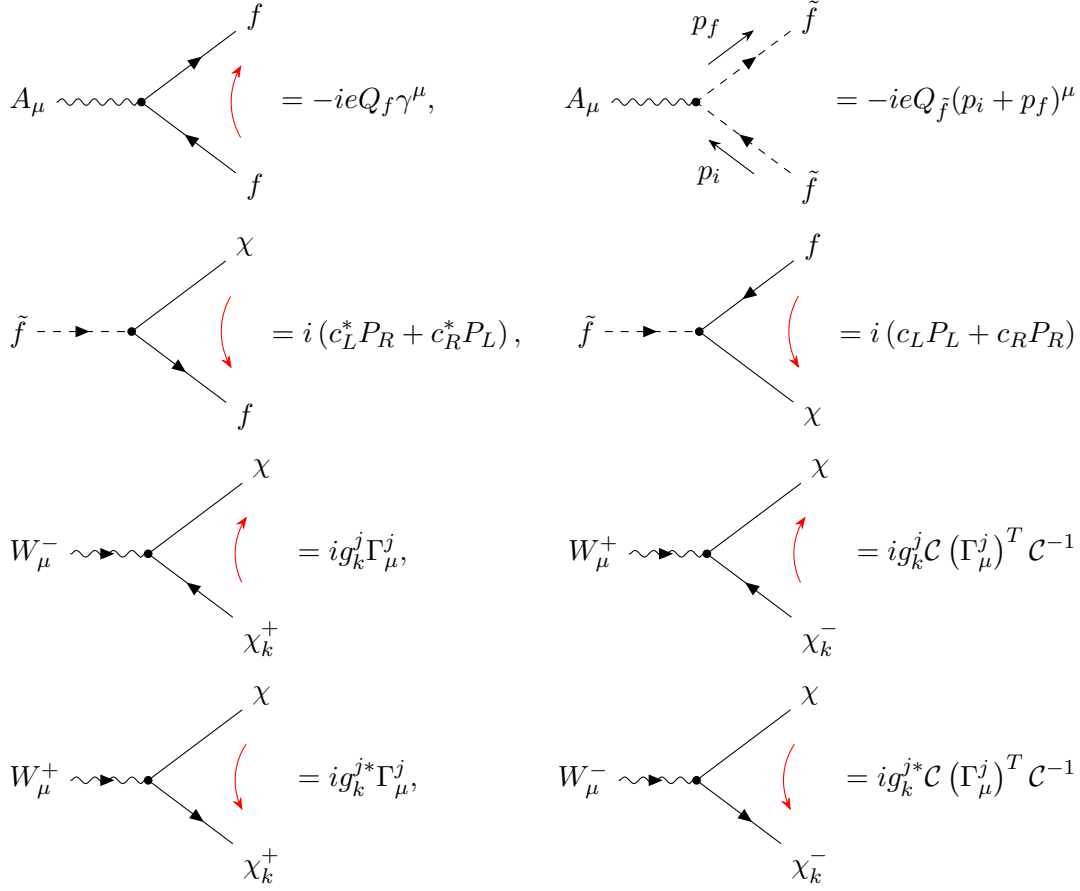


Figure C.1: Feynman rules based off the MSSM. The fields χ are Neutralino-like Majorana fermions, χ_k^+ chargino like charged Dirac fermion, f is a Dirac fermion like lepton or quark and \tilde{f} its spin-0 superpartner. The red arrow corresponds to the fermion flow in order to treat the Majorana vertices consistently, see text for details. [01.02.2022: wrong momentum arrow of \$p_f\$ of the scalar-photon interaction](#)

C.4 Vertices in the MSSM

In this section all vertices of the MSSM are listed which are needed for the calculation of the anapole moment of $\tilde{\chi}_1^0$. They are based on [25].

Chargino - Higgs - Neutralino

The Lagrangian describing the interaction between charginos, charged Higgs and neutralino is given by

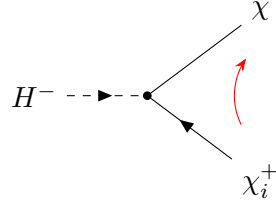
$$\mathcal{L} \supset -gH^-\bar{\chi} [Q_L^i P_L + Q_R^i P_R] \chi_i^+ + \text{h.c.} \quad (\text{C.17})$$

with

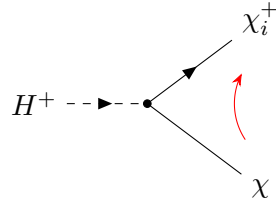
$$Q_L^i = \cos \beta \left[N_{14}^* V_{i1}^* + \frac{1}{\sqrt{2}} V_{i2}^* (N_{12}^* + \tan \theta_W N_{11}^*) \right] = -c_L^{iH} / g, \quad (\text{C.18a})$$

$$Q_R^i = \sin \beta \left[N_{13} U_{i1} - \frac{1}{\sqrt{2}} U_{i2} (N_{12} + \tan \theta_W N_{11}) \right] = -c_R^{iH} / g \quad (\text{C.18b})$$

and corresponding vertices



$$= i [c_L^{iH} P_L + c_R^{iH} P_R], \quad (\text{C.19a})$$



$$= i [c_L^{iH^*} P_R + c_R^{iH^*} P_L]. \quad (\text{C.19b})$$

The couplings are written in the generic way of appendix C.3 and take the form

$$c_L^{1H} = -g \cos \beta \left[N_{14}^* \cos \phi_R + \frac{1}{\sqrt{2}} \sin \phi_R (N_{12}^* + \tan \theta_W N_{11}^*) \right], \quad (\text{C.20a})$$

$$c_L^{2H} = -\epsilon_R g \cos \beta \left[-N_{14}^* \sin \phi_R + \frac{1}{\sqrt{2}} \cos \phi_R (N_{12}^* + \tan \theta_W N_{11}^*) \right], \quad (\text{C.20b})$$

$$c_R^{1H} = -g \sin \beta \left[N_{13} \cos \phi_L - \frac{1}{\sqrt{2}} \sin \phi_L (N_{12} + \tan \theta_W N_{11}) \right], \quad (\text{C.20c})$$

$$c_R^{2H} = -g \sin \beta \left[-N_{13} \sin \phi_L - \frac{1}{\sqrt{2}} \cos \phi_L (N_{12} + \tan \theta_W N_{11}) \right]. \quad (\text{C.20d})$$

for real chargino mixing matrices as in section 3.4.4.

Chargino - NGB - Neutralino

Since the charged Nambu-Goldstone boson (NGB) and the charged Higgs are related via eq. (3.83), the couplings between the chargino and charged NGB can be inferred from the chargino - charged Higgs vertex (explicit rules can be found in [149, Appendix A.7]) via $(\cos \beta, \sin \beta) \rightarrow (\sin \beta, -\cos \beta)$. Thus the couplings read:

$$c_L^{1G} = -g \sin \beta \left[N_{14}^* \cos \phi_R + \frac{1}{\sqrt{2}} \sin \phi_R (N_{12}^* + \tan \theta_W N_{11}^*) \right], \quad (\text{C.21a})$$

$$c_L^{2G} = -\epsilon_R g \sin \beta \left[-N_{14}^* \sin \phi_R + \frac{1}{\sqrt{2}} \cos \phi_R (N_{12}^* + \tan \theta_W N_{11}^*) \right], \quad (\text{C.21b})$$

$$c_R^{1G} = g \cos \beta \left[N_{13} \cos \phi_L - \frac{1}{\sqrt{2}} \sin \phi_L (N_{12} + \tan \theta_W N_{11}) \right], \quad (\text{C.21c})$$

$$c_R^{2G} = g \cos \beta \left[-N_{13} \sin \phi_L - \frac{1}{\sqrt{2}} \cos \phi_L (N_{12} + \tan \theta_W N_{11}) \right]. \quad (\text{C.21d})$$

Chargino - W - Neutralino

Here the relevant part of the Lagrangian is

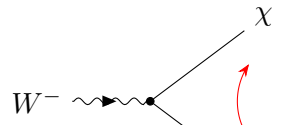
$$\mathcal{L} \supset g W_\mu^- \bar{\chi} \gamma_\mu (C_L^i P_L + C_R^i P_R) \chi_i^+ + \text{h.c.} \quad (\text{C.22})$$

with couplings

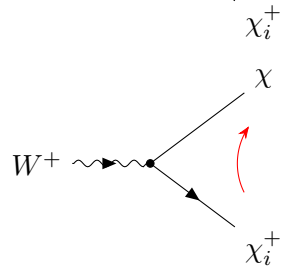
$$C_L^i = N_{12} V_{i1}^* - \frac{1}{\sqrt{2}} N_{14} V_{i2}^* = v_L^i / g, \quad (\text{C.23a})$$

$$C_R^i = N_{12}^* U_{i1} + \frac{1}{\sqrt{2}} N_{13}^* U_{i2} = v_R^i / g \quad (\text{C.23b})$$

and vertices



$$= i\gamma_\mu [v_L^i P_L + v_R^i P_R], \quad (\text{C.24a})$$



$$= -i\gamma_\mu [v_R^{i*} P_L + v_L^{i*} P_R]. \quad (\text{C.24b})$$

The expression for the second vertex has the left- and right projectors interchanged due to the fact that the reversed vertex as in [66, 67] was used. Explicitly the couplings are

$$v_L^1 = g \left[N_{12} \cos \phi_R - \frac{1}{\sqrt{2}} N_{14} \sin \phi_R \right], \quad (\text{C.25a})$$

$$v_L^2 = \epsilon_R g \left[-N_{12} \sin \phi_R - \frac{1}{\sqrt{2}} N_{14} \cos \phi_R \right], \quad (\text{C.25b})$$

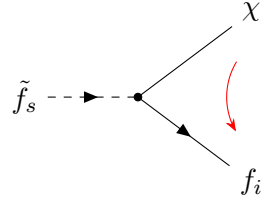
$$v_R^1 = g \left[N_{12}^* \cos \phi_L + \frac{1}{\sqrt{2}} N_{13}^* \sin \phi_L \right], \quad (\text{C.25c})$$

$$v_R^2 = g \left[-N_{12}^* \sin \phi_L + \frac{1}{\sqrt{2}} N_{13}^* \cos \phi_L \right]. \quad (\text{C.25d})$$

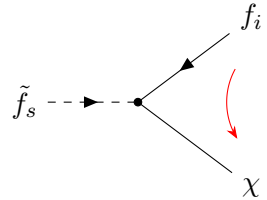
with real chargino mixing matrices as in section 3.4.4.

Sfermion - Fermion - Neutralino

The interaction including charged sfermions and fermions is described by the Feynman rules



$$= i \left(G_{is}^{fL*} P_R + G_{is}^{fR*} P_L \right), \quad (\text{C.26a})$$



$$= i \left(G_{is}^{fL} P_L + G_{is}^{fR} P_R \right). \quad (\text{C.26b})$$

The explicit couplings for the squark - quark¹ interactions are deduced from the Lagrangian

$$\mathcal{L} = \bar{\chi} \left[(G_{is}^{uL} P_L + G_{is}^{uR} P_R) \tilde{u}_s^\dagger u_i + (G_{is}^{dL} P_L + G_{is}^{dR} P_R) \tilde{d}_s^\dagger d_i \right] + \text{h.c.} \quad (\text{C.27})$$

¹The quark states are mass eigenstates here

with

$$G_{is}^{uL} = G^{uL} W_{j,s}^{\tilde{u}*} U_{ji}^{uL} - \frac{g}{\sqrt{2}m_W \sin \beta} m_{u_i} N_{14}^* W_{j+3,s}^{\tilde{u}*} U_{ji}^{uR}, \quad (\text{C.28a})$$

$$G_{is}^{uR} = G^{uR} W_{j+3,s}^{\tilde{u}*} U_{ji}^{uR} - \frac{g}{\sqrt{2}m_W \sin \beta} m_{u_i} N_{14} W_{j,s}^{\tilde{u}*} U_{ji}^{uL}, \quad (\text{C.28b})$$

$$G_{is}^{dL} = G^{dL} W_{j,s}^{\tilde{d}*} U_{ji}^{dL} - \frac{g}{\sqrt{2}m_W \cos \beta} m_{d_i} N_{13}^* W_{j+3,s}^{\tilde{d}*} U_{ji}^{dR}, \quad (\text{C.28c})$$

$$G_{is}^{dR} = G^{dR} W_{j+3,s}^{\tilde{d}*} U_{ji}^{dR} - \frac{g}{\sqrt{2}m_W \cos \beta} m_{d_i} N_{13} W_{j,s}^{\tilde{d}*} U_{ji}^{dL}, \quad (\text{C.28d})$$

where \tilde{q}_s , $s = 1, \dots, 6$, are six component squarks as in section 3.4.5, $j, i = 1, 2, 3$ being a generation index and G^{qL} and G^{qR} as in

$$G^{fL} = -\sqrt{2}g \left[T_{3L}^f N_{12}^* + \tan \theta_W (Q_f - T_{3L}^f) N_{11}^* \right], \quad (\text{C.29a})$$

$$G^{fR} = \sqrt{2}g \tan \theta_W Q_f N_{11}, \quad (\text{C.29b})$$

where Q_f and T_{3L}^f are the EM charge and third component of the weak isospin of the fermion f respectively. The mixing between sfermions is described by the matrices $W^{\tilde{f}}$. Here we will adopt the assumption that only L/R mixing is allowed, such that they simplify to (no summation implied)

$$W_{i,i}^{\tilde{f}} = W_{i+3,i+3}^{\tilde{f}} = \cos \theta_{\tilde{f}_i}, \quad (\text{C.30a})$$

$$W_{i,i+3}^{\tilde{f}} = -W_{i+3,i}^{\tilde{f}} = -\sin \theta_{\tilde{f}_i}. \quad (\text{C.30b})$$

The matrices U^{qL} and U^{qR} are unitary matrices diagonalizing the mass matrix of the quark q via a biunitary transformation, e.g.

$$(U^{uL\dagger} \mathbf{m}_u U^{uR})_{ij} \equiv m_{u_i} \delta_{ij}, \quad (U^{dL\dagger} \mathbf{m}_d U^{dR})_{ij} \equiv m_{d_i} \delta_{ij}. \quad (\text{C.31})$$

We will take the approximation in which

$$U^{qL} = U^{qR} = \mathbf{1}. \quad (\text{C.32})$$

This means that the interactions are "diagonal", e.g. only interactions between a squark - quark pair of the same flavor is allowed. Before writing down the couplings for quarks explicitly, lets discuss the slepton interactions first. The Lagrangian for charged leptons read

$$\mathcal{L} = \bar{\chi} [G_{is}^{eL} P_L + G_{is}^{eR} P_R] \tilde{e}_s^* e_i + \text{h.c.} \quad (\text{C.33})$$

with

$$G_{is}^{eL} = G^{eL} W_{i,s}^{\tilde{e}} - \frac{g}{\sqrt{2}m_W \cos \beta} m_{e_i} N_{13}^* W_{i+3,s}^{\tilde{e}} \quad (\text{C.34a})$$

$$G_{is}^{eR} = G^{eR} W_{i+3,s}^{\tilde{e}} - \frac{g}{\sqrt{2}m_W \cos \beta} m_{e_i} N_{13} W_{i,s}^{\tilde{e}} \quad (\text{C.34b})$$

Type	e	u	d
Q_f	-1	$+\frac{2}{3}$	$-\frac{1}{3}$
T_{3L}^f	$-\frac{1}{2}$	$+\frac{1}{2}$	$-\frac{1}{2}$

 Table C.1: Charge and Weak Isospin of SM fermions (excluding ν)

Mass [GeV]	e-Type	u-Type	d-Type
1st Generation	0.51×10^{-3}	2.16×10^{-3}	4.67×10^{-3}
2nd Generation	105.65×10^{-3}	1.27	93×10^{-3}
3rd Generation	1.78	4.18	172.76

 Table C.2: Masses of the SM fermions (excluding ν)

and G^{eL} , G^{eR} and $W^{\tilde{e}}$ as before. Contrary to the quark case, for leptons the mass- and gauge eigenstates are identical already, e.g.

$$(\mathbf{m}_e)_{ij} = m_{e_i} \delta_{ij}, \quad (\text{C.35})$$

such that no generation-mixing matrices appear.

Due to the simplification we made in the quark sector, both leptons and quarks exhibit a very similar structure of the couplings. Summing over the sfermion index s , while suppressing the fermion index i , e.g. $f_i \rightarrow f$, we can express the interaction Lagrangian for sfermion - fermion - neutralino as

$$\begin{aligned} \mathcal{L} = & \sum_f \bar{\chi} \left[(G^{\tilde{f}L} \cos \theta_{\tilde{f}} + H^{\tilde{f}R} \sin \theta_{\tilde{f}}) P_L + (G^{\tilde{f}R} \sin \theta_{\tilde{f}} + H^{\tilde{f}L} \cos \theta_{\tilde{f}}) P_R \right] \tilde{f}_1^\dagger f \\ & + \sum_f \bar{\chi} \left[(-G^{\tilde{f}L} \sin \theta_{\tilde{f}} + H^{\tilde{f}R} \cos \theta_{\tilde{f}}) P_L + (G^{\tilde{f}R} \cos \theta_{\tilde{f}} - H^{\tilde{f}L} \sin \theta_{\tilde{f}}) P_R \right] \tilde{f}_2^\dagger f \\ & + \text{h.c.} \end{aligned} \quad (\text{C.36})$$

with $G^{\tilde{f}L}$ and $G^{\tilde{f}R}$ as above and

$$H^{\tilde{f}L} = -\frac{g}{\sqrt{2}m_W} m_f \times \begin{cases} N_{14}/\sin \beta, & f = u \\ N_{13}/\cos \beta, & f = d, e \end{cases} \quad (\text{C.37a})$$

$$H^{\tilde{f}R} = H^{\tilde{f}L*} \quad (\text{C.37b})$$

The charge and weak isospin of the fermions are listed in table C.1, while the SM fermion masses of the PDG [125] are listed in table C.2.

Bibliography

- [1] N. Aghanim et al. »Planck 2018 results. VI. Cosmological parameters«. In: *Astron. Astrophys.* 641 (2020), A6. DOI: 10.1051/0004-6361/201833910. arXiv: 1807.06209 [astro-ph.CO].
- [2] Gianfranco Bertone, Dan Hooper and Joseph Silk. »Particle dark matter: Evidence, candidates and constraints«. In: *Phys. Rept.* 405 (2005), pp. 279–390. DOI: 10.1016/j.physrep.2004.08.031. arXiv: hep-ph/0404175.
- [3] Scott Dodelson. *Modern cosmology*. Acad. Press, 2003. ISBN: 0-12-219141-2.
- [4] Martin Bauer and Tilman Plehn. *Yet Another Introduction to Dark Matter: The Particle Physics Approach*. Vol. 959. Lecture Notes in Physics. Springer, 2019. DOI: 10.1007/978-3-030-16234-4. arXiv: 1705.01987 [hep-ph].
- [5] Fritz Zwicky. »Die Rotverschiebung von extragalaktischen Nebeln«. In: *Helvetica Physica Acta* (Nov. 1933).
- [6] Heinz Andernach and Fritz Zwicky. *English and Spanish Translation of Zwicky's (1933) The Redshift of Extragalactic Nebulae*. 2017. arXiv: 1711.01693 [astro-ph.IM].
- [7] Andrew McKellar. »Molecular Lines from the Lowest States of Diatomic Molecules Composed of Atoms Probably Present in Interstellar Space«. In: *Publications of the Dominion Astrophysical Observatory Victoria* 7 (Jan. 1941), p. 251.
- [8] A. A. Penzias and R. W. Wilson. »A Measurement of Excess Antenna Temperature at 4080 Mc/s.« In: *Astrophysical Journal* 142 (July 1965), pp. 419–421. DOI: 10.1086/148307.
- [9] C. L. Bennett et al. »NINE-YEAR WILKINSON MICROWAVE ANISOTROPY PROBE (WMAP) OBSERVATIONS: FINAL MAPS AND RESULTS«. In: *The Astrophysical Journal Supplement Series* 208.2 (Sept. 2013), p. 20. DOI: 10.1088/0067-0049/208/2/20. URL: <https://doi.org/10.1088/0067-0049/208/2/20>.
- [10] F. Bernardeau et al. »Large-scale structure of the Universe and cosmological perturbation theory«. In: *Physics Reports* 367.1 (2002), pp. 1–248. ISSN: 0370-1573. DOI: [https://doi.org/10.1016/S0370-1573\(02\)00135-7](https://doi.org/10.1016/S0370-1573(02)00135-7). URL: <http://www.sciencedirect.com/science/article/pii/S0370157302001357>.

- [11] Nicolás Bernal et al. »The Dawn of FIMP Dark Matter: A Review of Models and Constraints«. In: *Int. J. Mod. Phys. A* 32.27 (2017), p. 1730023. DOI: 10.1142/S0217751X1730023X. arXiv: 1706.07442 [hep-ph].
- [12] Graciela Gelmini and Paolo Gondolo. »DM Production Mechanisms«. In: (Sept. 2010), pp. 121–141. arXiv: 1009.3690 [astro-ph.CO].
- [13] Matthew D. Schwartz. *Quantum Field Theory and the Standard Model*. Cambridge University Press, Mar. 2014. ISBN: 978-1-107-03473-0.
- [14] Sven Krippendorff, Fernando Quevedo and Oliver Schlotterer. *Cambridge Lectures on Supersymmetry and Extra Dimensions*. 2010. arXiv: 1011.1491 [hep-th].
- [15] Stephen P. Martin. »A Supersymmetry primer«. In: *Perspectives on supersymmetry. Vol.2*. Ed. by Gordon L. Kane. Vol. 21. 2010, pp. 1–153. DOI: 10.1142/9789812839657_0001. arXiv: hep-ph/9709356.
- [16] G Kane and M Shifman. *The Supersymmetric World*. WORLD SCIENTIFIC, 2000. DOI: 10.1142/4611. eprint: <https://www.worldscientific.com/doi/pdf/10.1142/4611>. URL: <https://www.worldscientific.com/doi/abs/10.1142/4611>.
- [17] J. Terning. *Modern supersymmetry: Dynamics and duality*. Apr. 2006. DOI: 10.1093/acprof:oso/9780198567639.001.0001.
- [18] Rudolf Haag, Jan T. Lopuszanski and Martin Sohnius. »All Possible Generators of Supersymmetries of the s Matrix«. In: *Nucl. Phys. B* 88 (1975), p. 257. DOI: 10.1016/0550-3213(75)90279-5.
- [19] J. Wess and B. Zumino. »Supergauge Transformations in Four-Dimensions«. In: *Nucl. Phys. B* 70 (1974). Ed. by A. Salam and E. Sezgin, pp. 39–50. DOI: 10.1016/0550-3213(74)90355-1.
- [20] Abdus Salam and J.A. Strathdee. »Supergauge Transformations«. In: *Nucl. Phys. B* 76 (1974), pp. 477–482. DOI: 10.1016/0550-3213(74)90537-9.
- [21] Nathan Seiberg. »The Power of holomorphy: Exact results in 4-D SUSY field theories«. In: *Particles, Strings, and Cosmology (PASCOS 94)*. May 1994, pp. 0357–369. arXiv: hep-th/9408013.
- [22] Martin F. Sohnius and Peter C. West. »Conformal invariance in $N = 4$ supersymmetric Yang-Mills theory«. In: *Physics Letters B* 100.3 (1981), pp. 245–250. ISSN: 0370-2693. DOI: [https://doi.org/10.1016/0370-2693\(81\)90326-9](https://doi.org/10.1016/0370-2693(81)90326-9). URL: <http://www.sciencedirect.com/science/article/pii/0370269381903269>.

- [23] Stanley Mandelstam. »Light Cone Superspace and the Ultraviolet Finiteness of the N=4 Model«. In: *Nucl. Phys. B* 213 (1983), pp. 149–168. DOI: 10.1016/0550-3213(83)90179-7.
- [24] Nathan Seiberg. »Supersymmetry and Nonperturbative beta Functions«. In: *Phys. Lett. B* 206 (1988), pp. 75–80. DOI: 10.1016/0370-2693(88)91265-8.
- [25] Manuel Drees, Rohini Godbole and Probir Roy. *Theory and Phenomenology of Sparticles: An Account of Four-Dimensional N =1 Supersymmetry in High Energy Physics*. Jan. 2005, pp. 1–556. ISBN: 978-981-02-3739-4. DOI: 10.1142/4001.
- [26] B. C. Allanach. »SOFTSUSY: a program for calculating supersymmetric spectra«. In: *Comput. Phys. Commun.* 143 (2002), pp. 305–331. DOI: 10.1016/S0010-4655(01)00460-X. arXiv: hep-ph/0104145 [hep-ph].
- [27] Abdelhak Djouadi, Jean-Loic Kneur and Gilbert Moultaka. »SuSpect: A Fortran code for the supersymmetric and Higgs particle spectrum in the MSSM«. In: *Comput. Phys. Commun.* 176 (2007), pp. 426–455. DOI: 10.1016/j.cpc.2006.11.009. arXiv: hep-ph/0211331.
- [28] Serguei Chatrchyan et al. »Observation of a New Boson at a Mass of 125 GeV with the CMS Experiment at the LHC«. In: *Phys. Lett. B* 716 (2012), pp. 30–61. DOI: 10.1016/j.physletb.2012.08.021. arXiv: 1207.7235 [hep-ex].
- [29] Georges Aad et al. »Observation of a new particle in the search for the Standard Model Higgs boson with the ATLAS detector at the LHC«. In: *Phys. Lett. B* 716 (2012), pp. 1–29. DOI: 10.1016/j.physletb.2012.08.020. arXiv: 1207.7214 [hep-ex].
- [30] W. Hollik and H. Rzehak. »The Sfermion mass spectrum of the MSSM at the one loop level«. In: *Eur. Phys. J. C* 32 (2003), pp. 127–133. DOI: 10.1140/epjc/s2003-01387-9. arXiv: hep-ph/0305328.
- [31] Ian J.R. Aitchison. »Supersymmetry and the MSSM: An Elementary introduction«. In: (May 2005). arXiv: hep-ph/0505105.
- [32] Thomas Hahn. »Generating Feynman diagrams and amplitudes with FeynArts 3«. In: *Computer Physics Communications* 140.3 (Nov. 2001), pp. 418–431. ISSN: 0010-4655. DOI: 10.1016/S0010-4655(01)00290-9. URL: [http://dx.doi.org/10.1016/S0010-4655\(01\)00290-9](http://dx.doi.org/10.1016/S0010-4655(01)00290-9).
- [33] R. Mertig, M. Böhm and A. Denner. »Feyn Calc - Computer-algebraic calculation of Feynman amplitudes«. In: *Computer Physics Communications* 64.3 (1991), pp. 345–359. ISSN: 0010-4655. DOI: [https://doi.org/10.1016/0010-4655\(91\)90130-D](https://doi.org/10.1016/0010-4655(91)90130-D). URL: <http://www.sciencedirect.com/science/article/pii/001046559190130D>.

- [34] Vladyslav Shtabovenko, Rolf Mertig and Frederik Orellana. »New developments in FeynCalc 9.0«. In: *Computer Physics Communications* 207 (Oct. 2016), pp. 432–444. ISSN: 0010-4655. DOI: 10.1016/j.cpc.2016.06.008. URL: <http://dx.doi.org/10.1016/j.cpc.2016.06.008>.
- [35] Vladyslav Shtabovenko, Rolf Mertig and Frederik Orellana. »FeynCalc 9.3: New features and improvements«. In: *Computer Physics Communications* 256 (Nov. 2020), p. 107478. ISSN: 0010-4655. DOI: 10.1016/j.cpc.2020.107478. URL: <http://dx.doi.org/10.1016/j.cpc.2020.107478>.
- [36] Hiren H. Patel. *Package-X: A Mathematica package for the analytic calculation of one-loop integrals*. 2015. arXiv: 1503.01469 [hep-ph].
- [37] Vladyslav Shtabovenko. »FeynHelpers: Connecting FeynCalc to FIRE and Package-X«. In: *Computer Physics Communications* 218 (Sept. 2017), pp. 48–65. ISSN: 0010-4655. DOI: 10.1016/j.cpc.2017.04.014. URL: <http://dx.doi.org/10.1016/j.cpc.2017.04.014>.
- [38] Joshua P. Ellis. »TikZ-Feynman: Feynman diagrams with TikZ«. In: *Computer Physics Communications* 210 (2017), pp. 103–123. ISSN: 0010-4655. DOI: <https://doi.org/10.1016/j.cpc.2016.08.019>. URL: <http://www.sciencedirect.com/science/article/pii/S0010465516302521>.
- [39] C. Brogini, C. Giunti and A. Studenikin. »Electromagnetic Properties of Neutrinos«. In: *Adv. High Energy Phys.* 2012 (2012), p. 459526. DOI: 10.1155/2012/459526. arXiv: 1207.3980 [hep-ph].
- [40] Andrzej Czarnecki and Bernd Krause. »On the dipole moments of fermions at two loops«. In: *Acta Phys. Polon. B* 28 (1997). Ed. by S. Jadach, M. Skrzypek and Z. Was, pp. 829–834. arXiv: hep-ph/9611299.
- [41] P. Breitenlohner and D. Maison. »Dimensional Renormalization and the Action Principle«. In: *Commun. Math. Phys.* 52 (Feb. 1977). DOI: 10.1007/BF01609069.
- [42] Gerard t Hooft and M. Veltman. »Regularization and Renormalization of Gauge Fields«. In: *Nuclear Physics B* 44 (July 1972), pp. 189–213. DOI: 10.1016/0550-3213(72)90279-9.
- [43] S. A. Larin. »The Renormalization of the axial anomaly in dimensional regularization«. In: *Phys. Lett. B* 303 (1993), pp. 113–118. DOI: 10.1016/0370-2693(93)90053-K. arXiv: hep-ph/9302240.
- [44] M. J. Musolf and Barry R. Holstein. »Observability of the anapole moment and neutrino charge radius«. In: *Phys. Rev. D* 43 (1991), pp. 2956–2970. DOI: 10.1103/PhysRevD.43.2956.

- [45] J. Bernabeu et al. »On the charge radius of the neutrino«. In: *Phys. Rev. D* 62 (2000), p. 113012. DOI: 10.1103/PhysRevD.62.113012. arXiv: hep-ph/0008114.
- [46] Carlo Giunti and Alexander Studenikin. »Neutrino electromagnetic interactions: a window to new physics«. In: *Rev. Mod. Phys.* 87 (2015), p. 531. DOI: 10.1103/RevModPhys.87.531. arXiv: 1403.6344 [hep-ph].
- [47] A. Rosado. »Physical electroweak anapole moment for the neutrino«. In: *Phys. Rev. D* 61 (1 Nov. 1999), p. 013001. DOI: 10.1103/PhysRevD.61.013001. URL: <https://link.aps.org/doi/10.1103/PhysRevD.61.013001>.
- [48] Carlo Giunti and Alexander Studenikin. »Neutrino electromagnetic properties«. In: *Phys. Atom. Nucl.* 72 (2009), pp. 2089–2125. DOI: 10.1134/S1063778809120126. arXiv: 0812.3646 [hep-ph].
- [49] Carlo Giunti et al. »Electromagnetic neutrinos in laboratory experiments and astrophysics«. In: *Annalen Phys.* 528 (2016), pp. 198–215. DOI: 10.1002/andp.201500211. arXiv: 1506.05387 [hep-ph].
- [50] Ansgar Denner. »Techniques for calculation of electroweak radiative corrections at the one loop level and results for W physics at LEP-200«. In: *Fortsch. Phys.* 41 (1993), pp. 307–420. DOI: 10.1002/prop.2190410402. arXiv: 0709.1075 [hep-ph].
- [51] Norman Dombey and A. D. Kennedy. »Calculation of the Electron Anapole Moment«. In: *Phys. Lett. B* 91 (1980), pp. 428–430. DOI: 10.1016/0370-2693(80)91013-8.
- [52] J. Bernabeu, J. Papavassiliou and J. Vidal. »The Neutrino charge radius is a physical observable«. In: *Nucl. Phys. B* 680 (2004), pp. 450–478. DOI: 10.1016/j.nuclphysb.2003.12.025. arXiv: hep-ph/0210055.
- [53] J. Papavassiliou, J. Bernabeu and J. Vidal. *On the definition and observability of the neutrino charge radius*. 2002. arXiv: hep-ph/0210312 [hep-ph].
- [54] J. Papavassiliou et al. *The effective neutrino charge radius*. 2003. arXiv: hep-ph/0310028 [hep-ph].
- [55] J. Bernabéu, J. Papavassiliou and J. Vidal. »The neutrino charge radius as a physical observable«. In: *Nuclear Physics B* 680.1-3 (Mar. 2004), pp. 450–478. ISSN: 0550-3213. DOI: 10.1016/j.nuclphysb.2003.12.025. URL: <http://dx.doi.org/10.1016/j.nuclphysb.2003.12.025>.
- [56] Kazuo Fujikawa and Robert Shrock. »On a neutrino electroweak radius«. In: *Phys. Rev. D* 69 (2004), p. 013007. DOI: 10.1103/PhysRevD.69.013007. arXiv: hep-ph/0309329.

- [57] Maxim Dvornikov and Alexander Studenikin. »Electric charge and magnetic moment of massive neutrino«. In: *Phys. Rev. D* 69 (2004), p. 073001. DOI: 10.1103/PhysRevD.69.073001. arXiv: hep-ph/0305206.
- [58] Daniele Binosi and Joannis Papavassiliou. »Pinch technique: Theory and applications«. In: *Physics Reports* 479.1 (2009), pp. 1–152. ISSN: 0370-1573. DOI: <https://doi.org/10.1016/j.physrep.2009.05.001>. URL: <http://www.sciencedirect.com/science/article/pii/S0370157309001409>.
- [59] Ansgar Denner, G. Weiglein and S. Dittmaier. »Gauge invariance of Green functions: Background field method versus pinch technique«. In: *Phys. Lett. B* 333 (1994), pp. 420–426. DOI: 10.1016/0370-2693(94)90162-7. arXiv: hep-ph/9406204.
- [60] Ansgar Denner, Georg Weiglein and Stefan Dittmaier. »Application of the background field method to the electroweak standard model«. In: *Nucl. Phys. B* 440 (1995), pp. 95–128. DOI: 10.1016/0550-3213(95)00037-S. arXiv: hep-ph/9410338.
- [61] Henriette Elvang and Yu-tin Huang. »Scattering Amplitudes«. In: (Aug. 2013). arXiv: 1308.1697 [hep-th].
- [62] Joannis Papavassiliou. »Gauge independent transverse and longitudinal self energies and vertices via the pinch technique«. In: *Phys. Rev. D* 50 (1994), pp. 5958–5970. DOI: 10.1103/PhysRevD.50.5958. arXiv: hep-ph/9406258.
- [63] Shoji Hashimoto et al. »The Background field method: Alternative way of deriving the pinch technique’s results«. In: *Phys. Rev. D* 50 (1994), pp. 7066–7076. DOI: 10.1103/PhysRevD.50.7066. arXiv: hep-ph/9406271.
- [64] Joannis Papavassiliou. »On the connection between the pinch technique and the background field method«. In: *Phys. Rev. D* 51 (1995), pp. 856–861. DOI: 10.1103/PhysRevD.51.856. arXiv: hep-ph/9410385.
- [65] Howard E. Haber and Gordon L. Kane. »The Search for Supersymmetry: Probing Physics Beyond the Standard Model«. In: *Phys. Rept.* 117 (1985), pp. 75–263. DOI: 10.1016/0370-1573(85)90051-1.
- [66] Ansgar Denner et al. »Feynman rules for fermion number violating interactions«. In: *Nucl. Phys. B* 387 (1992), pp. 467–481. DOI: 10.1016/0550-3213(92)90169-C.
- [67] Ansgar Denner et al. »Compact Feynman rules for Majorana fermions«. In: *Phys. Lett. B* 291 (1992), pp. 278–280. DOI: 10.1016/0370-2693(92)91045-B.
- [68] Joachim Kopp, Lisa Michaels and Juri Smirnov. »Loopy Constraints on Leptophilic Dark Matter and Internal Bremsstrahlung«. In: *JCAP* 04 (2014), p. 022. DOI: 10.1088/1475-7516/2014/04/022. arXiv: 1401.6457 [hep-ph].

- [69] Michael J. Baker and Andrea Thamm. »Leptonic WIMP Coannihilation and the Current Dark Matter Search Strategy«. In: *JHEP* 10 (2018), p. 187. DOI: 10.1007/JHEP10(2018)187. arXiv: 1806.07896 [hep-ph].
- [70] Ta-Pei Cheng, Ling-Fong Li and David Gross. »Gauge Theory of Elementary Particle Physics«. In: *Physics Today - PHYS TODAY* 38 (Jan. 1985). DOI: 10.1063/1.2814821.
- [71] E. Aprile et al. »Excess electronic recoil events in XENON1T«. In: *Phys. Rev. D* 102.7 (2020), p. 072004. DOI: 10.1103/PhysRevD.102.072004. arXiv: 2006.09721 [hep-ex].
- [72] Amir N. Khan. »Can Nonstandard Neutrino Interactions explain the XENON1T spectral excess?«. In: *Phys. Lett. B* 809 (2020), p. 135782. DOI: 10.1016/j.physletb.2020.135782. arXiv: 2006.12887 [hep-ph].
- [73] W. B. Atwood et al. »The Large Area Telescope on the Fermi Gamma-ray Space Telescope Mission«. In: *Astrophys. J.* 697 (2009), pp. 1071–1102. DOI: 10.1088/0004-637X/697/2/1071. arXiv: 0902.1089 [astro-ph.IM].
- [74] R. Abbasi et al. »Search for GeV Neutrino Emission During Intense Gamma-Ray Solar Flares with the IceCube Neutrino Observatory«. In: (Jan. 2021). arXiv: 2101.00610 [astro-ph.HE].
- [75] Qihong Wang et al. »Results of dark matter search using the full PandaX-II exposure«. In: *Chin. Phys. C* 44.12 (2020), p. 125001. DOI: 10.1088/1674-1137/abb658. arXiv: 2007.15469 [astro-ph.CO].
- [76] D. S. Akerib et al. »First results from the LUX dark matter experiment at the Sanford Underground Research Facility«. In: *Phys. Rev. Lett.* 112 (2014), p. 091303. DOI: 10.1103/PhysRevLett.112.091303. arXiv: 1310.8214 [astro-ph.CO].
- [77] D. S. Akerib et al. »Improved Limits on Scattering of Weakly Interacting Massive Particles from Reanalysis of 2013 LUX Data«. In: *Phys. Rev. Lett.* 116.16 (2016), p. 161301. DOI: 10.1103/PhysRevLett.116.161301. arXiv: 1512.03506 [astro-ph.CO].
- [78] D. S. Akerib et al. »Results from a search for dark matter in the complete LUX exposure«. In: *Phys. Rev. Lett.* 118.2 (2017), p. 021303. DOI: 10.1103/PhysRevLett.118.021303. arXiv: 1608.07648 [astro-ph.CO].
- [79] D. S. Akerib et al. »Enhancing the sensitivity of the LUX-ZEPLIN (LZ) dark matter experiment to low energy signals«. In: (Jan. 2021). arXiv: 2101.08753 [astro-ph.IM].
- [80] Elena Aprile. »The XENON Dark Matter Experiment«. In: (Feb. 2005). arXiv: astro-ph/0502279.

- [81] Elena Aprile. »The XENON1T Dark Matter Search Experiment«. In: *Springer Proc. Phys.* 148 (2013). Ed. by David Cline, pp. 93–96. DOI: 10.1007/978-94-007-7241-0_14. arXiv: 1206.6288 [astro-ph.IM].
- [82] Paolo Beltrame. »Direct Dark Matter search with the XENON program«. In: *48th Rencontres de Moriond on Electroweak Interactions and Unified Theories*. 2013, pp. 143–148. arXiv: 1305.2719 [astro-ph.CO].
- [83] E. Aprile et al. »Projected WIMP sensitivity of the XENONnT dark matter experiment«. In: *JCAP* 11 (2020), p. 031. DOI: 10.1088/1475-7516/2020/11/031. arXiv: 2007.08796 [physics.ins-det].
- [84] Junjie Cao et al. »Explaining The XENON1T Excess With Light Goldstini Dark Matter«. In: (July 2020). arXiv: 2007.09981 [hep-ph].
- [85] M. Szydagis et al. »Investigating the XENON1T low-energy electronic recoil excess using NEST«. In: *Phys. Rev. D* 103.1 (2021), p. 012002. DOI: 10.1103/PhysRevD.103.012002. arXiv: 2007.00528 [hep-ex].
- [86] J. Aalbers et al. »DARWIN: towards the ultimate dark matter detector«. In: *JCAP* 11 (2016), p. 017. DOI: 10.1088/1475-7516/2016/11/017. arXiv: 1606.07001 [astro-ph.IM].
- [87] John Carr et al. »Prospects for Indirect Dark Matter Searches with the Cherenkov Telescope Array (CTA)«. In: *PoS ICRC2015* (2016), p. 1203. DOI: 10.22323/1.236.1203. arXiv: 1508.06128 [astro-ph.HE].
- [88] Yang Bai and Joshua Berger. »Lepton Portal Dark Matter«. In: *JHEP* 08 (2014), p. 153. DOI: 10.1007/JHEP08(2014)153. arXiv: 1402.6696 [hep-ph].
- [89] Julio F. Navarro, Carlos S. Frenk and Simon D. M. White. »The Structure of cold dark matter halos«. In: *Astrophys. J.* 462 (1996), pp. 563–575. DOI: 10.1086/177173. arXiv: astro-ph/9508025.
- [90] Alister W. Graham et al. »Empirical models for Dark Matter Halos. I. Non-parametric Construction of Density Profiles and Comparison with Parametric Models«. In: *Astron. J.* 132 (2006), pp. 2685–2700. DOI: 10.1086/508988. arXiv: astro-ph/0509417.
- [91] Anne M. Green. »Astrophysical uncertainties on direct detection experiments«. In: *Mod. Phys. Lett. A* 27 (2012), p. 1230004. DOI: 10.1142/S0217732312300042. arXiv: 1112.0524 [astro-ph.CO].
- [92] J. I. Read. »The Local Dark Matter Density«. In: *J. Phys. G* 41 (2014), p. 063101. DOI: 10.1088/0954-3899/41/6/063101. arXiv: 1404.1938 [astro-ph.GA].

- [93] Yoshiaki Sofue. »Rotation Curve of the Milky Way and the Dark Matter Density«. In: *Galaxies* 8.2 (2020). ISSN: 2075-4434. DOI: 10 . 3390/galaxies8020037. URL: <https://www.mdpi.com/2075-4434/8/2/37>.
- [94] Katherine Freese, Mariangela Lisanti and Christopher Savage. »Colloquium: Annual modulation of dark matter«. In: *Rev. Mod. Phys.* 85 (2013), pp. 1561–1581. DOI: 10 . 1103/RevModPhys . 85 . 1561. arXiv: 1209 . 3339 [astro-ph.CO].
- [95] Ralph Schönrich, James Binney and Walter Dehnen. »Local kinematics and the local standard of rest«. In: *Monthly Notices of the Royal Astronomical Society* 403.4 (Apr. 2010), pp. 1829–1833. ISSN: 1365-2966. DOI: 10.1111/j.1365-2966.2010.16253.x. URL: <http://dx.doi.org/10.1111/j.1365-2966.2010.16253.x>.
- [96] J.D. Lewin and P.F. Smith. »Review of mathematics, numerical factors, and corrections for dark matter experiments based on elastic nuclear recoil«. In: *Astroparticle Physics* 6.1 (1996), pp. 87–112. ISSN: 0927-6505. DOI: [https://doi.org/10.1016/S0927-6505\(96\)00047-3](https://doi.org/10.1016/S0927-6505(96)00047-3). URL: <http://www.sciencedirect.com/science/article/pii/S0927650596000473>.
- [97] V. A. Bednyakov and F. Simkovic. »Nuclear spin structure in dark matter search: The Finite momentum transfer limit«. In: *Phys. Part. Nucl.* 37 (2006), S106–S128. DOI: 10.1134/S1063779606070057. arXiv: hep-ph/0608097.
- [98] Torsten Bringmann et al. »DarkBit: A GAMBIT module for computing dark matter observables and likelihoods«. In: *Eur. Phys. J. C* 77.12 (2017), p. 831. DOI: 10.1140/epjc/s10052-017-5155-4. arXiv: 1705.07920 [hep-ph].
- [99] Jason Kumar and Danny Marfatia. »Matrix element analyses of dark matter scattering and annihilation«. In: *Phys. Rev. D* 88.1 (2013), p. 014035. DOI: 10.1103/PhysRevD.88.014035. arXiv: 1305.1611 [hep-ph].
- [100] Graciela B. Gelmini, Volodymyr Takhistov and Samuel J. Witte. »Casting a Wide Signal Net with Future Direct Dark Matter Detection Experiments«. In: *JCAP* 07 (2018). [Erratum: *JCAP* 02, E02 (2019)], p. 009. DOI: 10.1088/1475-7516/2018/07/009. arXiv: 1804.01638 [hep-ph].
- [101] Teresa Marrodán Undagoitia and Ludwig Rauch. »Dark matter direct-detection experiments«. In: *J. Phys. G* 43.1 (2016), p. 013001. DOI: 10 . 1088/0954-3899/43/1/013001. arXiv: 1509.08767 [physics.ins-det].
- [102] Gerard Jungman, Marc Kamionkowski and Kim Griest. »Supersymmetric dark matter«. In: *Phys. Rept.* 267 (1996), pp. 195–373. DOI: 10.1016/0370-1573(95)00058-5. arXiv: hep-ph/9506380.

- [103] Tom Banks, Jean-Francois Fortin and Scott Thomas. »Direct Detection of Dark Matter Electromagnetic Dipole Moments«. In: (July 2010). arXiv: 1007.5515 [hep-ph].
- [104] Peter Athron et al. »Global analyses of Higgs portal singlet dark matter models using GAMBIT«. In: *Eur. Phys. J. C* 79.1 (2019), p. 38. DOI: 10.1140/epjc/s10052-018-6513-6. arXiv: 1808.10465 [hep-ph].
- [105] Alejandro Ibarra and Sebastian Wild. »Dirac dark matter with a charged mediator: a comprehensive one-loop analysis of the direct detection phenomenology«. In: *JCAP* 05 (2015), p. 047. DOI: 10.1088/1475-7516/2015/05/047. arXiv: 1503.03382 [hep-ph].
- [106] Prateek Agrawal et al. »Flavored Dark Matter, and Its Implications for Direct Detection and Colliders«. In: *Phys. Rev. D* 86 (2012), p. 055002. DOI: 10.1103/PhysRevD.86.055002. arXiv: 1109.3516 [hep-ph].
- [107] Vernon Barger, Wai-Yee Keung and Danny Marfatia. »Electromagnetic properties of dark matter: Dipole moments and charge form factor«. In: *Phys. Lett. B* 696 (2011), pp. 74–78. DOI: 10.1016/j.physletb.2010.12.008. arXiv: 1007.4345 [hep-ph].
- [108] Maxim Pospelov and Tonnis ter Veldhuis. »Direct and indirect limits on the electromagnetic form-factors of WIMPs«. In: *Phys. Lett. B* 480 (2000), pp. 181–186. DOI: 10.1016/S0370-2693(00)00358-0. arXiv: hep-ph/0003010.
- [109] Spencer Chang, Neal Weiner and Itay Yavin. »Magnetic Inelastic Dark Matter«. In: *Phys. Rev. D* 82 (2010), p. 125011. DOI: 10.1103/PhysRevD.82.125011. arXiv: 1007.4200 [hep-ph].
- [110] Chiu Man Ho and Robert J. Scherrer. »Anapole Dark Matter«. In: *Phys. Lett. B* 722 (2013), pp. 341–346. DOI: 10.1016/j.physletb.2013.04.039. arXiv: 1211.0503 [hep-ph].
- [111] Pearl Sandick, Kuver Sinha and Fei Teng. »Simplified Dark Matter Models with Charged Mediators: Prospects for Direct Detection«. In: *JHEP* 10 (2016), p. 018. DOI: 10.1007/JHEP10(2016)018. arXiv: 1608.00642 [hep-ph].
- [112] Mathias Garny, Alejandro Ibarra and Stefan Vogl. »Signatures of Majorana dark matter with t-channel mediators«. In: *Int. J. Mod. Phys. D* 24.07 (2015), p. 1530019. DOI: 10.1142/S0218271815300190. arXiv: 1503.01500 [hep-ph].

- [113] Alexandre Alves, A.C.O. Santos and Kuver Sinha. »Collider Detection of Dark Matter Electromagnetic Anapole Moments«. In: *Phys. Rev. D* 97.5 (2018), p. 055023. DOI: 10.1103/PhysRevD.97.055023. arXiv: 1710.11290 [hep-ph].
- [114] Yu Gao, Chiu Man Ho and Robert J. Scherrer. »Anapole Dark Matter at the LHC«. In: *Phys. Rev. D* 89.4 (2014), p. 045006. DOI: 10.1103/PhysRevD.89.045006. arXiv: 1311.5630 [hep-ph].
- [115] Eugenio Del Nobile et al. »Direct detection of Light Anapole and Magnetic Dipole DM«. In: *JCAP* 06 (2014), p. 002. DOI: 10.1088/1475-7516/2014/06/002. arXiv: 1401.4508 [hep-ph].
- [116] Junji Hisano, Alejandro Ibarra and Ryo Nagai. »Direct detection of vector dark matter through electromagnetic multipoles«. In: *JCAP* 10 (2020), p. 015. DOI: 10.1088/1475-7516/2020/10/015. arXiv: 2007.03216 [hep-ph].
- [117] Junji Hisano, Ryo Nagai and Natsumi Nagata. »Singlet Dirac Fermion Dark Matter with Mediators at Loop«. In: *JHEP* 12 (2018), p. 059. DOI: 10.1007/JHEP12(2018)059. arXiv: 1808.06301 [hep-ph].
- [118] J. D. Hunter. »Matplotlib: A 2D graphics environment«. In: *Computing in Science & Engineering* 9.3 (2007), pp. 90–95. DOI: 10.1109/MCSE.2007.55.
- [119] Abdelhak Djouadi, Jean-Loic Kneur and Gilbert Moultaka. *SuSpect: a Fortran Code for the Supersymmetric and Higgs Particle Spectrum in the MSSM*. 2002. arXiv: hep-ph/0211331 [hep-ph].
- [120] Werner Porod. *SPheno, a program for calculating supersymmetric spectra, SUSY particle decays and SUSY particle production at e+ e- colliders*. 2003. arXiv: hep-ph/0301101 [hep-ph].
- [121] B.C. Allanach et al. »SUSY Les Houches Accord 2«. In: *Comput. Phys. Commun.* 180 (2009), pp. 8–25. DOI: 10.1016/j.cpc.2008.08.004. arXiv: 0801.0045 [hep-ph].
- [122] Andy Buckley. »PySLHA: a Pythonic interface to SUSY Les Houches Accord data«. In: *Eur. Phys. J. C* 75.10 (2015), p. 467. DOI: 10.1140/epjc/s10052-015-3638-8. arXiv: 1305.4194 [hep-ph].
- [123] G. Belanger et al. »MicrOMEGAs: A Program for calculating the relic density in the MSSM«. In: *Comput. Phys. Commun.* 149 (2002), pp. 103–120. DOI: 10.1016/S0010-4655(02)00596-9. arXiv: hep-ph/0112278.
- [124] G. Belanger et al. »micrOMEGAs: Version 1.3«. In: *Comput. Phys. Commun.* 174 (2006), pp. 577–604. DOI: 10.1016/j.cpc.2005.12.005. arXiv: hep-ph/0405253.

- [125] Particle Data Group et al. »Review of Particle Physics«. In: *Progress of Theoretical and Experimental Physics* 2020.8 (Aug. 2020). 083C01. ISSN: 2050-3911. DOI: 10.1093/ptep/ptaa104. eprint: <https://academic.oup.com/ptep/article-pdf/2020/8/083C01/34673722/ptaa104.pdf>. URL: <https://doi.org/10.1093/ptep/ptaa104>.
- [126] Luis G. Cabral-Rosetti, Myriam Mondragón and Esteban Reyes-Pérez. »Anapole moment of the lightest neutralino in the cMSSM«. In: *Nucl. Phys. B* 907 (2016), pp. 1–17. DOI: 10.1016/j.nuclphysb.2016.03.025. arXiv: 1504.01213 [hep-ph].
- [127] John Ellis and Keith A. Olive. »Revisiting the Higgs Mass and Dark Matter in the CMSSM«. In: *Eur. Phys. J. C* 72 (2012), p. 2005. DOI: 10.1140/epjc/s10052-012-2005-2. arXiv: 1202.3262 [hep-ph].
- [128] Howard Baer, Vernon Barger and Azar Mustafayev. »Neutralino dark matter in mSUGRA/CMSSM with a 125 GeV light Higgs scalar«. In: *JHEP* 05 (2012), p. 091. DOI: 10.1007/JHEP05(2012)091. arXiv: 1202.4038 [hep-ph].
- [129] Subhaditya Bhattacharya et al. »Non-universal SUGRA at LHC: Prospects and Discovery Potential«. In: *Phys. Rev. D* 89.1 (2014), p. 015004. DOI: 10.1103/PhysRevD.89.015004. arXiv: 1309.0036 [hep-ph].
- [130] E. Bagnaschi et al. »Likelihood Analysis of the Minimal AMSB Model«. In: *Eur. Phys. J. C* 77.4 (2017), p. 268. DOI: 10.1140/epjc/s10052-017-4810-0. arXiv: 1612.05210 [hep-ph].
- [131] Konstantin A. Kouzakov and Alexander I. Studenikin. »Electromagnetic interactions of neutrinos in processes of low-energy elastic neutrino-electron scattering«. In: *J. Phys. Conf. Ser.* 1342.1 (2020). Ed. by Ken Clark et al., p. 012120. DOI: 10.1088/1742-6596/1342/1/012120. arXiv: 1711.00517 [hep-ph].
- [132] O. M. Boyarkin and I. O. Boyarkina. *Solar neutrinos as indicators of the Sun's activity*. 2020. arXiv: 2004.10056 [astro-ph.SR].
- [133] Riccardo Catena, Timon Emken and Julia Ravanis. »Rejecting the Majorana nature of dark matter with electron scattering experiments«. In: *JCAP* 06 (2020), p. 056. DOI: 10.1088/1475-7516/2020/06/056. arXiv: 2003.04039 [hep-ph].
- [134] Gaetano Lambiase et al. »Constraints on electromagnetic form factors of sub-GeV dark matter from the Cosmic Microwave Background anisotropy«. In: (Feb. 2021). arXiv: 2102.04840 [hep-ph].

- [135] Carola F. Berger et al. »Supersymmetry Without Prejudice«. In: *JHEP* 02 (2009), p. 023. DOI: 10.1088/1126-6708/2009/02/023. arXiv: 0812.0980 [hep-ph].
- [136] V.M. Dubovik and V.V. Tugushev. »Toroid moments in electrodynamics and solid-state physics«. In: *Physics Reports* 187.4 (1990), pp. 145–202. ISSN: 0370-1573. DOI: [https://doi.org/10.1016/0370-1573\(90\)90042-Z](https://doi.org/10.1016/0370-1573(90)90042-Z). URL: <http://www.sciencedirect.com/science/article/pii/037015739090042Z>.
- [137] Dragos-Victor Anghel and Amanda Teodora Preda. »Observables compatible to the toroidal moment operator«. In: (Jan. 2021). arXiv: 2101.05889 [quant-ph].
- [138] Vladimir M. Dubovik and Valentin E. Kuznetsov. »The Toroid moment of Majorana neutrino«. In: *Int. J. Mod. Phys. A* 13 (1998), pp. 5257–5278. DOI: 10.1142/S0217751X98002419. arXiv: hep-ph/9606258.
- [139] Elena N. Bukina, Vladimir M. Dubovik and Valentin E. Kuznetsov. »Transition radiation of the neutrino toroid dipole moment«. In: *Phys. Lett. B* 435 (1998), pp. 134–138. DOI: 10.1016/S0370-2693(98)00776-X. arXiv: hep-ph/9805491.
- [140] F. Jegerlehner. »Facts of life with γ_5 «. In: *Eur. Phys. J. C* 18 (2001), pp. 673–679. DOI: 10.1007/s100520100573. arXiv: hep-th/0005255.
- [141] Er-Cheng Tsai. »Gauge Invariant Treatment of γ_5 in the Scheme of 't Hooft and Veltman«. In: *Phys. Rev. D* 83 (2011), p. 025020. DOI: 10.1103/PhysRevD.83.025020. arXiv: 0905.1550 [hep-th].
- [142] Er-Cheng Tsai. »The Advantage of Rightmost Ordering for γ_5 in Dimensional Regularization«. In: (May 2009). arXiv: 0905.1479 [hep-th].
- [143] A. M. Bruque, A. L. Cherchiglia and M. Pérez-Victoria. »Dimensional regularization vs methods in fixed dimension with and without γ_5 «. In: *JHEP* 08 (2018), p. 109. DOI: 10.1007/JHEP08(2018)109. arXiv: 1803.09764 [hep-ph].
- [144] Roberto Pittau. »A four-dimensional approach to quantum field theories«. In: *JHEP* 11 (2012), p. 151. DOI: 10.1007/JHEP11(2012)151. arXiv: 1208.5457 [hep-ph].
- [145] Warren Siegel. »Supersymmetric dimensional regularization via dimensional reduction«. In: *Physics Letters B* 84.2 (1979), pp. 193–196. ISSN: 0370-2693. DOI: [https://doi.org/10.1016/0370-2693\(79\)90282-X](https://doi.org/10.1016/0370-2693(79)90282-X). URL: <http://www.sciencedirect.com/science/article/pii/037026937990282X>.
- [146] Ruggero Ferrari. »Managing γ_5 in Dimensional Regularization and ABJ Anomaly«. In: (Mar. 2014). arXiv: 1403.4212 [hep-th].

- [147] Andrzej J. Buras and Peter H. Weisz. »QCD nonleading corrections to weak decays in dimensional regularization and 't Hooft-Veltman schemes«. In: *Nuclear Physics B* 333.1 (1990), pp. 66–99. ISSN: 0550-3213. DOI: [https://doi.org/10.1016/0550-3213\(90\)90223-Z](https://doi.org/10.1016/0550-3213(90)90223-Z). URL: <http://www.sciencedirect.com/science/article/pii/055032139090223Z>.
- [148] G. Altarelli et al. »QCD non-leading corrections to weak decays as an application of regularization by dimensional reduction«. In: *Nuclear Physics B* 187.3 (1981), pp. 461–513. ISSN: 0550-3213. DOI: [https://doi.org/10.1016/0550-3213\(81\)90473-9](https://doi.org/10.1016/0550-3213(81)90473-9). URL: <http://www.sciencedirect.com/science/article/pii/0550321381904739>.
- [149] John F Gunion et al. *The Higgs hunter's guide*. Vol. 80. Upton, NY: Brookhaven Nat. Lab., 1989. URL: <https://cds.cern.ch/record/425736>.